POWER QUALITY CONTROL
USING POWER ELECTRONICS CONVERTERS

BY

YUEXIN YIN

A DISSERTATION PRESENTED TO THE GRADUATE SCHOOL
OF THE UNIVERSITY OF FLORIDA IN PARTIAL FULFILLMENT OF THE
REQUIREMENTS FOR THE DEGREE OF
DOCTOR OF PHILOSOPHY

UNIVERSITY OF FLORIDA

1995

UNIVERSITY OF FLORIDA LIBRARIES

To my wife, Dai Lu, and my family

ACKNOWLEDGEMENTS

The author would like to thank his advisor, Dr. Dennis P. Carroll, for his guidance and support in the author's research and other academic pursuits. Dr. Carroll's counsel and encouragement have inspired the author's will to achieve and have provided both personal and academic philosophies that will serve as invaluable, life-long models.

The author wishes to express gratitude to Dr. Khai D. T. Ngo, for his advice on power electronics applications and the sponsored research project from which this dissertation was generated. Additional thanks go to Dr. Martin A. Uman, Dr. Haniph A. Latchman, and Dr. Barney L. Capehart for serving as the committee members.

The author also wishes to thank the other students involved in the sponsored research project, Xu Huang and Ray-Shyang Lai. Their knowledge in the area of power electronics was very helpful.

Finally, the author wishes to acknowledge the Electric Power Research Institute (EPRI) for partially funding the research project as part of CUSTOM POWER initiative. Special thanks to Westinghouse Electric Corporation, Marine Division, for the fellowship granted to the author so that he was able to complete his PhD program.

TABLE OF CONTENTS

ACKNOWLEDGEMENTS iii

ABSTRACT vii

CHAPTER 1 INTRODUCTION 1

1.1 Power Quality 1
1.2 Dissertation Results versus Previous Work 3
1.3 Major Contributions 9

CHAPTER 2 POWER QUALITY ISSUES 10

2.1 General Description 10
2.1.1 Terminology and Definition 10
2.1.2 Causes and Impacts 11
2.2 A miniature Distribution System for Power Quality Study 14
2.3 Power Quality Phenomena Duplication 19
2.4 Power Quality with Electric Machine Loads 31

CHAPTER 3 POWER ELECTRONICS CONVERTERS: PWM DC-AC INVERTERS 38

3.1 PWM DC-AC Inverter Fundamentals 39
3.2 Single-Phase PWM DC-AC Inverter Modeling 44
3.3 Three-Phase PWM DC-AC Inverter with Uncoupled Network Loads 49
3.4 Three-Phase PWM DC-AC Inverter with Dynamic Machine Loads 58

CHAPTER 4 CONTROL SYSTEM ANALYSIS 63

4.1 General Description 63
4.2 Load Dynamics 66
4.3 Control System for the Inverter with Uncoupled Network Loads 75

4.4 Control System for the Inverter with Dynamic Machine Loads 78
4.5 Adaptive Control 84
4.6 Effect of Distribution System 90
4.7 Conclusion 92

CHAPTER 5 SIMULATION RESULTS 93

5.1 Introduction 93
5.2 Power Quality Improvement for Uncoupled Network Loads 98
5.2.1 Blocking Feeder Harmonics 98
5.2.2 Compensating Voltage Sags 99
5.2.3 Absorbing Voltage Swells 99
5.2.4 Compensating Voltage Outage 100
5.2.5 Absorbing Impulses in Feeder Voltage 101
5.3 One-Cycle-Switching 122
5.4 Power Quality Improvement for Dynamic Machine Loads 128
5.5 Power Electronic Controller using Adaptive Control 135

CHAPTER 6 IMPLEMENTATION ISSUES 147

6.1 A State-of-the-Art Technique for Converter Supply 147
6.2 Harmonic Rejection and Sensitivity Analysis 154
6.2.1 Harmonic Rejection 154
6.2.2 Sensitivity Analysis 158

CHAPTER 7 CONCLUSION 161

APPENDIX A INDUCTION MOTOR DATA 166

APPENDIX B ALGEBRAIC EQUATIONS OF TRANSFORMATION MATRICES 167

B-1 Transformation between abc and 0fb Variables 167
B-2 Transformation between abc and qd0 Variables 169

APPENDIX C PARAMETERS USED IN THE DISSERTATION 171

C-1 Laboratory Model Distribution System 171
C-2 Inverter Filter Parameters 172
C-3 Control System 172

APPENDIX D DIGITAL ALGORITHMS 173

REFERENCES 176

BIOGRAPHICAL SKETCH 181

Abstract of Dissertation Presented to the Graduate School of the
University of Florida in Partial Fulfillment of the Requirements for the Degree of
Doctor of Philosophy

POWER QUALITY CONTROL USING POWER ELECTRONICS CONVERTERS

By
Yuexin Yin

December 1995

Chairman: Dr. Dennis P. Carroll
Major Department: Electrical and Computer Engineering

This dissertation describes power electronics applications in distribution power quality enhancement.

The dissertation first deals with power quality phenomena which are of concern in distribution engineering. The typical power quality phenomena such as harmonic distortions, voltage sags, voltage swells, impulses, outages, transients, noises, etc. are examined through waveforms acquired from both a real distribution system and computer simulations based on a typical distribution system. The duplication of the waveforms in the computer simulation helps to explain power quality phenomena and provides in-depth knowledge of each phenomenon. The impacts of power quality problems on distribution systems and customer loads are discussed.

By using power electronics converters, basically PWM DC-AC inverters, high quality power is maintained at an important load or bus no matter what power quality

phenomena exist in the distribution system. The idea is using DC-AC inverters to either compensate voltage and/or current, or absorb excessive voltage and/or current at critical loads to maintain high quality power.

Depending on the distribution loads, several topologies of the control systems are developed to serve as multi-functional controller for power quality improvement. The dissertation generalizes the control systems for the static loads and dynamic machine loads, respectively. Furthermore, an adaptive control system is developed to follow the changes in the supported loads. In all of the control systems, a closed-loop structure is included in order to reject disturbances, from either the distribution system or converter DC bus voltage. The dissertation investigates the details of attenuating the disturbances by the closed-loop system.

The dissertation not only provides theory and concept in this area, but the computer simulations are used throughout the dissertation to verify the concept.

CHAPTER 1

INTRODUCTION

1.1 Power Quality

Electric distribution systems provide connections between bulk sources and customer loads through distribution components. Distribution power quality has a direct impact on the supplied customers and distribution components. Due to various disturbances or changes in system operation, distribution systems suffer from both short duration transient problems and long-term abnormal conditions. In general, distribution systems have little control over these problems without using mitigation techniques. Distribution systems are therefore vulnerable to these power quality problems.

In the present distribution systems, more and more customers require high quality power supply to maintain normal operations. Such typical customer loads are computer facilities or some high precision equipment. These loads are sensitive to the supplied power because of the electronic devices which operate in very low power ratings and are built in a highly compacted form. Industrial process controls involving electric motors are also vulnerable to short power interruptions. On the other hand, more and more customers are creating power quality problems by using unconventional techniques because these techniques can provide some flexibilities which are impossible or very difficult to achieve using conventional approaches. The typical example is Adjustable

Speed Drives (ASDs) which provide efficient control capabilities for rotating electric machinery. The ASDs are designed with power electronics converters which normally create waveform distortions to the power supply. In distribution systems, power electronics equipment is the main reason for the harmonic waveform distortions.

Power quality problems are a concern of electric utilities which coordinate bulk power sources and various customer loads. For both efficiency and economy, power quality has a great impact on the utility systems because it directly affects the distribution components such as subtransmission lines, substations, distribution transformers, metering, etc. Considering electricity as a product, high quality power is more meaningful to customers. The "end users" of the power--customers--are concerned about power quality as well because the power supply may affect their equipment, network, or appliances. Utilities must maintain high quality power, for their customers and for their own sake.

Because of this, the Electric Power Research Institute (EPRI), a major utility coordination organization headquartered in Palo Alto, California, USA, sponsored the CUSTOM POWER strategy under the leadership of Dr. Narain Hingorani [1,2]. Dr. Hingorani had previously coined the term FACTS, Flexible AC Transmission Systems. FACTS are developed to increase the capability of the transmission systems [3,4], while CUSTOM POWER is intended to increase the capability of the distribution systems. Both use power electronics converters as controllers. In CUSTOM POWER, power electronics controllers are used to improve power quality within the distribution systems. From theoretical analyses and computer simulations as performed for this dissertation,

power electronics converters with high power ratings have the capability of isolating the disturbances or other transients occurring in utility systems from sensitive and important customer loads. Also, power electronics converters can immunize electric utilities against some customer loads which cause power quality problems such as harmonic distortions.

1.2 Dissertation Results versus Previous Work

The research as described in this dissertation follows the directions of the CUSTOM POWER strategy and applies power electronics to power quality improvement. The dissertation begins with a power quality problems analysis, then proceeds to power electronics converter analysis, the multi-functional control system design for power electronics converters, the implementation issues, and ends with a conclusion and discussion of the further development.

In power quality problems analysis, the dissertation mainly simulates the power quality phenomena based on a typical distribution system. According to the literature, systematic and detailed power quality analysis, including the causes and impacts on distribution systems, is not available. Some literature illustrates power quality phenomena from the industrial point of view. For instance, IEEE Tutorial Courses [5] and Rice [6] address harmonics caused by Adjustable Speed Drives (ASDs). McGranaghan et al [7] discuss voltage sags in industrial systems. J. Harvey [8] covers more details in this field. This dissertation discusses various power quality phenomena of concern in present distribution systems as supported by sample waveforms. The

waveforms from real systems are compared with computer simulations. A quantitative agreement is achieved. On the other hand, the dissertation shows some waveforms which are difficult to obtain in real systems.

In addition to studying the impact of power quality problems on general static loads, the dissertation investigates a typical industrial load--dynamic rotating electric machinery as well. The results based on computer simulations uncover some facts which are not shown in the literature before. The voltage sags in the system cause currents to increase rather than current sags. This phenomenon is explained in the dissertation in detail. Due to this phenomenon, dynamic loads are examined in addition to the static loads in power electronics applications.

Since the dissertation deals with a new topic in electric power engineering, many ideas and implementations are novel in this area. Although there are similar achievements in power quality improvement, the techniques as developed in this dissertation are quite different from other techniques. Furthermore, the dissertation describes a control method which can solve many of the power quality problems, while the other methods normally solve only one particular problem as described below.

The conventional power conditioner is used as a power source to the protected equipment, as described by Chen and Divan [9]. Therefore, full power is attained through the power conditioner. As long as the load or bus draws rated current and voltage, the power conditioner operates with full power as well. The input to the power conditioner can be a battery or rectified DC source. The typical equipment of using battery is the Uninterruptible Power Supplies (UPS). By using a rectified DC source,

the power conditioner serves as an on-line protective equipment for the supported customer load. If the input to the power conditioner losses full voltage such as in the case of voltage sags or outages, the energy stored in the storage element capacitor serves as the source to the inverter to support the customer. In this way, the power conditioner supports the loads depending on the charge on the capacitor. This demands a high rating for the capacitor. Normally, the higher the capacitance, the better. The power conditioner using the same topology is widely used in motor drive applications where variable voltage and frequency are normally desired. The capacitor in drive applications is only used as a filter element rather than an energy storage component.

F.Z. Peng et al introduce a new topology of power conditioning which is valid for harmonic compensation [10,11]. The idea is using shunt and series converters to block harmonics caused by both customer and utilities. This technique is discussed in this dissertation to explain the principle of the converter applications. However, Peng et al do not solve the other power quality problems covered in this dissertation. In addition, various other literature addresses this topic [12,13,14].

Another important application of the power conditioner is in that of balancing three-phase systems which suffer unbalanced voltages due to sequence currents. The power conditioner injects sequence quantities to bring the system into balance. Campos et al [15] and Bhavaraju et al [16] describe the details of power electronics converter applications in balancing three-phase systems.

The phenomena as described above are normally steady-state in which the problems are easy to solve to some extent. In fact, in this area, there are significant

achievements accompanying advanced technologies such as digital signal processing and adaptive control [13]. Nevertheless, there is little progress in dealing with transient power quality problems. Typical examples are voltage sags which occur very often in electric utilities because of breaker operations. The distribution industry reports this kind of phenomena from time to time, as discussed by McGranaghan et al [7], and Dugan et al [17]. These authors present the challenges from the industrial point of view and claim that voltage sags have a big impact on both system operations and economics. They also urge the use of high technological power conditioners to deal with these fast transient power quality problems. Nevertheless, there is little progress seen in this area.

In addition to voltage sags, there are various other transient phenomena such as voltage swells, and surges, existing in distribution systems. Smith and Standler [18] report the effects of electrical surges on domestic appliances. Normally, electrical surges are protected by surge arresters. However, surge arresters only work when electric surges exceed the protective level. If the surges are higher than the system voltage but lower than the protective level, the surge arresters do not operate.

According to the industry, power quality problems become most challenging in distribution systems. Although there are some technologies to deal with specific power quality phenomenon, such as those as described above, they are not designed for other applications. Instead of solving one particular distribution power quality problem, the development as described in this dissertation solves several power quality problems using power electronics converters. The significance is that the multi-functional power electronic controller is developed based on various industrial loads.

The dissertation first addresses the power quality issues concerned in the distribution engineering. Various power quality phenomena are simulated in a typical distribution system, and supported by the waveforms acquired from a real distribution system. The simulation provides an in-depth knowledge of these phenomena. A power quality phenomenon based on the typical distribution system load--rotating electrical machinery is also discussed in detail.

The dissertation then discusses power electronics converters used to improve the power quality. Specifically, a three-phase DC-AC inverter is studied. Based on the different distribution system loads, different topologies are used for analysis. For static loads, a single-phase topology can be used for analysis and compensator design. The dissertation provides a detailed analysis of the inverter system with only static load installed. For rotating machinery loads, a transformation from the conventional three-phase abc coordinate system to a rotating reference frame qd0 is used. It appears from the literature little progress has been made in these areas.

In the three-phase PWM DC-AC inverter applications, three fundamental models are used for analysis and compensator design of the control system. The first one is based on the conventional abc domain, where the three phases are treated separately. Kusko et al [19], Nabae et al [20], Yao et al [21], Min et al [22], Pouliquen et al [23], Dzieniakowski et al [24], and Hoang [25] adopt this model. The second one is based on qd0 domain in which all the three-phase systems are transformed to a two-phase system, assuming no zero sequence currents exist. This model is widely used in rotating electrical machinery and drive systems. Only a few applications are cited herein.

Krause [26] uses the abc-qd0 transformation for the analysis of all electrical machinery. Murai et al [27] also adopt qd0 models for electrical drive analysis, and Kawabata [28] uses it for general inverter applications. The third model is based on a qd0 model but combined with symmetrical components technique, the so-called 0fb model by Ngo [29] and White [30]. Campos et al [15] use the qd0 model and symmetrical components technique separately, to study the unbalanced system. The 0fb model is a complex number transformation as a result of using symmetrical components.

The above three models are used in different applications. The dissertation covers each model. Also, it provides a detailed analysis of transformations used in different applications. The dynamic equations of the inverter system are also developed based on each transformation.

Depending on the distribution loads, the control systems are discussed in detail. The dissertation models various distribution loads. A generalized control structure based on qd0 system is developed. Of special interest is using the adaptive control to deal with the system plant changing in rotating machinery application. The adaptive control is different from those used as hysteresis control, or "Bang-Bang" control, in that the coefficients of the compensator are adjusted based on a recursive algorithm. The adaptive "Bang-Bang" control is used widely, as discussed by Zoos et al [31]. Nevertheless, it can not adjust its compensator to follow the plant model changes. Also, the adaptive control used is different from a conventional open-loop adaptive control as used widely, in that the closed-loop structure is applied. The adaptive control based on minimizing the error is a new application in the inverter control system.

In addition to the theoretical analysis, implementation issues with computer simulations are provided in the dissertation. The computer simulations are mainly based on the power system simulation package ElectroMagnetic Transients Program (EMTP). The EMTP package models most conventional power system components. In addition, it has the capabilities for simulations of power electronics and control systems [32,33].

1.3 Major Contributions

The dissertation provides the following contributions to electrical distribution engineering and related areas:

(1) The dissertation addresses the power quality issues by discussing various power quality phenomena, the causes and their impacts on distribution systems.

(2) The dissertation provides a detailed analysis and computer simulations of power electronic converters in solving power quality problems. Various distribution system loads are analyzed including coupled dynamic loads.

(3) Based on different distribution loads, a multi-functional control system is designed, which solves many power quality problems. The computer simulations are performed to verify the concepts and design approaches.

(4) The application of adaptive control is introduced to deal with uncertainties in distribution system loads.

CHAPTER 2

POWER QUALITY ISSUES

This chapter addresses power quality issues and describes most of power quality phenomena by definitions or explanations. Some real system waveforms are illustrated and the waveforms are duplicated by computer simulation results using EMTP. To carry out research in power quality enhancement, a state-of-the-art distribution system model is designed. The simulation results from the distribution system model help to explain the causes and impacts of the power quality phenomena.

2.1 General Description

In general, high quality power provides little waveform distortion from the standard: a pure sinusoidal waveform with constant amplitude and frequency. Any waveform distortions from the standard are said to have power quality problems. According to different situations, the following terminologies and definitions are provided to understand power quality phenomena [34].

2.1.1 Terminology and Definition

Harmonic distortions refer to the waveforms which have periodic deviation from normal sinusoidal waveforms. Harmonics exist in both voltage and current waveforms, and are normally evaluated by Total Harmonic Distortion (THD) [5,6].

Voltage sags refer to momentary voltage drops from rated or normal voltage. Sag rate is the percentage of the voltage amplitude in reference to the rated voltage amplitude. The duration of voltage sags is typically several cycles.

Voltage swells refer to momentary voltage boosts over rated voltage. The duration of voltage swells is typically several cycles.

Voltage outages refer to a complete loss of power for a longer period in contrast to voltage sags.

Undervoltages refer to the voltage drops from rated voltage and by definition have a longer duration compared to voltage sags.

Overvoltages refer to the voltage increase over rated voltage and by definition have a longer duration compared to voltage swells.

Surges or impulses refer to the voltage increase in a very short duration with high amplitude. Surges or impulses may trigger voltage or current oscillations.

Noises refer to high frequency oscillation parasitic on normal waveforms.

Low power factor normally refers to the system or customer loads whose power factor is lower than the demanded power factor defined by the utilities industry.

2.1.2 Causes and Impacts

The previous descriptions cover most of the distribution power quality phenomena. The causes of these phenomena may be multifarious due to the complex nature of the power systems, but they still fall into uniform classifications. Some of the problems may be caused by natural phenomena and some by power system operations. Steady-state harmonic distortions are normally caused by nonlinear power electronics

loads. In the last decade, power electronics equipment has been increasingly used in power systems for various purposes including control of rotating electric machinery, increase of transmission or distribution system capabilities, and conservation of energy consumption which otherwise is wasted because of changing operations. Switching operations of power electronics converters which are connected to the electric utility side causes current waveform distortion of the power supply. The current distortion causes voltage distortion depending on the capacity of the power electronics non-linear loads at this bus. Due to the long term duration, harmonic distortions are steady-state power quality phenomena which need long-term considerations.

In transient power quality, some natural phenomena occurring in power systems cause voltage abnormality. Lightning normally causes overvoltage and overcurrent to a power system for very short periods (typically in micro-second levels). Similarly, power system switching operations cause the same phenomena, but the durations are normally longer. Power system faults such as line to ground faults cause line voltage outage and remote system voltage sag. Some large loads such as large motors tripped-off from distribution systems cause voltage swells. Also, voltage sags may exist during motor start-up because of the voltage drops on the line caused by high inrush current. A line-to-ground fault in one of the three phases of ungrounded transformers results in voltage swells in other two phases as well. Many of these abnormal behaviors in distribution systems are accompanied by transient oscillations.

A low power factor is normally caused by customer loads which absorb too much reactive power. Reactive power corresponds to the power consumed in reactive

components--inductive loads. Many industrial loads are inductive because rotating electric machinery relies on the inductive component to transfer the energy. The power factor is determined by how much reactive power is consumed compared with real power.

The impact of these power quality phenomena takes multiple forms. Harmonics increase losses of equipment which is designed to operate in normal conditions. The extra losses cause equipment to overheat. For instance, harmonics in rotating electric machinery increase winding losses without contributing any useful energy transfers. Furthermore, harmonics cause torque pulsations which may trigger mechanical system oscillation. In transformers, harmonics increase winding losses and decrease efficiency as in rotating electric machinery. Harmonics also cause saturation of transformers.

Electric surges or impulses are suppressed by surge arresters if the surges exceed the coordinated protection level. Nevertheless, non-operation or failure of surge arresters is often reported, which actually degrades protection for the protected equipment or network. On the other hand, frequent firing of surge arresters causes aging problems which shortens the life of arresters and eventually results in surge arrester failure. Normally, arresters are rated higher than the rated system or equipment voltage. Suppression of surges or impulses may actually cause overvoltages. Overvoltages or voltage swells increase losses and cause equipment to overheat, gradually destroying the insulation materials of equipment. Undervoltages may cause abnormal operations of customer loads. For example, the speed decreases in rotating machinery, and memory may be lost in a computer, if the voltage supply drops.

Power quality also affects utility meters. Misreading of industrial or residential meters may be the results of harmonics or transient phenomena in distribution systems. The meters, like other electrical equipment, contain electrical components such as inductor windings, designed to operate in normal conditions. Errors may occur in metering due to harmonics or transient phenomena.

In conclusion, power quality problems as described herein have direct impacts on the electric utilities and their supplied customers. The power quality has a direct effect on efficiency, protective insulations, system capabilities, etc. Sensitive loads such as computer facilities and high precision equipment suffer in wasting human effort, if low quality power is responsible for the loss of the computer memory or loss of a valuable product. Maintaining high quality power benefits both the electric utilities and customers.

2.2 A Miniature Distribution System for Power Quality Study

A power system as shown in Figure 2.1 is studied to simulate a typical distribution system. The system has a capacity of 25 MVA and the substation has 13.8 kV voltage. Two feeders noted as FEEDER 1 and FEEDER 2 connect to the substation through short distribution lines. FEEDER 3 represents the rest of the loads connected to the source. FEEDER 1 and FEEDER 2 have a tie-line connection to provide exchange of the feeders in case one fails. The Solid-State-Breaker (SSB) provides fast switching operations, which are simulated by electronically controlled switches. Distribution systems could benefit from a SSB capable of switching in less than one cycle

because it can reduce the time interval of voltage outages or sags due to breaker operations. This actually is one of the techniques to provide high quality power to customers. The SSBs connected on the feeders are normally closed and the SSB serving as a tie-line connection is normally open.

This system reflects most of the distribution features such as source, feeders, distribution system lines, breakers, transformers and loads with their power factor correction capacitors. Notice that this system is also capable of simulating power quality phenomena which will be described in the next section.

In order to make the system manageable in the laboratory, a scaled down distribution system model is derived with 15 kVA and 208 V rating, as shown in Figure 2.2. The load noted by V_{cus} is the critical or important load which needs a high quality power. The transformer feeding V_{cus} is used to provide isolation between the critical load and the substation. The load itself is variable with a range of 0.3 ~ 3 kVA.

With the help of the computer simulation package EMTP, the distribution system was designed with all the components selected. Figure 2.3 shows the distribution model with all the parameters labeled. Due to laboratory availability, the isolation transformers with voltage ratings of 208V/208V are replaced by two 208V/480V transformers. The new components which are not seen in the previous figures are the INVERTER and RECTIFIER blocks, that represent the power electronics converters. The idea is to use the FEEDER 2 as the supply for the converter which is designed to maintain high quality power for the important load. The branch connected to FEEDER 1, noted as SSR (Solid-State-Relay), is used to simulate a line-to-ground fault.

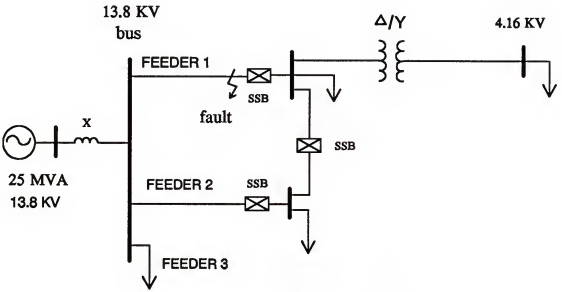

Figure 2.1 A typical distribution system

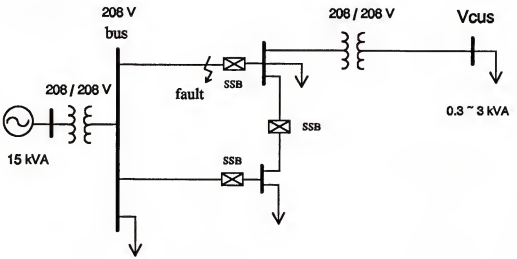

Figure 2.2 Scaled down distribution system model

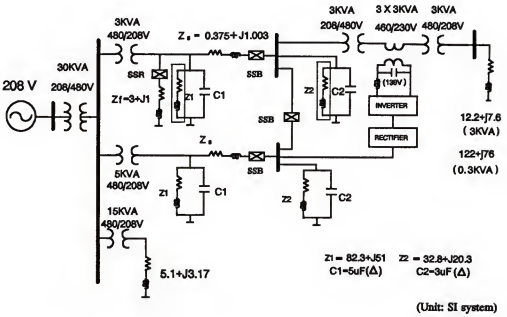

Figure 2.3 Laboratory model distribution system

The systems as shown above are based on one-line diagrams, but they are actually a three-phase system. All the phenomena studied are based on a three-phase system. Some parameters do not reflect real system parameters but provide convenience in laboratory construction. For instance, the feeder distribution line impedances are larger than those in a real system. Increasing line impedance allows observation of a typical sag rate at the custom bus when there is a fault in the distribution line. Nevertheless, the system features are the same as in a real system.

2.3 Power Quality Phenomena Simulation

With the support of local electric utilities, some power quality waveforms were acquired in real power systems. Figure 2.4 and Figure 2.5 show the typical harmonic distortions caused by power electronics rectifiers. Figure 2.4 is the voltage and current waveform caused by a single-phase rectifier, and Figure 2.5 is for a three-phase rectifier. The current waveforms are highly distorted, and the voltage waveforms are slightly distorted because of the balance of other linear loads connected at the same bus. It can be shown that low frequency harmonic components in current waveforms have more severe effects than higher order harmonics. Figure 2.6 shows voltage sags which are caused by a remote fault in the systems. A line-to-ground fault in one phase causes a severe voltage sag to this phase voltage at a remote site. Also, mutual coupling of distribution lines causes voltage sags in the other two phases as well. Figure 2.7 shows impulses with unknown causes. Thus, one phase experiences a voltage impulse, and the other two phases incur noises obviously caused by the same reason.

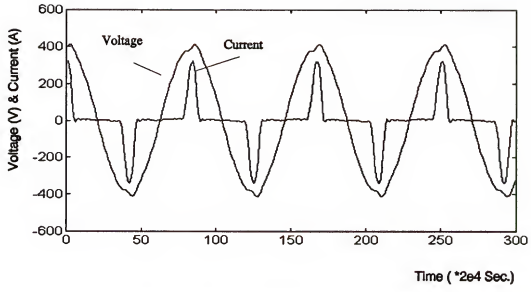

Figure 2.4 Harmonic voltage and current from real system:Single-phase rectifier

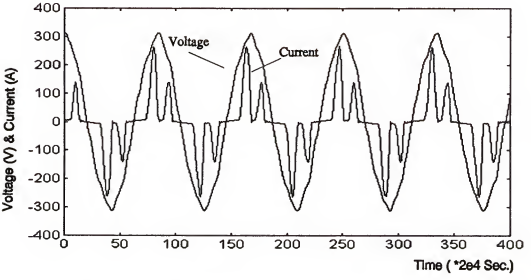

Figure 2.5 Harmonic voltage and current from real system: Three-phase rectifier

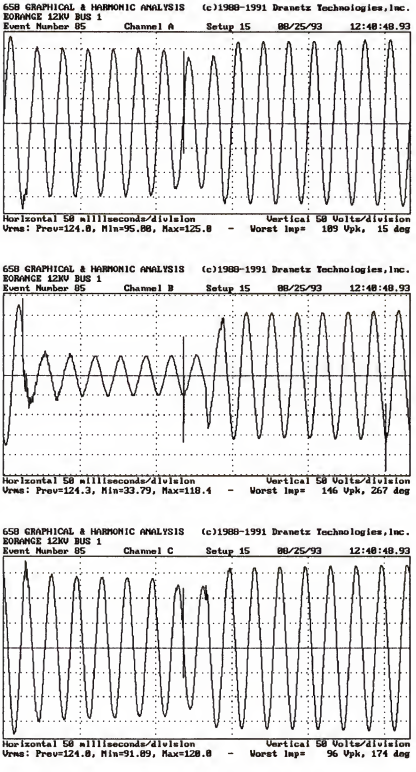
658 GRAPHICAL & HARMONIC ANALYSIS (c)1988-1991 Dranetz Technologies,Inc.
EORANGE 12KV BUS 1
Event Number 85 Channel A Setup 15 08/25/93 12:48:48.93
Horizontal 50 milliseconds/division Vertical 50 Volts/division
Vrms: Prev=124.8, Min=95.88, Max=125.8 - Worst Imp= 189 Vpk, 15 deg
658 GRAPHICAL & HARMONIC ANALYSIS (c)1988-1991 Dranetz Technologies,Inc.
EORANGE 12KV BUS 1
Event Number 85 Channel B Setup 15 08/25/93 12:48:48.93
Horizontal 50 milliseconds/division Vertical 50 Volts/division
Vrms: Prev=124.3, Min=33.79, Max=118.4 - Worst Imp= 146 Vpk, 267 deg
658 GRAPHICAL & HARMONIC ANALYSIS (c)1988-1991 Dranetz Technologies,Inc.
EORANGE 12KV BUS 1
Event Number 85 Channel C Setup 15 08/25/93 12:48:48.93
Horizontal 50 milliseconds/division Vertical 50 Volts/division
Vrms: Prev=124.8, Min=91.89, Max=128.8 - Worst Imp= 96 Vpk, 174 deg

Figure 2.6 Measured voltage sags from real system (Top to bottom phase A, B, C)

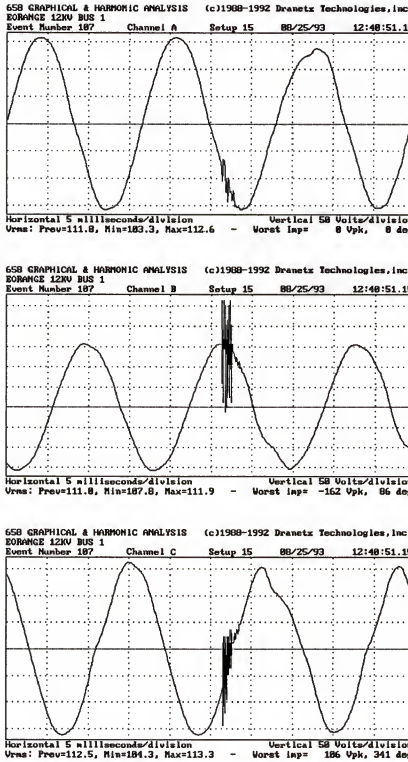
658 GRAPHICAL & HARMONIC ANALYSIS (c)1988-1992 Dranetz Technologies,Inc.
EORANGE 12KV BUS 1
Event Number 107 Channel A Setup 15 08/25/93 12:40:51.15
Horizontal 5 milliseconds/division Vertical 58 Volts/division
Vrms: Prev=111.8, Min=103.3, Max=112.6 - Worst Imp= 0 Vpk, 0 deg
658 GRAPHICAL & HARMONIC ANALYSIS (c)1988-1992 Dranetz Technologies,Inc.
EORANGE 12KV BUS 1
Event Number 107 Channel B Setup 15 08/25/93 12:40:51.15
Horizontal 5 milliseconds/division Vertical 58 Volts/division
Vrms: Prev=111.8, Min=107.8, Max=111.9 - Worst Imp= -162 Vpk, 86 deg
658 GRAPHICAL & HARMONIC ANALYSIS (c)1988-1992 Dranetz Technologies,Inc.
EORANGE 12KV BUS 1
Event Number 107 Channel C Setup 15 08/25/93 12:40:51.15
Horizontal 5 milliseconds/division Vertical 58 Volts/division
Vrms: Prev=112.5, Min=104.3, Max=113.3 - Worst Imp= 186 Vpk, 341 deg

Figure 2.7 Measured impulses from real system (Top to bottom: Phase A, B, C)

Based on the laboratory miniature distribution system model, some power quality phenomena were simulated using EMTP. The waveforms are similar to those from the real distribution systems. The waveforms are acquired at the critical load bus as mentioned before. In the following text, the term Custom Power bus or Custom bus will be used for this critical bus which is actually defined by CUSTOM POWER technology.

Figure 2.8 shows the current and voltage waveforms when the Custom Power bus is installed with a three-phase rectifier load. Both current and voltage waveforms are highly distorted; because there are no other loads at this bus to balance the power electronics nonlinear load. It is observed that the simulation provides a better current waveform than that from the real system. Unlike the real system, the miniature distribution system model has more inductance in the feeder side which enables current flow continuously within each half cycle. Figure 2.9 shows the similar waveform as that from the real system without filtering inductance. The waveform is acquired from an equivalent system model without a filtering component. The current waveform is highly distorted. Figure 2.10 shows the current and voltage waveforms at the custom bus when the feeder side has harmonic sources. The feeder voltage is highly distorted, therefore, the custom bus voltage is highly distorted as well. The current waveform at custom bus has little distortion because of the filtering inductance. These are three-phase harmonic distortion phenomena with balanced power electronics rectifier loads. Figure 2.11 and Figure 2.12 show the current and voltage waveforms when the custom bus has an unbalanced load with one phase of rectifier load and the other two phases of regular load. The regular load is equivalent to an impedance. Due to the mutual coupling of the

transformers, the other two phases which are not installed in the rectifier are also distorted, as can be seen in the voltage waveforms in Figure 2.12. Mapping the voltage and current waveforms together for the phase which has a single-phase rectifier load will yield similar waveforms as those from a real system, as in Figure 2.13, which is compared to the waveforms in Figure 2.4.

Figure 2.14 shows voltage sags at the Custom Power bus when there is a line-to-ground fault at FEEDER 1 distribution line, referring to Figure 2.3. Voltage sags from EMTP simulations are similar to those obtained in the real system as in Figure 2.6, which verifies that voltage sags result from a remote fault. Figure 2.15 shows voltage swells. As described previously, voltage swells may be caused by a large motor load tripped off from the system, or a single line-to-ground fault with ungrounded transformers. The voltage swells in Figure 2.15 result form the load trip-off which is connected to the source, as can be seen in Figure 2.1. FEEDER 3 represents a large motor load which is connected to the system.

Finally, the simulation of one-cycle switching is shown in Figure 2.16. One-cycle switching allows feeders to switch-over within one cycle without causing a long time voltage outage at the important bus. One-cycle-switching may result in voltage surges when the reclosing time coincides with the peak time of the voltage (phase A in the figure). In addition, one-cycle-switching causes high frequency oscillations because of the breaker operation. The switching of the breakers is controlled by the so-called Solid-State-Breaker (SSB), which is actually the power electronics devices.

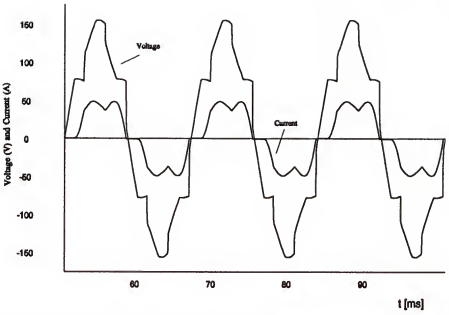

Figure 2.8 Voltage and current waveforms of custom bus with rectifier load

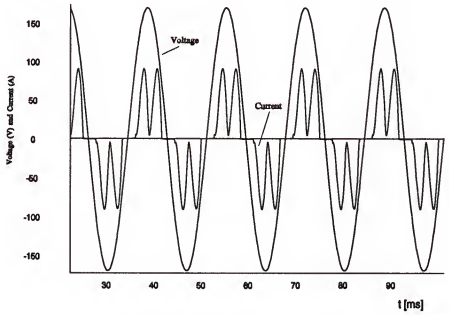

Figure 2.9 Voltage and current waveforms of three-phase rectifier without line inductance

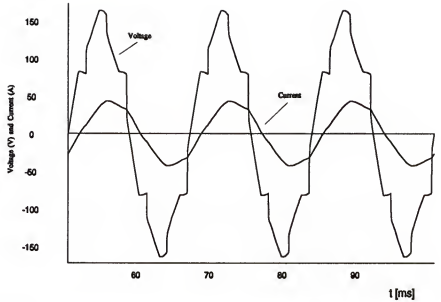

Figure 2.10 Voltage and current waveforms at Custom bus with harmonics in feeder

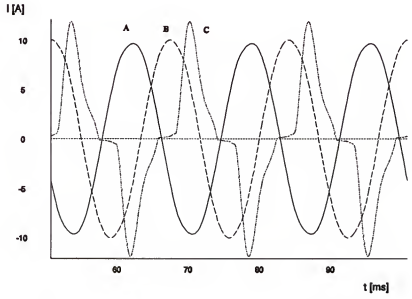

Figure 2.11 Three-phase current with one phase of rectifier load (unbalance load)

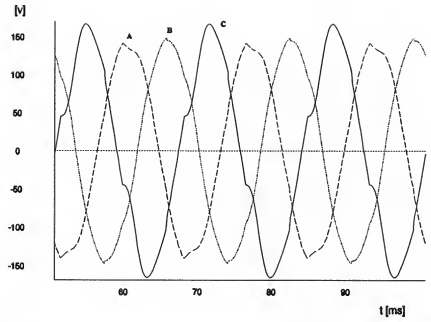

Figure 2.12 Three-phase voltage with unbalanced load (single-phase rectifier load)

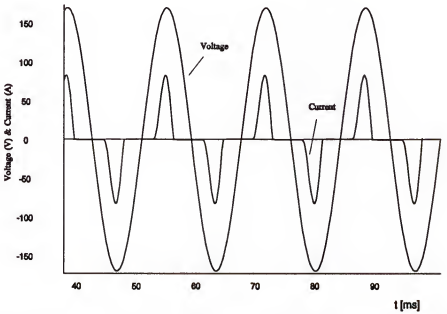

Figure 2.13 Voltage and current of single-phase rectifier without line inductance

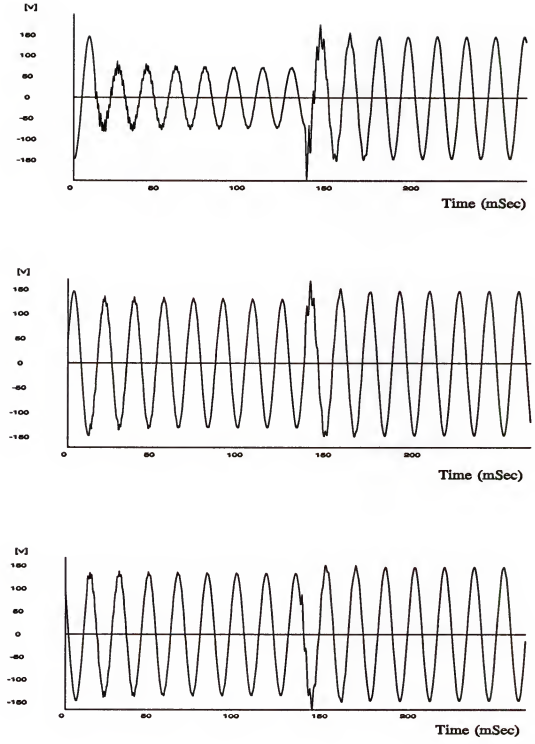

Figure 2.14 Voltage sags at Custom bus (Top to bottom: phase A,B,C)

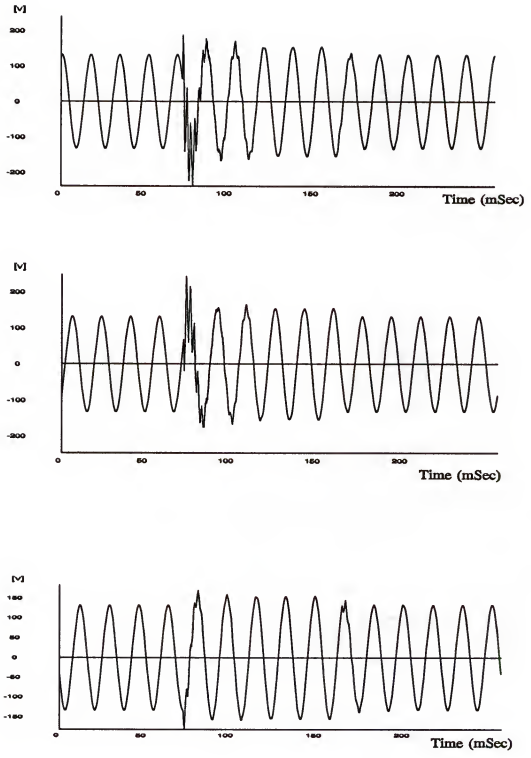

Figure 2.15 Voltage swells at Custom bus (Top to bottom: phase A,B,C)

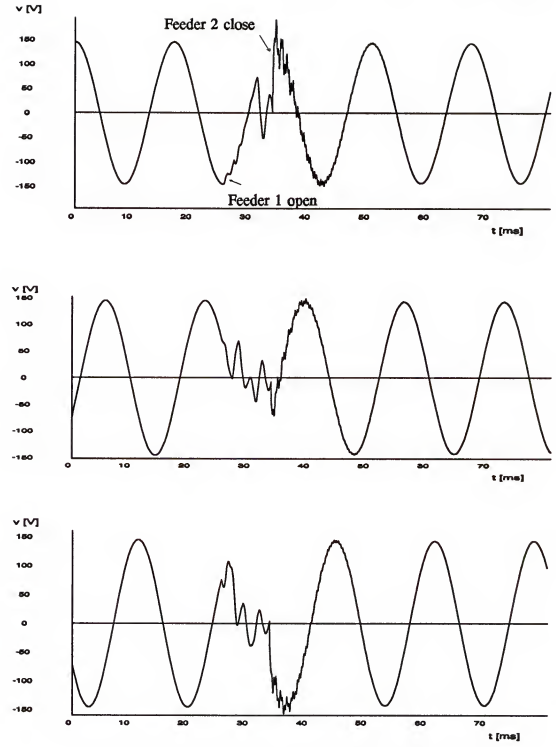

Figure 2.16 Voltage at Custom bus of one cycle switching
(Top to bottom: phase A,B,C)

2.4 Power Quality with Electric Machine Loads

The following example illustrates how the power quality problems affect a typical distribution system load--rotating machinery. A three-phase induction motor is installed at the Custom Power bus. From Figure 2.3, the static load at the Custom bus is replaced by a dynamic machinery load of similar size. Assume that voltage sags as discussed before exist in the Feeder 1 side. We will see the motor phenomena under the voltage sags at its terminal.

Using an EMTP simulation, the system is modelled as before. To model the induction motor, the Universal Machine module in EMTP is used which allows study of the dynamics of rotating machinery. The induction motor data are used in Yin [35,36] and listed in Appendix A. The modeling technique is not covered herein, only the simulation results are shown.

In order to evaluate the overall performance of the induction motor, the simulation covers the induction motor with start-up and voltage sags after motor start-up. Due to the Y-Δ isolation transformer between the substation feeder and the Custom bus (other than the converter transformer), the voltage sag in one phase will cause a voltage increase in the other two phases. Therefore, the Y-Δ isolation transformer is replaced by Y-Y isolation transformer to see the pure sag phenomena.

During voltage sag, the motor current actually increases rather than decreases. This happens to other two phases as well. This is a significant difference between the static load and the dynamic machine load. In the static load such as an equivalent impedance, the voltage sag results in current sag because of the linearity. Nevertheless,

the voltage sag causes current swell in induction motor load. This is due to the reaction of the induction motor mechanical system. According to the machine theory [30], the mechanical output is determined by the mechanical speed and electromagnetic torque, as shown in (2.1).

$$P_{out} \sim T*\omega_m \tag{2.1}$$

where T is the load torque and ω_m is the mechanical angular speed.

The relationship of the mechanical speed and torque is shown in equation (2.2), where J is the moment of inertia, and D is the damping coefficient.

$$J\frac{d\omega_m}{dt} + D\omega_m = \Delta T \tag{2.2}$$

ΔT is the torque difference of electromagnetic torque and load torque.

The mechanical transient phenomena are determined by the time constant in the mechanical system. For the specific machine which has the parameters listed in Appendix A, the mechanical time constant can be derived.

$$\tau = \frac{J}{D} = \frac{0.063}{0.02} = 3.15(Sec.) \tag{2.3}$$

Therefore, changes in the mechanical system are slow, as far as a short-term voltage sag is concerned. Meanwhile, the motor power flow must be maintained during the voltage sag, as in equation (2.4). where P_{loss} is the total loss of the motor. The input power is determined by the voltage and current as in equation (2.5).

$$P_{in} = P_{out} + P_{loss} \tag{2.4}$$

where P_{loss} is the total of the motor. The input power is determined by the voltage and current as in equation (2.5).

$$P_{in} \sim vi \cos\theta \tag{2.5}$$

Therefore, less voltage demands more current to maintain a constant power flow inside the motor during the voltage sag. In fact, the motor operates in the generation mode, in which the mechanical system drives the machine due to the mechanical inertia.

As extreme cases, the motor terminal may be shorted to ground or open. In the former case, the terminal voltage is forced to zero. The maximum current is limited by the leakage impedance of the motor. If the machine terminal is an open-circuit, the current is zero, while the voltage maintains high. In either case, the power flow is balanced by the losses which include winding losses and friction losses.

The above analysis is verified by EMTP simulations. Figure 2.17 shows the voltage sag in phase A at the motor terminal and Figure 2.18 is the motor armature winding current. The transient at the beginning is the motor inrush current during start-up. Figure 2.19 and Figure 2.20 illustrate the mechanical system reacting to the electrical changes. Figure 2.19 is the electromagnetic torque which has a double frequency torque pulsation during voltage sags. The average torque is almost constant during the voltage sag. The speed drops about 2 % under 40 % voltage sag rate. Therefore, the mechanical output power which is proportional to the product of torque and speed can be taken to be constant.

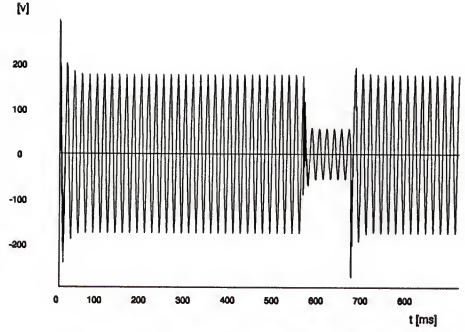

Figure 2.17 Phase A voltage at motor terminal

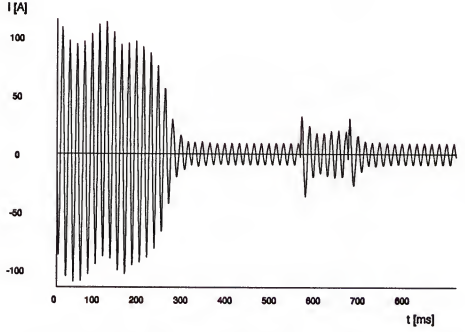

Figure 2.18 Phase A armature winding current of the motor

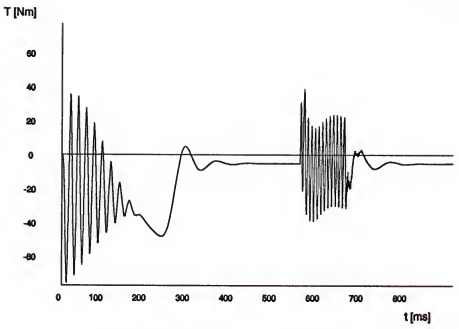

Figure 2.19 Electromagnetic torque

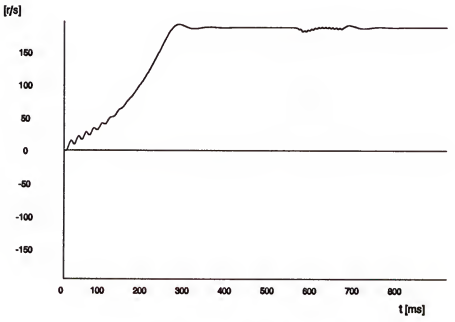

Figure 2.20 Rotor angular speed

This example shows that the voltage sags affect the machine operation by increasing the transient inrush currents, causing very severe torque pulsating in the mechanical system and reducing the motor speed. Also, it affects the feeder side by drawing more current to balance the power flow in the machinery. Furthermore, unbalanced sequence currents result from unbalanced voltage sags, caused by a single line-to-ground fault.

From this example, it is seen that the impact of power quality problems is significant, and the analysis is very complicated, considering all the components. A similar study was performed by Martinez [37]. The analysis helps to explain the phenomena in this field. Furthermore, by inserting the Y-Δ isolation transformer between the high voltage side and low voltage side, a configuration which is the case in many utility applications, the results may be completely different. The reliance on a nonlinear computer simulation such as EMTP is necessary to fully understand the various phenomena.

In summary, this chapter discusses power quality issues in electric distribution systems. The waveforms characterizing major power quality phenomena such as harmonics and voltage sags are duplicated using an EMTP simulation based on a typical distribution system model. The duplication of the waveforms help utility engineers to better understand distribution power quality phenomena. Some of the power quality problems can be mitigated by existing means based on understanding the phenomena. However, some of the problems are beyond control without installing new equipment such as the power electronics converters. The waveforms simulated in this chapter may

be used in the following chapters to verify the concept of using power electronics converters to improve power quality.

The next two chapters will concentrate on the analysis of power electronics converter applications in power quality improvement and control system designing for power electronics converters. The combination of the converters and control systems yields multi-functional power electronics converters which have the capability of suppressing many of the power quality problems.

CHAPTER 3

POWER ELECTRONICS CONVERTERS: PWM DC-AC INVERTERS

Chapter 2 deals with power quality issues and describes many of the distribution power quality phenomena. This chapter addresses power electronics converter applications in power quality improvement. The particular power electronics converters used here are DC-AC inverters which invert a Direct Current (DC) source to Alternating Current (AC). In order to verify the concept, the miniature distribution system model as described in the last chapter is simplified and power quality phenomena are based on the simplified system. The objective is to maintain high quality power at the Custom bus V_{cus} as in Figure 2.2. By installing DC-AC inverters at the Custom bus, the distorted waveforms resulting from the feeder side can be blocked from the Custom load. The Custom bus will maintain high quality power no matter what power quality phenomena exist in the feeder side. As described, the feeder side may bring distorted waveforms into the Custom load, such as harmonics, voltage sags, voltage swells, high frequency impulses, and transients. All these power quality problems can be suppressed by power electronic converters installed between the feeder bus and the Custom load bus. Also, a power electronics converter with a different topology is capable of blocking the harmonics resulting from the Custom load itself to the feeder side, thus the voltage at the

Custom bus is maintained sinusoidal. As a result, the Custom bus maintains a high quality power with a clean sinusoidal waveform.

This chapter is intended to illustrate power electronics converter applications. The theoretical background of the converters is discussed in detail with the simplified distribution system model. In Chapter 5, the detailed distribution system will be used with detailed converter models and detailed control system.

3.1 PWM DC-AC Inverter Fundamentals

The DC-AC inverters invert a DC source to an AC source by a switching operation of power electronics devices. There are various topologies available in DC-AC inverters for different applications. Figure 3.1 and Figure 3.2 show two topologies of single-phase DC-AC inverters. Depending on the DC source to the inverter input, a DC-AC inverter is classified as either a Voltage Source Inverter (VSI) or a Current Source Inverter (CSI). The VSI has a constant voltage source directly connected to the inverter input, as in Figure 3.1. In Figure 3.2, the DC source V_g and large inductor L_s are equivalent to a current source to the inverter input. By controlling the power electronics devices, which are IGBTs with anti-parallel diodes as in Figure 3.1 or series diodes as in Figure 3.2, the output voltage or current of the inverter will be a series of pulses. The pulses with high voltage or current then pass an L-C filter which partially filters out harmonics. The load is equivalent to a resistance R. These are two fundamental topologies of the DC-AC inverter used in power electronics applications. In the analysis of this dissertation, the VSI inverter as in Figure 3.1 is used in most cases.

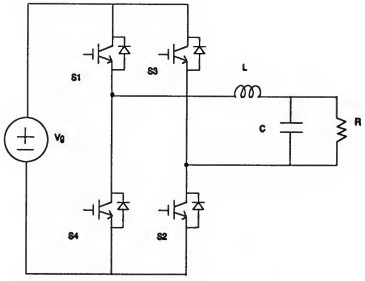

Figure 3.1 DC-AC VSI inverter

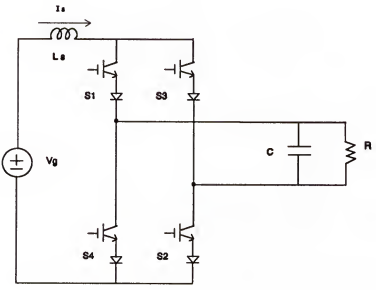

Figure 3.2 DC-AC CSI inverter

There are various switching patterns to control the switching devices S1 ~ S4. A simple example is that each half leg conducts a half cycle on the basis of 60 Hz. The output of the inverter will be a square wave with peak-to-peak value being V_g in VSI or I_s in CSI respectively. Nevertheless, the square waveform contains very rich harmonics, especially low order harmonics which obviously do not meet the requirement here. On the other hand, the square wave output does not provide the flexibility of changing the fundamental component in the output. The fundamental component in the output is determined by the DC voltage or current which is not flexible to change [38,39].

Another very popular control technique of switching devices is Pulse-Width-Modulation (PWM) in which the pulses have variable width and high frequency. The on and off states of the devices correspond to the pulses with a pattern of "1" or "0". The PWM pulses are generated by comparing two signals, with one being the high frequency carrier signal and the other being the low frequency control signal. The carrier signal is periodic and normally is a high frequency ramp or triangle function. The control signal determines the pattern of the output of the converter if the peak value of the control signal is smaller than that of the carrier. Figure 3.3 and Figure 3.4 show the relationship of the these signals. When the control signal is greater than the carrier signal at a particular instance, the pattern is "1"; otherwise it is "0". All of the signals are low power and low voltage which are normally used as gate drives with buffers for power electronics devices.

The advantage of PWM DC-AC inverters is significant. The PWM, based on the variable width of pulses and fast switching, has little harmonic distortion in the output

waveforms. Fast switching eliminates low order harmonics. Also, the fundamental output is controllable by the gate signal pattern without changing the DC source. Therefore, the PWM technique has two advantages: 1) It decreases harmonic distortions, and 2) It offers flexibility of control according to the requirement in the power line. Due to these advantages, the PWM technique is used for power quality improvement, because this application requires low harmonic distortion in the output, and control of the fundamental voltage in the power system.

The input to output relationship of the DC-AC inverter has a different form, as we will see in the following chapters when dealing with the dynamics of the converters. Nevertheless, a simple relationship between input and output can be used to explain the inverter. Taking the VSI as an example, assuming the control signal is a pure sinusoidal function as in Figure 3.3, the output voltage of the VSI is determined by the DC voltage source and a ratio of control signals, as in equation (3.1):

$$V_o = m_a * \frac{V_g}{2} \tag{3.1}$$

where V_o is the peak value of output voltage and V_g is the DC voltage. The m_a is the modulation index which is determined by the ratio of the peak of carrier and control signals, as in equation (3.2).

$$m_a = \frac{V_{peak\ of\ carrier}}{V_{peak\ of\ control}} \tag{3.2}$$

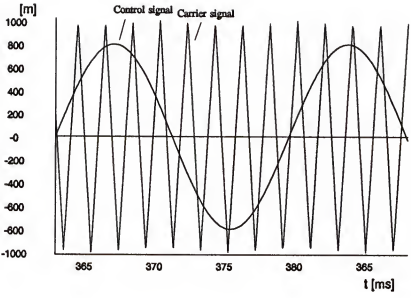

Figure 3.3 Carrier waveform and control waveform

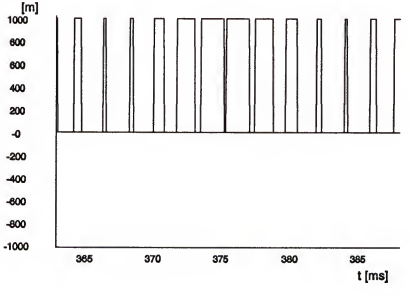

Figure 3.4 Pulse-Width-Modulation waveform

From equation (3.1), the maximum peak value of the output voltage is 0.5 V_s. The modulation index is normally kept under 1 to avoid waveform distortions. The relationship between input voltage and output fundamental voltage is important because the DC voltage can be determined by the required maximum output.

Another factor is the frequency ratio, defined as the ratio of carrier signal to control signal, assuming the frequency of control signal is kept constant. It is required that this ratio be high enough to achieve low harmonic distortions. The switching frequency is restricted by the power electronics device turn-on and turn-off time. Consequently, high switching frequency increases switching losses which ultimately reduces the efficiency of the converter. These facts are important in PWM DC-AC inverters.

A detailed analysis of CSI PWM DC-AC inverters is provided by Ngo [29]. In the following, a detailed analysis of the VSI PWM DC-AC inverters is performed, for the applications in power quality improvement. The analysis is based on the different distribution loads at the Custom bus. Several models are discussed for analysis and linear control system design, as described in the next chapter.

3.2 Single-Phase PWM DC-AC Inverter Modeling

This section will study the single-phase PWM DC-AC inverter modeling from a control viewpoint. The next section will develop the dynamic three-phase PWM DC-AC inverter modeling. The models as developed are based on the low frequency describing functions, for which the details are discussed by Ngo [29].

A widely used nonlinear low frequency model is based on the State-Space - Averaging (SSA), in which the state space equations are derived from different operation modes [40,41]. In the following analysis, it is assumed that the switching frequency of the PWM is arbitrarily high. Thus, the equations as described herein only contain the low frequency features compared to the high frequency switching [29].

Figure 3.5 shows a single-phase DC-AC bridge inverter system with a simplified distribution line. The inverter supply voltage V_g is assumed to be a constant voltage source. The distribution line has two nodes with one being the feeder bus V_{bus}, and the other the Custom bus V_{cus}. The Custom load is assumed to have a static load with equivalent resistor and inductor to ground. An isolation single-phase transformer is used to connect the inverter to the distribution line.

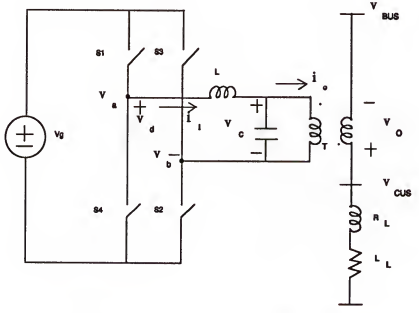

Figure 3.5 Series converter with simplified system model

In the inverter circuit, each phase leg has a switch pair, e.g. S1/S4 and S2/S3. The voltages at V_a and V_b are related to the DC bus voltage by the duty ratios. Assuming the duty ratio for each phase leg of the inverter is $d_a(t)$ and $d_b(t)$ respectively, the voltages at V_a and V_b will be $d_a(t)*V_g$ and $d_b(t)*V_g$, referring to the negative point of the DC bus. Notice that the duty ratios only reflect the low frequency features.

By defining the effective duty ratio d(t) as in (3.3),

$$d(t) = d_a(t) - d_b(t) \tag{3.3}$$

one can relate the voltage difference v_{ab} to the effective duty ratio by

$$v_{ab} = d(t)\, V_g \tag{3.4}$$

Thus, the state space equations in the filter circuit of the inverter can be derived based on the SSA technique [40,41].

$$L\frac{di_1}{dt} = -v_c + d(t)\, V_g \tag{3.5}$$

$$C\frac{dv_c}{dt} = i_1 - i_o \tag{3.6}$$

The current of the transformer i_o is related to the Custom bus voltage through an impedance with an equivalent resistance R_L and inductance L_L.

$$L_L\frac{di_o}{dt} = v_{cus} - R_L i_o \tag{3.7}$$

The Custom bus voltage v_{cus} is related to the inverter output voltage v_o as in (3.8). It is also noticed that the capacitor voltage v_c is actually the inverter output voltage v_o.

$$V_o = V_{cus} - V_{bus} \tag{3.8}$$

$$V_o = V_c \tag{3.9}$$

Thus, the unknown variables in the above state space equations are only the state variables, the inputs and output voltage. Notice that there are two inputs in the state space equations. One is the effective duty ratio d(t), the other is the feeder voltage v_{bus}.

Solving the equations (3.5) ~ (3.9) by first taking the Laplace transform, one can obtain the dynamic equations in the frequency domain.

$$V_o(S) = \frac{(R_L + SL_L)\, V_g}{Y(S)} D(S) - \frac{SL}{Y(S)} V_{bus}(S) \tag{3.10}$$

where Y(S) is given by (3.11), which indicates a third order system.

$$Y(S) = R_L + (L_L + L)\, S + LR_L CS^2 + L_L LCS^3 \tag{3.11}$$

In order to obtain the control-to-output transfer function, the feeder voltage V_{bus} is assumed to be zero, which yields

$$H(S) = \frac{V_o(S)}{D(S)} = \frac{(R_L + SL_L)\, V_g}{Y(S)} \tag{3.12}$$

The effect of the distribution system voltage V_{bus} on the Custom bus voltage V_{cus}, will be discussed in detail in the next chapter. The equation (3.12) is the dynamic model of the single-phase PWM DC-AC inverter, based on the State-Space-Averaging technique. In order to verify the validity of the developed model, a comparison of the results from both the dynamic model based on the State-Space-Averaging technique and the real inverter circuit is made.

By substituting the inverter and Custom load parameters from the miniature distribution system model, the transfer function can be obtained for a particular case. As introduced in Chapter 2, the power system is 208 V line-to-line thus a 120 V phase voltage. The maximum Custom load is 3 kVA which has an equivalent impedance based on 208 V:

R_L = 12.2 Ω, L_L=20 mH,

The DC voltage supply is V_g=180 V. The inverter filter parameters are as follows:

L = 0.256 mH, C = 95 uF,

with a corner frequency of 1.02 kHz.

Figure 3.6 shows three curves overlapping together with the desired waveform, the output voltage waveform with the real converter and that using the transfer function. They are so close that little difference is observed. Therefore, it appears that the transfer function may be used for analysis and control system design.

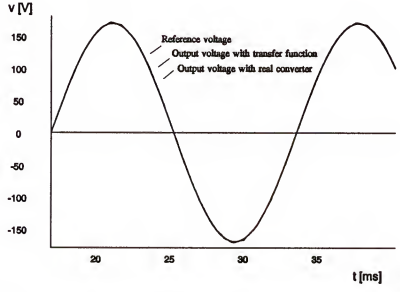

Figure 3.6 A comparison of output voltage with converter and transfer function

3.3 Three-Phase PWM DC-AC Inverter with Uecoupled Network Loads

The previous section derives the dynamic model of the single-phase PWM DC-AC inverter, in which the power system is equivalent to a single-phase, simplified system. The DC-AC inverter is a single-phase full-bridge circuit. However, the distribution power systems are three-phase, as shown in Figure 2.2 and Figure 2.3. Therefore, the three-phase DC-AC inverter must be applied in general. In this section, a dynamic model of the three-phase DC-AC inverter is developed.

A widely used three-phase DC-AC inverter based on the voltage source supply is shown in Figure 3. 7. The three-phase feeder voltages are $V_{bus\text{-}a}$, $V_{bus\text{-}b}$, and $V_{bus\text{-}c}$. The Custom voltages are $V_{cus\text{-}a}$, $V_{cus\text{-}b}$, and $V_{cus\text{-}c}$. The inverter has three phase legs with six switches. Each phase leg has two complementary switches. As in the case of many three-phase systems, the three phases of this inverter are coupled. Nevertheless, the control signals, which are the duty ratios of each phase leg, are independent. This is due to the fact that the applications as discussed in this dissertation may include an unbalanced situation. One typical example is the line-to-ground fault, which causes unbalanced voltage sags at the Custom bus. Therefore, the control function for each phase must be developed.

In the case of unbalanced and coupled three-phase systems, the three phases may be decoupled by using a transformation of variables from the abc domain to another reference frame. There are several transformations, depending on the different applications. As introduced in Chapter 1, the transformation from an abc system to a 0fb system can be applied to three-phase inverter applications. The detailed theoretical

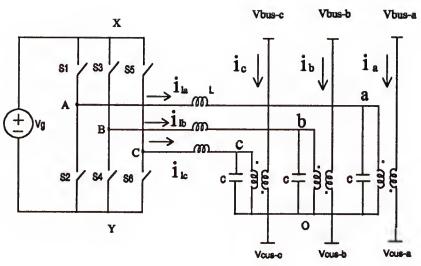

Figure 3.7 Three-phase DC-AC inverter

background is provided by White [30]. Appendix B-1 lists the transformation matrices and their related operations. As will be shown later, the coupled three-phase inverter system can be transformed to a decoupled two-phase system. It will be further shown that the original three-phase inverter system is equivalent to three single-phase system, from the control point of view.

In deriving the dynamic equations for the three-phase PWM DC-AC inverter with static load, certain assumptions are applied as follows.

(1) The reference frame, in which the transformation matrices are applied, has a fixed frequency. The frequency is assumed to be the base frequency of the distribution system, i.e. 60 Hz.

(2) The inverter has a fixed DC voltage supply. This assumption is made

to exclude the DC voltage as a control variable. Nevertheless, the DC bus voltage may have harmonic ripple.

(3) The duty ratios of the switches in the three-phase inverter are the only control signals for the inverter.

(4) The load of the inverter is a decoupled static load.

Under these assumptions, the dynamic equations of the three-phase system, as shown in Figure (3.7), can be derived according to the Kirchhoff's Voltage Laws (KVL).

$$V_{AY} = V_{Aa} + V_{ao} + V_{oY} \tag{3.13}$$

$$V_{BY} = V_{Bb} + V_{bo} + V_{oY} \tag{3.14}$$

$$V_{CY} = V_{Cc} + V_{co} + V_{oY} \tag{3.15}$$

As in a single-phase DC-AC inverter, the duty ratio at each phase leg is taken as a pair. Assuming the duty ratio switch pairs for the three-phase inverter are d_{a1}/d_{a2}, d_{b1}/d_{b2},and d_{c1}/d_{c2}, one can obtain the voltages at each half leg, as described in the previous sections. Meanwhile, the voltage drop at each filter inductor can be expressed in terms of its current. Thus, the equations (3.13)~(3.15) can be rewritten as in (3.16)~(3.18), respectively.

$$d_{a2}V_g = L\frac{di_{1a}}{dt} + V_{ao} + V_{oY} \tag{3.16}$$

$$d_{b2}V_g = L\frac{di_{1b}}{dt} + V_{bo} + V_{oY} \tag{3.17}$$

$$d_{c2}V_g = L\frac{di_{1c}}{dt} + V_{co} + V_{oY} \tag{3.18}$$

Because of the ungrounded neutral point of the inverter, the sum of the three-phase inductor currents is zero, so is the sum of their derivatives.

$$\frac{di_{1a}}{dt} + \frac{di_{1b}}{dt} + \frac{di_{1c}}{dt} = 0 \tag{3.19}$$

Adding equations (3.16) ~ (3.17) and applying (3.19), one can obtain the unknown variable V_{oY}. Then, the state space equations can be rewritten, in a matrix form as (3.20). For convenience, the duty ratios d_{a2}, d_{b2}, and d_{c2} are replaced by d_a, d_b, and d_c respectively.

$$\begin{bmatrix} L & 0 & 0 \\ 0 & L & 0 \\ 0 & 0 & L \end{bmatrix} \begin{bmatrix} \frac{di_{1a}}{dt} \\ \frac{di_{1b}}{dt} \\ \frac{di_{1c}}{dt} \end{bmatrix} = - \begin{bmatrix} \frac{2}{3} & -\frac{1}{3} & -\frac{1}{3} \\ -\frac{1}{3} & \frac{2}{3} & -\frac{1}{3} \\ -\frac{1}{3} & -\frac{1}{3} & \frac{2}{3} \end{bmatrix} \begin{bmatrix} v_{ao} \\ v_{bo} \\ v_{co} \end{bmatrix} + \begin{bmatrix} \frac{2}{3} & -\frac{1}{3} & -\frac{1}{3} \\ -\frac{1}{3} & \frac{2}{3} & -\frac{1}{3} \\ -\frac{1}{3} & -\frac{1}{3} & \frac{2}{3} \end{bmatrix} \begin{bmatrix} d_a \\ d_b \\ d_c \end{bmatrix} V_g \tag{3.20}$$

Meanwhile, the currents at nodes a,b,c must obey the constraint, according to the Kirchhoff's Current Laws (KCL). A matrix form is provided in (3.21), in which the currents i_a, i_b and i_c represent the load currents. Assuming the inverter supplies a full voltage to the Custom load, i.e. the feeder voltage is zero, and the Custom load is a

$$\begin{bmatrix} C & 0 & 0 \\ 0 & C & 0 \\ 0 & 0 & C \end{bmatrix} \begin{bmatrix} \frac{dv_{ao}}{dt} \\ \frac{dv_{bo}}{dt} \\ \frac{dv_{co}}{dt} \end{bmatrix} = \begin{bmatrix} i_{1a} \\ i_{1b} \\ i_{1c} \end{bmatrix} - \begin{bmatrix} i_a \\ i_b \\ i_c \end{bmatrix} \tag{3.21}$$

static load with an equivalent resistance R_L and inductance L_L, one can obtain the equations for inverter output voltages and currents.

$$\begin{bmatrix} L_L & 0 & 0 \\ 0 & L_L & 0 \\ 0 & 0 & L_L \end{bmatrix} \begin{bmatrix} \frac{di_a}{dt} \\ \frac{di_b}{dt} \\ \frac{di_c}{dt} \end{bmatrix} = - \begin{bmatrix} R_L & 0 & 0 \\ 0 & R_L & 0 \\ 0 & 0 & R_L \end{bmatrix} \begin{bmatrix} i_a \\ i_b \\ i_c \end{bmatrix} + \begin{bmatrix} v_{ao} \\ v_{bo} \\ v_{co} \end{bmatrix} \tag{3.22}$$

The equations (3.20) ~ (3.22) constitute the basic state space equations in the inverter circuit including the Custom load. The equations are linear in that the coefficients are constant. Nevertheless, three subequations in (3.20) are coupled each other. Therefore, a transformation to another coordinate system is needed.

As used by Ngo [29] and White [30], the transformation from the abc domain to the 0fb domain, is applied to transform the above equations (3.20) ~ (3.22). Appendix B-1 lists the transformation matrix T and its related algebraic operations. For convenience, the equation (3.20) is first substituted by (3.21). Thus, the transformation is only applied to three sets of matrices, as in (3.23) ~ (3.25).

$$\begin{bmatrix} d_a \\ d_b \\ d_c \end{bmatrix} = T \begin{bmatrix} d_o \\ d_f \\ d_b \end{bmatrix} \tag{3.23}$$

$$\begin{bmatrix} v_{ao} \\ v_{bo} \\ v_{co} \end{bmatrix} = T \begin{bmatrix} v_o \\ v_f \\ v_b \end{bmatrix} \tag{3.24}$$

$$\begin{bmatrix} i_a \\ i_b \\ i_c \end{bmatrix} = T \begin{bmatrix} i_o \\ i_f \\ i_b \end{bmatrix} \tag{3.25}$$

It is also noticed that in the 0fb system, the zero components are zero because of the fact that the sum of the three inductor currents is zero. Therefore, each matrix in (3.20) ~ (3.22) is reduced to a second-order matrix with only f and b components. After applying the transformation equations and algebraic matrix operations as listed in Appendix B-1, one can obtain a new set of the differential equations in the 0fb domain, as in (3.26) and (3.27).

$$\begin{bmatrix} LC & 0 \\ 0 & LC \end{bmatrix} \begin{bmatrix} \frac{d^2 v_f}{dt^2} \\ \frac{d^2 v_b}{dt^2} \end{bmatrix} + 2 \begin{bmatrix} -j\omega LC & 0 \\ 0 & j\omega LC \end{bmatrix} \begin{bmatrix} \frac{dv_f}{dt} \\ \frac{dv_b}{dt} \end{bmatrix} + \begin{bmatrix} -\omega^2 LC & 0 \\ 0 & -\omega^2 LC \end{bmatrix} \begin{bmatrix} v_f \\ v_b \end{bmatrix}$$

$$+ \begin{bmatrix} 1 & 0 \\ 0 & 1 \end{bmatrix} \begin{bmatrix} v_f \\ v_b \end{bmatrix} + \begin{bmatrix} L & 0 \\ 0 & L \end{bmatrix} \begin{bmatrix} \frac{di_f}{dt} \\ \frac{di_b}{dt} \end{bmatrix} + \begin{bmatrix} -j\omega LC & 0 \\ 0 & j\omega LC \end{bmatrix} \begin{bmatrix} i_f \\ i_b \end{bmatrix}$$

$$= \begin{bmatrix} 1 & 0 \\ 0 & 1 \end{bmatrix} \begin{bmatrix} d_f \\ d_b \end{bmatrix} V_g \tag{3.26}$$

$$\begin{bmatrix} L_L & 0 \\ 0 & L_L \end{bmatrix} \begin{bmatrix} \frac{di_f}{dt} \\ \frac{di_b}{dt} \end{bmatrix} + \begin{bmatrix} R_L - j\omega L_L C & 0 \\ 0 & R_L + j\omega L_L C \end{bmatrix} \begin{bmatrix} i_f \\ i_b \end{bmatrix} = \begin{bmatrix} 1 & 0 \\ 0 & 1 \end{bmatrix} \begin{bmatrix} V_f \\ V_b \end{bmatrix} \qquad (3.27)$$

It is noticed that the equations in (3.26) and (3.27) are decoupled. By taking the Laplace transform, one can obtain the transfer functions in both f and b axes.

$$H_f(S) = \frac{V_f(S)}{D_f(S)} = \frac{V_g}{LCS^2 - 2j\omega LCS - \omega^2 LC + 1 + \frac{LS - j\omega L}{L_L S + R_L - j\omega L_L}} \qquad (3.28)$$

$$H_b(S) = \frac{V_b(S)}{D_b(S)} = \frac{V_g}{LCS^2 + 2j\omega LCS - \omega^2 LC + 1 + \frac{LS + j\omega L}{L_L S + R_L + j\omega L_L}} \qquad (3.29)$$

The transfer functions (3.28) and (3.29) are not in the standard form, because it is found that this form is more convenient to use than the standard form.

By using the inverse transformation from the 0fb to the abc system, three control signals in the abc domain can be obtained, according to the inverse transformation, as listed in Appendix B-1.

$$d_a = e^{-j\theta} d_f + e^{j\theta} d_b \qquad (3.30)$$

$$d_b = e^{-j(\theta - 120^\circ)} d_f + e^{j(\theta - 120^\circ)} d_b \qquad (3.31)$$

$$d_c = e^{-j(\theta + 120^\circ)} d_f + e^{j(\theta + 120^\circ)} d_b \qquad (3.32)$$

The Laplace transform of (3.30) ~ (3.32) yields

$$D_a(S) = D_f(S+j\omega) + D_b(S-j\omega) \tag{3.33}$$

$$D_b(S) = e^{j120°}D_f(S+j\omega) + e^{-j120°}D_b(S-j\omega) \tag{3.34}$$

$$D_c(S) = e^{-j120°}D_f(S+j\omega) + e^{j120°}D_b(S-j\omega) \tag{3.35}$$

On the other hand, one can obtain the output voltages in abc domain by using the same inverse transformation.

$$V_{ao} = e^{-j\theta}v_f + e^{j\theta}v_b \tag{3.36}$$

$$V_{bo} = e^{-j(\theta-120°)}v_f + e^{j(\theta-120°)}v_b \tag{3.37}$$

$$V_{co} = e^{-j(\theta+120°)}v_f + e^{j(\theta+120°)}v_b \tag{3.38}$$

The Laplace transform of (3.36)~(3.38) yields

$$V_{ao}(S) = V_f(S+j\omega) + V_b(S-j\omega) \tag{3.39}$$

$$V_{bo}(S) = e^{j120°}V_f(S+j\omega) + e^{-j120°}V_b(S-j\omega) \tag{3.40}$$

$$V_{co}(S) = e^{-j120°}V_f(S+j\omega) + e^{j120°}V_b(S-j\omega) \tag{3.41}$$

The right side of (3.39)~(3.41) can be substituted by the transfer functions of (3.28) and (3.29). It is noticed that the operators of the transfer functions have to be changed to S+jω and S-jω for $H_f(S)$ and $H_b(S)$, respectively. From (3.28) and (3.29), one obtains

$$V_f(S+j\omega) = \frac{D_f(S+j\omega)\,V_g}{LCS^2+1+\frac{LS}{L_LS+R_L}} \tag{3.42}$$

$$V_b(S-j\omega) = \frac{D_b(S-j\omega)\,V_g}{LCS^2+1+\frac{LS}{L_LS+R_L}} \tag{3.43}$$

Using (3.42) and (3.43) to substitute into (3.39) ~ (3.41), and further substituted by (3.33) ~ (3.35), one can obtain the output voltage for each phase.

$$V_{ao}(S) = \frac{(R_L+SL_L)\,V_g}{R_L+(L_L+L)\,S+LR_LCS^2+L_LLCS^3}D_a(S) \tag{3.44}$$

$$V_{bo}(S) = \frac{(R_L+SL_L)\,V_g}{R_L+(L_L+L)\,S+LR_LCS^2+L_LLCS^3}D_b(S) \tag{3.45}$$

$$V_{co}(S) = \frac{(R_L+SL_L)\,V_g}{R_L+(L_L+L)\,S+LR_LCS^2+L_LLCS^3}D_c(S) \tag{3.46}$$

The results in (3.44) ~ (3.46) show that the three-phase output voltages are determined by their own control signals, i.e. the duty ratios. There is no coupling between phases. The transfer functions of the three phases are independent and have the same form as in (3.47).

$$H(S) = \frac{V(S)}{D(S)} = \frac{(R_L+SL_L)\,V_g}{R_L+(L_L+L)\,S+LR_LCS^2+L_LLCS^3} \tag{3.47}$$

From the analysis in the previous section, where a single-phase inverter system is used, the transfer function of the three-phase system (3.47) is the same as that of the single-phase inverter (3.12).

Therefore, from an analysis point of view, the three-phase inverter can be equivalent to three single-phase inverters. Also, the compensator design in the control system can be based on each phase rather than a three-phase 0fb model. This simplifies the analysis and control system design to a great extent. This conclusion is based on the special assumptions made in this section. An additional constraint is that the neutral point of the inverter filter is floating, thus, the sum of three-phase currents is zero. The conclusion derived in this section is also verified in Chapter 5 by comparing the detailed simulation results of the three-phase inverter and three single-phase inverters.

3.4 Three-Phase PWM DC-AC Inverter with Dynamic Machine Loads

In the previous section, a static load without coupling between the phases was assumed at the Custom bus. It was shown in a detailed derivation, that an equivalent single-phase DC-AC bridge inverter can be used for analysis. In this section, a typical three-phase dynamic load in distribution systems (rotating electrical machinery) is considered. Accordingly, the control system design will be based on this different application, as discussed in the next chapter.

It is assumed that the Custom bus serves a typical three-phase squirrel cage induction motor load. The dynamic equations including the three-phase inverter and motor will have a higher order than the static load. As discussed before, the transformation from one coordinate system to another is applied. The main difficulty is that the inverter and motor load have to be transformed to the same reference frame. In the previous section, a system based on the backward and forward elements was

discussed. In transforming rotating machinery, the equations based on the 0fb system are still coupled during the transient [30]. Therefore, the overall system equations will be coupled, due to the coupling in the motor load.

Krause [26] adopts an abc-qd0 rotating reference frame transformation, based on real numbers for the transformation matrices. Murai et al [27] et al use abc-qd0 transformation for inverter and motor drive applications. In rotating machinery, the abc model equations contain time-varying coefficients, with both the magnitude and phase angle changing. By using an appropriate transformation from the abc domain to the qd0 domain, the coefficients become time-invariant. Nevertheless, the equations on the q and d axes are still coupled, but the coupling is weakened. Since our system equations are coupled anyway, the abc-qd0 transformation will be used to transform the equations. Also, a reference frame based on the motor synchronous speed is assumed for all of the transformations. Thus, the reference frame has an angular speed with the base frequency of the power system.

As discussed in Chapter 2, the electrical transient is much faster than the mechanical transient in the motor load. Therefore, only the electrical transient is important in Custom Power applications. A constant mechanical speed is assumed in all of the applications. Under this assumption, the dynamic equations of the induction motor become linear with a fixed speed, but with electrical transients taken into account. The Laplace transformed induction motor equations based on the assumed qd0 system can be derived from Krause [26], as listed below.

$$V_{qs}(S) = (r_s + SL_s) I_{qs}(S) + X_{ss} I_{ds}(S) + SL_m I_{qr}(S) + X_m I_{dr}(S) \quad (3.48)$$

$$V_{ds}(S) = -X_{ss}I_{qs}(S) + (r_s+SL_s)\,I_{ds}(S) - X_m I_{qr}(S) + SL_m I_{dr}(S) \quad (3.49)$$

$$V_{qr}(S) = SL_m I_{qs}(S) + nX_m I_{ds} + (r_r+SL_r)\,I_{qs}(S) + nX_r I_{dr}(S) \quad (3.50)$$

$$V_{dr}(S) = -nX_m I_{qs}(S) + SL_m I_{ds}(S) - nX_r I_{qr}(S) + (r_r+SL_r)\,I_{ds}(S) \quad (3.51)$$

or in matrix form

$$\begin{bmatrix} V_{qds}(S) \\ V_{qdr}(S) \end{bmatrix} = \begin{bmatrix} A & B \\ C & D \end{bmatrix} \begin{bmatrix} I_{qds}(S) \\ I_{qdr}(S) \end{bmatrix} \quad (3.52)$$

where n is the motor slip and given by (3.53),

$$n = \frac{\omega_s - \omega_r}{\omega_s} \quad (3.53)$$

and A,B,C,D are given as follows.

$$A = \begin{bmatrix} r_s+SL_s & X_{ss} \\ -X_{ss} & r_s+SL_s \end{bmatrix} \quad (3.54)$$

$$B = \begin{bmatrix} SL_m & X_m \\ -X_m & SL_m \end{bmatrix} \quad (3.55)$$

$$C = \begin{bmatrix} r_r+SL_r & X_{rr} \\ -X_{rr} & r_r+SL_r \end{bmatrix} \quad (3.56)$$

$$D = \begin{bmatrix} SL_m & nX_m \\ -nX_m & SL_m \end{bmatrix} \quad (3.57)$$

The machine parameters used in this study are listed in Appendix A.

Assuming a squirrel cage motor is used, where $V_{dr}(S)=V_{qr}(S)=0$, one can obtain the transfer functions between the machine terminal stator voltages and currents in matrix form.

$$V_{qd}(S) = (A - BC^{-1}D)\, I_{qd}(S) \tag{3.58}$$

From the equations (3.48) ~ (3.58), the q-axis and d-axis of the motor equations are coupled. The coupling is not obvious from the machine parameters and also is a function of the motor speed. Therefore, computer simulations are recommended to investigate the diagonal and off-diagonal transfer functions, which is discussed in next chapter.

Also, the three-phase inverter can be transformed to the qd0 domain using the same transformation. One can start from the equations (3.20) and (3.21) as used in the last section and apply the abc-qd0 transformation as listed in Appendix B-2. Also, the feeder voltage is assumed to be zero, thus the inverter supplies a full voltage to the Custom load. Corresponding to the results based on the transformation between the abc domain and 0fb domain, as performed in the last section, the dynamic equations of the inverter in qd0 domain can be obtained.

$$V_{qd}(S) = E^{-1}FI_{qd}(S) + E^{-1}D_{qd}(S) \tag{3.59}$$

where the matrices E and F are given by (3.60) and (3.61).

$$E = \begin{bmatrix} S^2LC-\omega^2LC+1 & 2S\omega LC \\ -2S\omega LC & S^2LC-\omega^2LC+1 \end{bmatrix} \tag{3.60}$$

$$F = \begin{bmatrix} SL & \omega L \\ -\omega L & SL \end{bmatrix} \tag{3.61}$$

Combining the equations (3.58) and (3.59), one can obtain the transfer function including the inverter and motor load as follows.

$$\frac{V_{qd}(S)}{D_{qd}(S)} = E^{-1}(I-E^{-1}F(A-BC^{-1}D))^{-1} \tag{3.62}$$

Under the assumption of high frequency switching, the transfer function is linear, if the motor speed is assumed fixed. Nevertheless, the two axes are coupled together. The mutual coupling is highly dependent on the machine parameters in both motor load and inverter filter circuit. With a fixed inverter filter, the transfer function varies with different machine parameters. In the next chapter, the transfer functions will be plotted for typical motor parameters and speed conditions, in dealing with the compensator design.

In this chapter, the dynamic equations of the inverter are derived for different applications. The next chapter will use these equations for specific control system analysis. The theory and design techniques will be verified by computer simulations.

CHAPTER 4

CONTROL SYSTEM ANALYSIS

4.1 General Description

This chapter discusses the control techniques used for the DC-AC inverter in power quality improvement. The criterion of designing is that the control system should be flexible to follow changes in the power system. The changes are unknown in a sense that the feeder suffers random abnormal power quality phenomena. The control system is designed in such a way that it blocks all the power quality problems from the important load which is the Custom Power bus.

In addition, the Custom load has uncertainties as well. The load types may be changing in different time intervals. This chapter investigates a variety of loads as used in distribution systems. Also, the different operating conditions of these loads are examined.

In the application of harmonic cancellation as described in the literature, the DC-AC inverter is controlled in such a way that the harmonics are blocked at the feeder side without passing into the Custom bus side. The control technique used in blocking harmonics is based on the harmonic compensations, as used by Peng et al [10,11]. The output of the DC-AC inverter compensates the system by subtracting the harmonics from the line. Figure 4.1 and Figure 4.2 shows a simplified model and control system for the

inverter. Figure 4.1 shows the simplified power system and the converter model relationship with the feeder bus (noted as V_{bus}) and the Custom bus (noted as V_{cus}). In Figure 4.2, the PWM control technique is used in which the control signal is derived by filtering the feeder bus. In filter design, Nabae et al [20] propose a high-pass filter based on the dq model to subtract the harmonics. Chicharo et al [12] apply an adaptive signal processing technique to retrieve and estimate the harmonic contents. In both these applications, the control signal is derived from the feeder side. There is no control to the load side, i.e. the Custom bus, because both actually adopt the open-loop control structure.

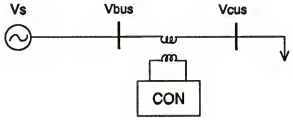

Figure 4.1 Simplified power system and converter model

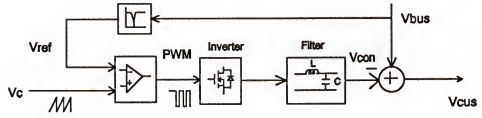

Figure 4.2 Feedforward open-loop PWM control

In both applications, it is clear that the inverter output is "known" so that the exact harmonics can be produced by inverters and fed into the system. The Custom bus remains fundamental because the feeder has fundamental voltage and fundamental current. If the feeder does not contain the fundamental voltage or if the feeder voltage has sags, as in the cases of voltage outages or voltage sags corresponding to the power quality phenomena, this technique is not valid. Therefore, a more flexible control technique needs to be developed to deal with all power quality phenomena.

The closed-loop control based on "Bang-Bang" control, as shown in Figure 4.3, partially fulfills the requirement in power quality improvement. Using an automatic tracking system, one can include the uncertainty of the feeder voltage inside the closed-loop. In Figure 4.3, the measurement factor, i.e. the feedback gain is assumed to be unity. Therefore, the closed-loop system is actually tracking the reference, which is a sinusoidal waveform with specified amplitude and frequency. The compensator is designed to achieve high performance of the closed-loop system. The "Bang-Bang" switch provides output pulses according to the error. The "Bang-Bang" switching is adaptive in the sense that the pulse widths are adjustable, depending on the error band.

The closed-loop tracking system based on the "Bang-Bang" control has the advantage of following the reference, even if the feeder loses power. Nevertheless, the output may contain harmonics which are unpredictable. The frequencies of the harmonics may be low, if a wide band exists. The unpredictable low frequency harmonics increase the difficulties in filter design. Also, the fixed compensator in the closed-loop system can not follow the changes in the Custom load.

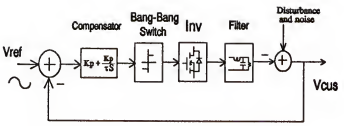

Figure 4.3 Closed-loop "Bang-Bang" control

In the following sections, detailed analysis will be provided in the inverter and system modelling, with different load types. A suitable control system will be proposed for each type of loads. The effect of model changes will be investigated as well. Because of the uncertainties of the load types and load operation conditions, a closed-loop adaptive control technique is also developed.

4.2 Load Dynamics

Two major load types are concerned herein, as discussed in Chapter 3. One is the uncoupled static load, and the other is the coupled dynamic machine load. The static load may have a different configuration. Chapter 3 assumes an equivalent impedance installed at the Custom bus. Based on the equivalent impedance load, some other load topologies may exist. For example, a capacitor may be installed to correct the power factor at the Custom bus. Also, the impedance may change depending on the load capacity.

A typical dynamic load used in the distribution systems is rotating machinery. Rotating machines are very different from static loads in that the mechanical system may be involved. In addition, the three phases in dynamic machine loads are strongly coupled to each other, and the coupling is time-varying during the transients. Chapter 2 reveals a fundamental difference between the static load and dynamic machine load, in reacting to power quality problems. As discussed before, the rotating machine typically boosts its terminal currents during a voltage sag, while a static load results in a current sag responding to the voltage sag.

In the following analysis, the load types will be discussed with the transfer functions based on the derivations in Chapter 3. The transfer functions are described in the Bode plots. The input and output of the transfer functions are all the same, i.e. the input is the duty ratio and the output is the Custom bus voltage, assuming the inverter supplies a full voltage to the Custom bus.

The Bode plot of the transfer function with a basic load type is shown in Figure 4.4, according to (3.12) and the parameters following the equation. The equation (3.12) describes a third-order system, but the high frequency region has only a 40 dB/decade negative slope. This is due to the zero in the transfer function, which produces a 20 dB positive slope in the high frequency region.

If the Custom load is changed from 3 kVA to 0.3 kVA, the transfer function changes slightly. The comparison can be seen in Figure 4.5. However, if the load topology changes, the dynamic behavior can change dramatically, as can be seen in Figures 4.6 ~ 4.9.

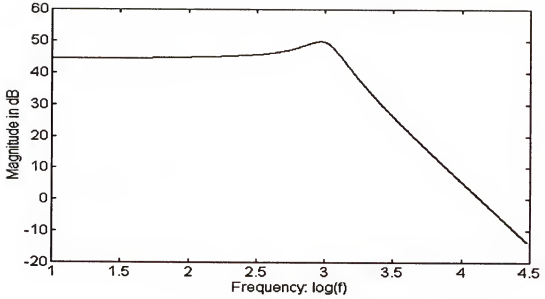

(a)

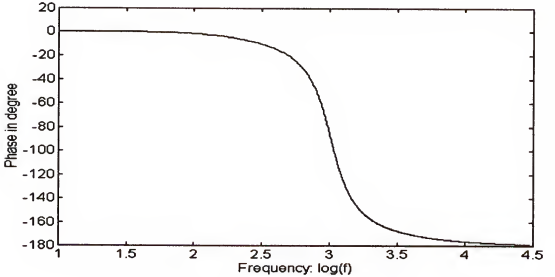

(b)

Figure 4.4 Bode plot of the transfer function with 3 kVA static load at the Custom bus (a) Magnitude, (b) Phase angle

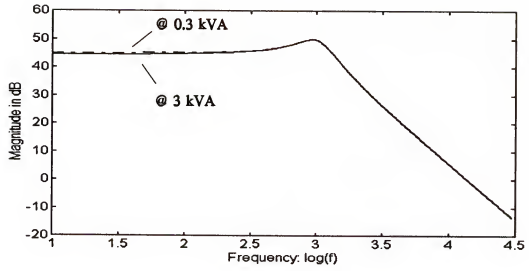

(a)

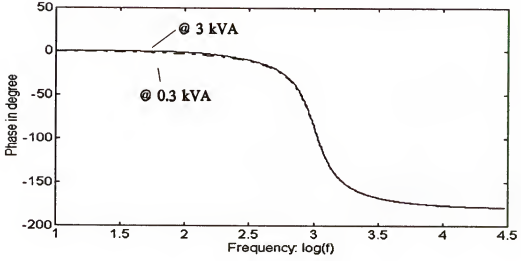

(b)

Figure 4.5 Comparison of the Bode plot of the Custom load with 3 kVA and 0.3 kVA (a) Magnitude, (b) Phase angle

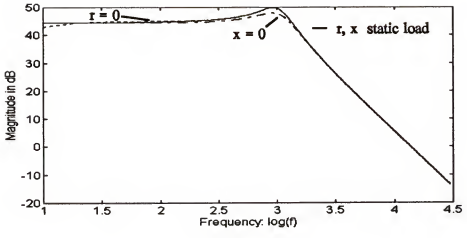

(a)

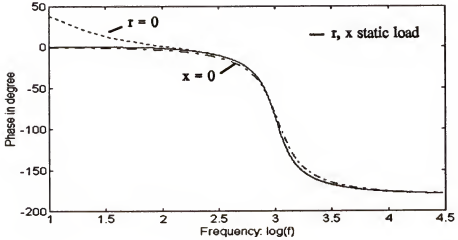

(b)

Figure 4.6 Bode plot of the transfer functions with extreme cases: (1) R=0, (2) X=0
(a) Magnitude, (b) Phase angle

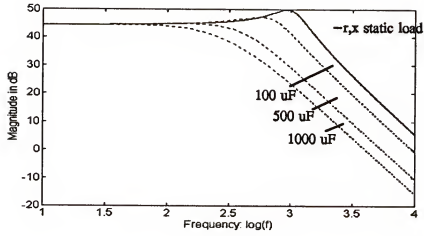

(a)

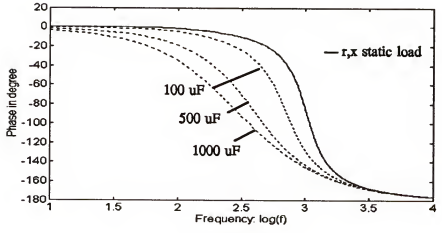

(b)

Figure 4.7 Bode plots in the cases of the static load in parallel with capacitors
(a) Magnitude, (b) Phase angle

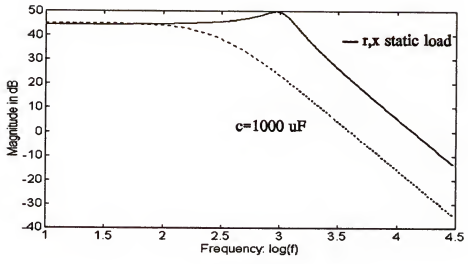

(a)

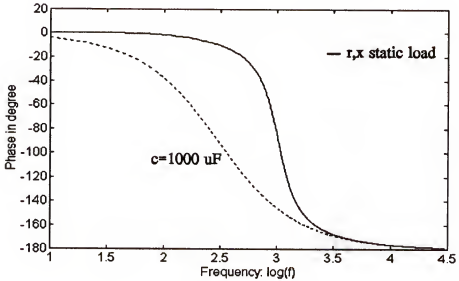

(b)

Figure 4.8 Bode plot with only capacitor load at the Custom bus
(a) Magnitude, (b) Phase angle

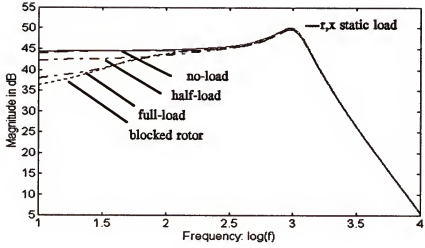

(a)

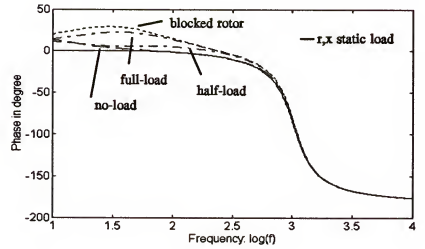

(b)

Figure 4.9 Bode plot in the case of dynamic machine load with different operation conditions (a) Magnitude, (b) Phase angle

Each of the Bode plots shown as follows is compared to the base case, i.e. the equivalent impedance load with 3 kVA 208 V ratings. If the load has only a resistor or reactor, the magnitude changes slightly. Also, the high frequency region is not affected. Nevertheless, the phase shift changes in the low frequency region, as can be seen in Figure 4.6. The deviations are more significant in the case of the capacitive loads. Figure 4.7 shows the Bode plots of the transfer functions when the Custom bus has a variable power factor capacitor. The magnitude of the low frequency region is little affected, but the phase shift becomes larger and larger with increasing the capacitance. The high frequency region becomes narrower with increasing the capacitance. The same phenomenon exists in the case where the Custom bus has only a capacitor load, as shown in Figure 4.8.

Furthermore, the Bode plot in the case of a dynamic machine load is shown in Figure 4.9. This plot is derived from a uncoupled single-phase equivalent induction motor load. In general, the dynamic behavior is different from the static load. As shown in Figure 4.9, both the magnitude and phase angle at the low frequency region are affected. The effect is different for different operating conditions.

The above analysis can be further extended to the control system performance studies. The detailed design approaches are provided in the following sections. From the control point of view, the loop gain is assumed to be high over a wide range. If a closed-loop control system is designed, the gain of the converter should be high, so that the output follows the reference. Meanwhile, the phase shift should be small at the base operating frequency, i.e. 60 Hz. Most of the cases discussed above have a high gain in

the low frequency region except for the dynamic motor loads. Moreover, the capacitor loads decrease bandwidth. These are the main concerns in the control system analysis.

Based on the previous analysis, the control systems are developed depending on the different load types. The load types fall into two categories, with one being the static load, and the other being the dynamic load. Furthermore, an adaptive control technique is proposed to deal with the model changes as revealed in this section. In all of the control systems developed, the closed-loop system is used. This is determined by the fact that the closed-loop system is capable of rejecting disturbances and noises.

4.3 Control System for the Inverter with Uncoupled Network Loads

If the Custom load is a static load without mutual coupling, a single-phase equivalent can be used as a model for control system design. This was discussed in Chapter 3 and adopted in the literature as in [19,20,21,22,23,24,25]. In addition, the dynamic equations as derived in Chapter 3 and Bode plots as shown in the last section can be used for design purposes. Furthermore, the classical closed-loop control system, similar to that shown in Figure 4.3 may be used with appropriate modifications. Figure 4.10 shows the basic control diagram.

In Figure 4.10, the "Bang-Bang" switch is replaced by the PWM comparator. Also, the disturbance and noise are replaced by the feeder voltage V_{bus}. Because the feeder voltage is treated as a disturbance, the closed-loop system should have a high loop gain to reject the effect of the feeder bus. In the last section of this chapter, an investigation into the effect of the feeder bus on the Custom bus voltage is performed.

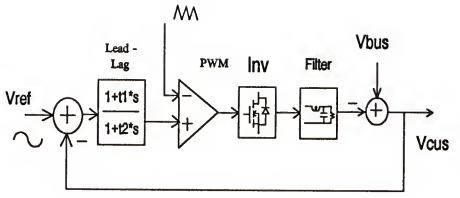

Figure 4.10 Closed-loop system with PWM control

From Figure 4.5 ~ Figure 4.7, the gain in the low frequency region in all cases is high, because of the nature of the DC-AC inverter. Nevertheless, the phase shift is different during steady state. If the loop gain is maintained high, which can be achieved by increasing the gain of the compensator, the phase shift may not be so significant in the overall closed-loop system. Assuming a unity feedback, the compensator can be only a phase compensator with a lead or lag phase shift. Under this circumstance, a phase lead compensator can be designed to increase the phase margin of the loop gain, because the gain margin is high in all cases. The increase of the phase margin can increase the bandwidth. Thus, the dynamic response can be fast.

As an example of the compensator design, the phase margin can be increased to 40° for the inductive static load, as can be seen in Figure 4.11. Unfortunately, the gain is also increased in the high frequency region, which may amplify the high frequency resonance. These are the trade-offs in the compensator design for the closed-loop system. The detailed design techniques are found in [42,43]. The transfer function of the resulting phase lead compensator is described in the equation (4.1).

$$H(S) = \frac{1+7.54*10^{-5}S}{1+1.3*10^{-5}S} \qquad (4.1)$$

4.4 Control System for the Inverter with Dynamic Machine Loads

The analysis of the static loads without mutual coupling was based on a single-phase system. However, this technique is not valid for dynamic machine loads which have strong mutual coupling between phases. In the abc domain, the mutual coupling is time-varying in that the machine parameters are changing with different rotor positions. In rotating electrical machine analysis, the qd0 model is widely used to change the time-varying parameters into time-invariant. Nevertheless, the q and d axes are still coupled after the transformation, as discussed in Chapter 3. The coupling varies with different machines, however, it is usually weak. Taking the specific machine used in this dissertation as an example, one can obtain the dynamic equations for the inverter and motor system. The dynamic equations of the motor load and inverter system based on the qd0 system have been derived as a transfer function. The relationship of output voltages and input duty ratios are rewritten as in (4.2).

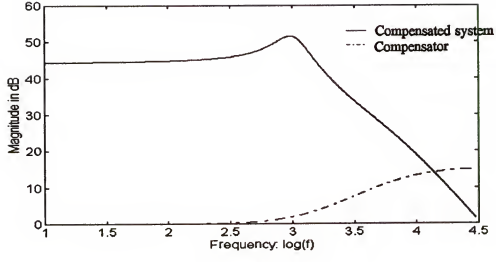

(a)

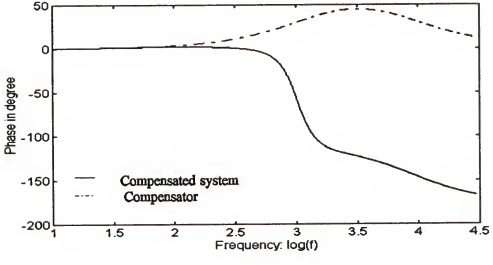

(b)

Figure 4.11 Bode-plot of the loop gain and its compensator
(a) Magnitude, (b) Phase angle

$$V_{qd}(S) = \begin{bmatrix} H_{qq}(S) & H_{qd}(S) \\ H_{dq}(S) & H_{dd}(S) \end{bmatrix} D_{qd}(S) \qquad (4.2)$$

where $H_{qq}(S)$ and $H_{dd}(S)$, $H_{dq}(S)$ and $H_{qd}(S)$ are the diagonal and off-diagonal elements, which are determined by (3.62).

The diagonal elements $H_{qq}(S)$, and $H_{dd}(S)$ are equal if the three phases of the machine are symmetrical. The off-diagonal elements $H_{qd}(S)$, and $H_{dq}(S)$ determine the mutual coupling, and normally differ only in phase angle. With the machine parameters as listed in Appendix A, the transfer functions can be plotted, as shown in Figure 4.12.

The Bode plot of the magnitude shows the diagonal elements, which are the transfer functions on the q and d axes, are stronger than the off-diagonal elements. The irregular phase diagram of the off-diagonal $H_{dq}(S)$ is caused by the software, which bounds between 180° and -180°. The phase angle of $H_{qd}(S)$ is not shown in the figure, because it actually is complementary to that of $H_{dq}(S)$. From the transfer functions of the diagonal elements, they are similar to those in the static loads.

From Figure 4.12, the transfer functions of the diagonal elements are similar to those in the equivalent r and x loads, as well as the steady state dynamic machine load in no-load case, as shown in Figure 4.4 and 4.9. Therefore, the closed-loop control system as used in the uncoupled static load is proposed here for both q and d axes. Due to the high loop gain of the closed-loop system, the effect of coupling between q and d axes on the output voltage can be reduced dramatically, as will be shown later. Figure 4.13 shows a complete general control system for three-phase applications.

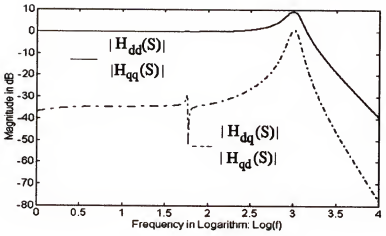

(a)

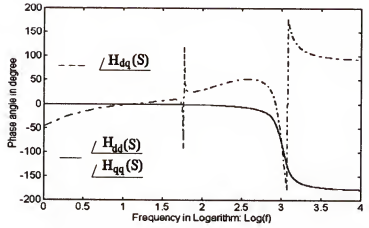

(b)

Figure 4.12 Bode plot of the transfer function in inverter and motor system
(a) Magnitude, (b) Phase angle

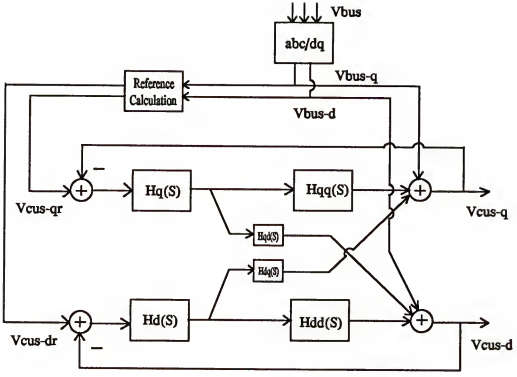

Figure 4.13 General control structure for dq model

In Figure 4.13, the three-phase feeder voltages are first transformed into qd components to serve as the reference voltages for both q and d axes, if the zero component is taken to be zero. Assuming the feeder voltage is a balanced three-phase system during steady state, one can obtain the transformed components on both q and d axes. In case the feeder contains harmonics, a low pass filter can be used to extract the fundamental component. Nabae et al [20] have described this application. As a result, the nominal reference voltage can be set to 1 pu for one axis and zero for another. Since the objective is to maintain a full voltage for the Custom bus, the magnitude should be kept constant at all times. However, the phase angle at the Custom bus may need to be changed to follow changes at V_{bus}. Since this is dependent upon the load flow of the system for different system conditions, the phase shift change is much slower compared to the transient phenomena. Therefore, a continuous update of the reference can be based on the calculations over a longer period. Thus, the reference can be adjusted for the phase angle without changing the magnitude.

In Figure 4.13, a closed-loop control system is used for both q and d axes. The output will track the reference as set by calculation, assuming the closed-loop has a high gain for both axes. Thus, the mutual coupling, as determined by $H_{qd}(S)$ and $H_{dq}(S)$ in (4.1), can be taken as a disturbance, as in the case of feeder voltages V_{bus-q}, V_{bus-d}. Starting from the tracking error on one axis, one can derive the coupling effect from this axis to another. As an example, the tracking error on the q axis is assumed to be $E_q(S)$ in the Laplace form. The voltage output on the d-axis V_{cus-d} resulting from the coupling can be derived as follows.

$$V_{dlq}(S) = \frac{H_q(S)\,H_{qd}(S)}{1+H_q(S)\,H_{dd}(S)}\,E_q(S) \tag{4.3}$$

Furthermore, some approximation can be assumed to simplify the equation. Assuming the loop gain $H_q(S)H_{dd}(S)$ is high, and the compensators on both axes are the same, the voltage output on the d axis, due to the coupling from the q axis can be rewritten as

$$V_{dlq}(S) \approx M_{dq}(S)\,E_q(S) \tag{4.4}$$

where $M_{dq}(S)$ is the coupling factor and determined by

$$M_{dq}(S) = \frac{H_{dq}(S)}{H_{dd}(S)} \tag{4.5}$$

From Figure 4.12, the coupling factor is much smaller than one in our application, especially at low frequency region and very high frequency region. Therefore, the coupling is weakened by the closed-loop system. Furthermore, the right side of (4.4) is also determined by the error. The error is small during the steady state. Nevertheless, a large error at the resonant frequency should be avoided, in order to reduce the coupling effect.

According to the above analysis, the compensator design can be based on both q and d axes separately. Due to the factor that the loop gain of the closed-loop system is already high in the unity feedback, a simple phase lead compensator can be used for both axes to increase the bandwidth, as described in the last section. Nevertheless, increasing the bandwidth also increases high frequency ripple. These are concerns in the real system design.

The above analysis does not take into account the load changes. The control system design is only valid for the specific load type under specific operating condition. In case of load changes, the adaptive control must be applied to follow the changes at the Custom bus.

4.5 Adaptive Control

The previous two sections deal with the applications for specific loads, namely uncoupled static loads and coupled dynamic loads. The control systems are designed separately for each specific application. Both cases assume the load topologies are the same. Also, the operating conditions are not changing. However, changing of the operation conditions changes dynamic behavior, as in the cases of variable capacitance in the equivalent impedance load, and variable speed in the dynamic machine load. As revealed in section 4.2, the load change has a significant effect on the transfer functions, especially in the dynamic machine loads and capacitor loads.

This section describes a control system which deals with the uncertainties involving different Custom loads. Specifically, the following two cases are examined: (1) changes in the operating conditions with the same load topology, (2) changes in the load topology.

The criterion to select the control system must take the following two facts into account. One is that the feeder voltage is treated as a disturbance. Moreover, the feeder voltage may have large voltage changes. Therefore, the closed-loop control has to be used to reject the effect of the feeder voltage changing. The frequency range caused by

the sudden changing may not be so high, because power systems normally have a high damping ratio due to local distribution components. The second is that the load changing causes the plant model to change. The plant model change is time-varying, in that the changes of different load types and operating conditions are unknown. The fixed compensator may not be capable of tracking of the desired reference.

In dealing with plant model changes of a control system, an adaptive control technique can be used. In addition, in order to reject and attenuate the effect of feeder voltage and mutual coupling in dynamic machine model, a closed-loop adaptive control system must be applied. This section will discuss the details for using adaptive control in the application of power quality improvement.

Before introducing the adaptive control, a study of the inverter system with different load conditions is performed. According to the dynamic models described by the Bode plots as shown in Figure 4.4～4.9, the common features can be derived as the follows:

(1) Each system has a high gain in the low frequency region, due to the nature of the DC-AC inverter.

(2) In the high frequency region, a negative 40 dB/slope appears, which resembles a second order system.

(3) The phase margin is small for all the cases.

From these features, it is concluded that a same control law can be used for all the cases, if a closed-loop control system is applied. Under this circumstance, the parameters of the controller can be adjusted by using an adaptive control algorithm.

In deriving the adaptive control system for the applications as described before, one should develop a plant model which has the same characteristics as those in real system. Since the plant model is unknown in a sense that the plant parameters are changing, an on-line parameter estimation and model identification technique is used. The estimation is based on the measurement from the real plant input and output. With the estimated plant model approaching the real system, the parameters of the controller are updated according to a formula derived from the desired criterion. Figure 4.14 shows a general diagram of a closed-loop adaptive control. The notations in the figure are simplified, but the original notations are shown in parenthesis as well. In the following, the control system terminologies of plant and plant model are used, which represent the inverter system and inverter model respectively.

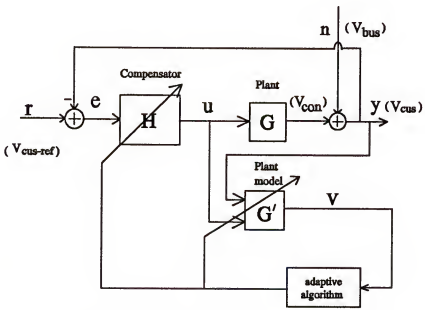

Figure 4.14 Closed-loop adaptive control system

In Figure 4.14, the compensator parameters are calculated based on the plant model. Dahlin [44] proposes an algorithm to synthesize the compensator by setting a desired closed-loop behavior. From the general frequency characteristics as shown before, a desired closed-loop system is specified as follows.

$$K(S) = \frac{\lambda}{S+\lambda} \tag{4.6}$$

where λ is determined by the bandwidth of the closed-loop system.

According to the closed-loop system, which takes the plant model G' as the controlled system, the closed-loop transfer function can be written as follows

$$K = \frac{HG'}{1+HG'} \tag{4.7}$$

Then, the compensator H can be represented by the closed-loop transfer function and plant model G'.

$$H = \frac{1}{G'}\frac{K}{1-K} \tag{4.8}$$

The transfer function K(S) is replaced by K for generality. In the following, the digital domain notations will be used for implementation purposes. The transformation from a continuous time equation to discrete time equation is provided in Appendix D. Thus, the discrete time equation for (4.6) can be obtained, as described in Appendix D.

$$K(Z) = \frac{T_s\lambda}{T_s\lambda+2}\frac{Z+1}{Z+\frac{T_s\lambda-2}{T_s\lambda+2}} \tag{4.9}$$

where T_s is the sample rate of the digital system.

Assuming the plant model is a second order system

$$G' = \frac{\sum_{i=0}^{2} b_i Z^{-i}}{1 - \sum_{j=1}^{2} a_j Z^{-j}} \tag{4.10}$$

The compensator H then can be derived as in (4.11), which is the general synthesis formula according to Dahlin [44].

$$H(Z^{-1}) = \frac{\sum_{i=0}^{3} h_{1i} Z^{-i}}{\sum_{j=0}^{3} h_{2j} Z^{-j}} \tag{4.11}$$

where h_{1i} and h_{2j} are determined from equation (4.10) by comparing the coefficients of operator Z^{-1}, Z^{-2}, Z^{-3} and so on.

In the adaptive control, the coefficients in the general control law as in (4.11) are calculated each step from the plant model, while the plant model is determined by an adaptive algorithm. There are various adaptive algorithms. The general rule is using a recursive formula to estimate the plant model. Touchstone et al [45] and Corripio et al [46] developed a recursive formula which may be implemented in this application.

According to the assumption of the second order system for plant model, the output of the plant model can be determined by a recursive formula as in (4.12),

$$v_k = \hat{a}_1 v_{k-1} + \hat{a}_2 v_{k-2} + \hat{b}_0 u_k + \hat{b}_1 u_{k-1} + \hat{b}_2 u_{k-2} \tag{4.12}$$

where v is the output of the plant model and u is its input. The same input is fed into the plant. The coefficients a_1, a_2, b_o, b_1, and b_2 are the estimated parameters of the plant model.

Define a column vector containing the input u and measured output y as follows

$$x_k^T = [y_k \; y_{k-1} \; u_k \; u_{k-1} \; u_{k-2}] \tag{4.13}$$

and a column vector containing the input u and output of the plant model v as follows

$$z_k^T = [v_k \; v_{k-1} \; u_k \; u_{k-1} \; u_{k-2}] \tag{4.14}$$

and a vector of the model parameters

$$\Phi = [\hat{a}_1 \; \hat{a}_2 \; \hat{b}_0 \; \hat{b}_1 \; \hat{b}_2] \tag{4.15}$$

By setting suitable initial values, the following recursive formula can be used to update the model parameters Φ.

$$K_k = (1+z_k^T P_k x_k)^{-1} z_k^T P_k \tag{4.16}$$

$$\Phi_{k+1} = \Phi_k + (y_{k+1} - \Phi_k x_k) K_k \tag{4.17}$$

$$P_{k+1} = P_k - P_k x_k K_k \tag{4.18}$$

where the matrix P_k is a weighting matrix. In all the equations, the subscript k represents the iteration steps.

By applying the above algorithm, simulation results will be provided in Chapter 5. Comparing Corripio's adaptive control with the fixed system of power quality control, there are two fundamental differences which might be of concern in the real system design. One is that the inverter in the power quality control has a high gain, which could make the adapter diverge. The other is the sudden changes of the disturbance input, i.e. the feeder voltage. These facts make more critical the selection

of initial conditions. The authors in [45] suggest a trial-and-error technique, which is efficient only after enough experience is accumulated for the various applications.

In order to verify that the adaptive control is needed, a study of using the fixed controller with a non-nominal load at the Custom bus is performed. Figure 4.15 shows the Custom bus voltage and the reference voltage, where the Custom load has a power factor correction capacitor in parallel with the static load. The capacitance of the capacitor is 100 uF, which is selected when the Custom bus has unit power factor after installing the capacitor.

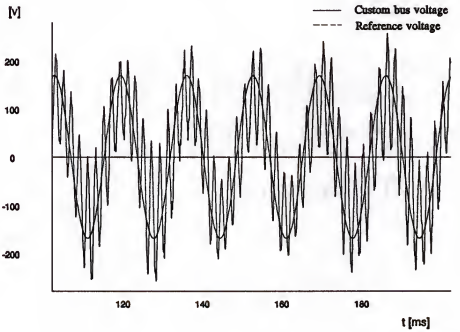

Figure 4.15 Custom bus and reference voltages with a 100 uF capacitor at the Custom bus

4.6 Effect of Distribution System

In all of the analysis so far, the feeder voltage input is assumed to be zero for control design purpose. The inverter supplies the only voltage to the Custom load. In fact, the feeder voltage itself is the second system input, which is considered to be a disturbance function in this application. Cutting the system at V_{bus}, one can use the dynamic equations as developed in Chapter 3 for further analysis. From equations (3.8) and (3.10), the transfer function from the feeder bus V_{bus} to the Custom bus is as follows

$$H_{bus-cus}(S) = \frac{R_L + L_L S + LR_L CS^2 + L_L LCS^3}{Y(S)} \tag{4.19}$$

where Y(S) is given by (3.11).

The Bode plot of the transfer function $H_{bus-cus}(S)$, as in Figure 4.16, shows that the magnitude of the transfer function from the feeder bus to the Custom bus is near zero dB. In the cases of voltage outages, the feeder bus voltage change may be significant. Nevertheless, the effect of the sudden change of the feeder bus is attenuated by the high loop gain if a closed-loop system is applied, as can be seen in equation (4.20).

$$V_{cus|bus}(S) = \frac{H_{bus-cus}(S)}{1+HG} V_{bus}(S) \tag{4.20}$$

where HG represents the loop gain in the closed-loop system.

From equation (4.20), the effect of Vbus is attenuated by a factor of approximately HG, if the loop gain is kept high. Chapter 6 will discuss this point quantitatively.

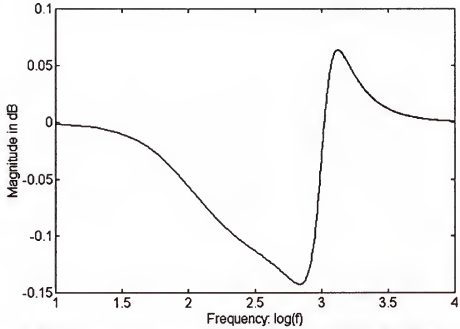

Figure 4.16 Bode plot of the transfer function from feeder voltage to the Custom bus voltage

4.7 Conclusion

Based on the different distribution system applications, various distribution system loads are examined in this chapter. Accordingly, suitable control systems are developed for each type of load. For static loads, a simple closed-loop control with phase lead compensator can be used. Furthermore, the compensator design can be based on a single-phase equivalent system for an uncoupled static load. In the case of a dynamic machine load, a qd0 reference model is developed which takes the mutual coupling and disturbance attenuations into account. The next chapter will utilize the techniques developed in this chapter in a real system. Various simulation results are provided to support the analysis, as performed in Chapter 3 and Chapter 4.

CHAPTER 5

SIMULATION RESULTS

5.1 Introduction

This chapter utilizes the theory and techniques developed in previous chapters to cope with the power quality problems. The detailed distribution system model is used and the power quality phenomena are simulated based on the detailed distribution model, referring to Figure 2.3. The detailed power electronic converter models are connected to the distribution system to serve as an on-line power quality controller. The closed-loop automatic control system is used for the converters as well. Again, the objective is to maintain a high quality power at the Custom Power bus in the distribution system. Concerning the distribution system, power electronics converters are used as a controller to achieve high quality power. In the following, the term "power electronic controller" is used when dealing with power systems in referring to the power electronics converter.

The detailed analysis of the closed-loop control with phase lead compensator was discussed in the last chapter where the inverter and filter were represented by a simplified transfer function. In all the applications from this chapter on, a detailed converter switching model with a PWM control technique is used. The norminal switching frequency at each device is 20 kHz with a 10 kHz triangular carrier waveform. The doubling frequency effect is achieved by a three-stage PWM technique rather than

the bipolar PWM. A similar technique is discussed by Lai and Ngo [47]. Only the simulation results are shown herein to support the analysis.

In order to verify the three-stage PWM technique, a frequency spectrum analysis at the output waveforms can be performed. Due to the high switching frequency, counting the major harmonic ripples is used rather than using the frequency spectrum. Figure 5.1 shows a sampled one cycle waveform at the Custom bus, when the inverter is injecting the harmonics to compensate the line. Figure 5.2 shows the expanded waveform of Figure 5.1 using a larger scale. From Figure 5.2, there are 20 major harmonic ripples within one milli-Second. Thus, the major harmonic frequency is 20 kHz, which agrees with the desired switching frequency. It should be pointed out that the waveform in Figure 5.2 was taken with the detailed distribution system. The interactions with the power system causes distortion in the observed harmonic ripples. Figure 5.3 shows the actual three-stage PWM signal.

A prelimary simulation study was also performed to compare three-phase inverter results with three separate single-phase inverters. As discussed in Chapter 3, an equivalent single-phase bridge PWM inverter can be used to simplify the compensator design in the control system, if the Custom load is a static load without mutual coupling. Figure 5.4 shows a comparison at the Custom bus voltage. Two curves are overlapped together, and the difference is not seen.

In addition, a comparison of using different switching frequency is provided. The 10 kHz and 5 kHz switching frequency are examined, with the results shown in Figure 5.5 and Figure 5.6 respectively.

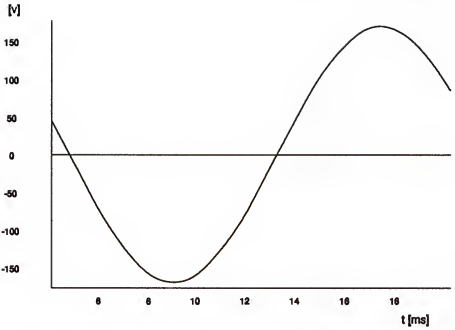

Figure 5.1 Sampled voltage waveform at the Custom bus

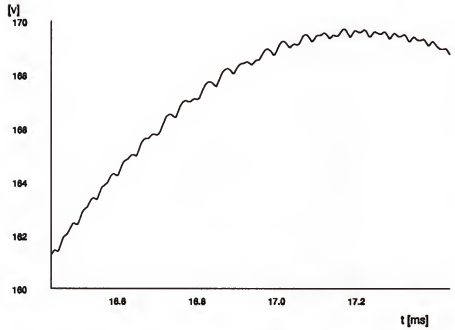

Figure 5.2 Expanded waveform of the Custom bus voltage

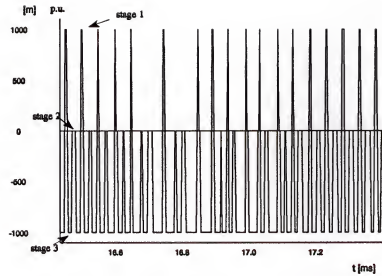

Figure 5.3 Three-stage PWM inverter output voltage

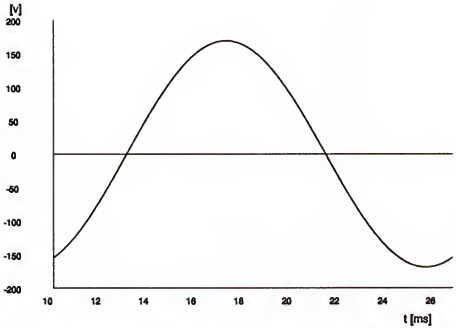

Figure 5.4 Custom voltages comparison with three-phase inverter and three single-phase inverters

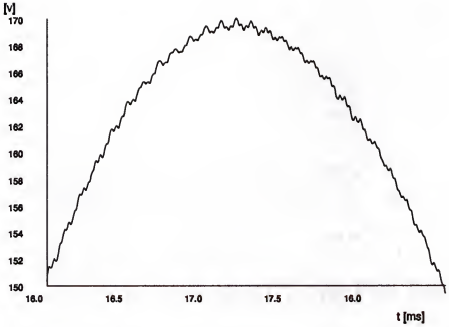

Figure 5.5 Expanded waveform of the Custom bus voltage with 10 kHz switching frequency

Figure 5.6 Expanded waveform of the Custom bus voltage with 5 kHz switching frequency

5.2 Power Quality Improvement for Uncoupled Network Loads

In the following, detailed EMTP simulations are used to illustrate the nonlinear performance of Custom Power controller for an uncoupled static load. A three-phase inverter is used in all of the applications. Also, the control system is based on a single-phase lead compensator design, as discussed in Chapter 4, referring to Figure 4.10 and equation (4.1). The three-phase inverter and its connection to the system are shown in Figure 3.7. The results emphasize the comparison between the feeder bus voltage and the Custom bus voltage, since the power electronics controller is installed between these two buses. The comparison is similar to that of the Custom bus voltages with and without applying the power electronic controller. All results discussed in Section 5.2.1 ~ 5.2.5 was taken for the nominal system data given in Appendix C, with a 3 kVA Custom load.

5.2.1 Blocking Feeder Harmonics

In this application, the feeder voltages have unbalanced harmonic distortion, as shown in Figure 5.7. The three-phase unbalanced harmonics are injected into the system on the feeder side. Thus, as far as the Custom bus is concerned, the harmonics affect the Custom bus as a voltage source. The three-phase tracking system with a series inverter is capable of providing unbalanced voltage harmonics to subtract the harmonic components in the feeder voltage. The simulation results as shown in Figure 5.7 ~ 5.10 verify this application. Because high frequency switching is used, the Custom voltage is nearly a pure sinusoidal waveform, as shown in Figure 5.8. Figure 5.9 shows the filtered three-phase converter output voltage which actually represents the harmonic

content in the feeder voltages. The three-phase filter inductor currents are unbalanced because of the unbalanced voltage output, as shown in Figure 5.10.

5.2.2 Compensating Voltage Sags

The voltage sags are caused by an unbalanced line-to-ground fault through a reactance in the feeder side. Figure 5.11 shows the three-phase feeder voltages and Figure 5.12 the three-phase Custom bus voltages. It is noticed that the fault in the feeder side not only causes deviation in the voltage magnitude, but the phase angles are affected as well. This can be seen in the voltage waveforms in phase C. During the sag, the voltage deviation of phase C is small compared to that of the other phases. Nevertheless, the converter output voltage in phase C verifies that there is a phase shift during the sag. In Figure 5.13, close investigation into the other two phases yields the same conclusion. Therefore, the converter injects a sequence voltage into the system to balance the three-phase voltages. Figure 5.14 shows the three-phase inverter filter currents in which high frequency harmonic ripples appear.

5.2.3 Absorbing Voltage Swells

Due to a large motor load tripped off in the system, a voltage swell occurs at the Custom bus. Since this big load is on the source side, the disturbance is designed in such a way that it will not cause large voltage increases to the loads between the source and substation bus, for which the power electronic controller has no control. Therefore, a reduced voltage compared to the normal voltages is maintained in the system prior to the swell. The undervoltage at the Custom bus before the motor is tripped off is compensated by the power electronics controller. Therefore, the converter not only

absorbs the overvoltages which are caused by tripping-off of the large load, but it initially compensates the undervoltages as well.

Figure 5.15, Figure 5.16 and Figure 5.17 show the feeder voltage, Custom bus voltage and converter output respectively. Again, nearly sinusoidal waveforms at the Custom bus are achieved.

5.2.4 Compensating Voltage Outages

A one-phase voltage outage is shown in Figure 5.18 in which the phase A feeder voltage is completely lost, i.e. a simple line-to-ground fault at the feeder bus. The waveform shows the best case when the voltage disappears at the instant that it crosses zero. Normally, if the voltage outage happens at other instances, i.e., sudden changes at a high peak, the converter output may spike. Fortunately, the high frequency spike would probably be attenuated because the real system has more damping than the miniature distribution system model. Therefore, the voltage outage normally is accompanied with resonant oscillation. It is also true that the high frequency oscillation in the output depends on the switching frequency and the sampling rate of a digital control system. In this example, the voltage outage at one phase causes voltage sags at the other two phases, because of the coupling between the phases on the feeder side. The inverter again operates in an unbalanced mode for which the inverter provides an unbalanced three-phase voltages. Figure 5.19 shows the Custom bus voltages, and 5.20 shows the inverter output voltages.

Another study is performed to illustrate the worst case in which an outage of all three phases occurs. For convenience, the three-phase voltage outage is caused by a

three-phase line-to-ground fault internally on the feeder side, referring to the distribution system model in Figure 2.3. Thus, the feeder voltage goes to zero after resonant oscillation.

Figure 5.21 shows the three-phase feeder voltage. By using the power electronics controller, the Custom voltages maintain a sinusoidal waveform except for short duration glitches, as shown in Figure 5.22. Figure 5.23 shows the inverter output voltages.

5.2.5 Absorbing Impulses in Feeder Voltage

Voltage impulses caused by lightning surges normally have high peaks and fast transient responses. These surges have a very short rise time, in the range of micro-seconds. According to IEEE standards [48], a 1.2 μsec. rise time is typical when lightning directly hits transmission lines. Because of this, the power electronics converters are not capable of recognizing such a fast surge because the switching frequency of the converters is much lower than that. Therefore, fast rise time surges are normally suppressed by surge arresters. In this study, slower rise time impulses are considered which result from some types of switching surges, or lightning surges interacting with power system apparatus or protective devices.

Figure 5.24 shows an example of a slow impulse on the feeder voltage phase A. Figure 5.25 and 5.26 shows how the inverter suppresses the impulse and maintains a sinusoidal waveform at the Custom bus. The peak time of the impulse does not matter as far as the inverter is concerned. The inverter produces the same quantity no matter where and when the impulse appears. This compares with surge arresters, which will not suppress the surges if the voltage peak does not exceed the protective level.

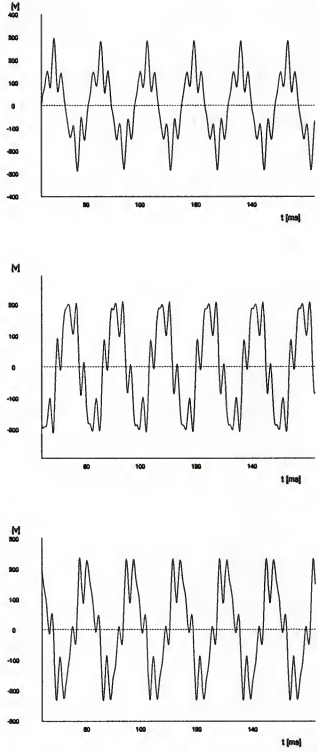

Figure 5.7 Three-phase feeder voltage with unbalanced harmonic distortion

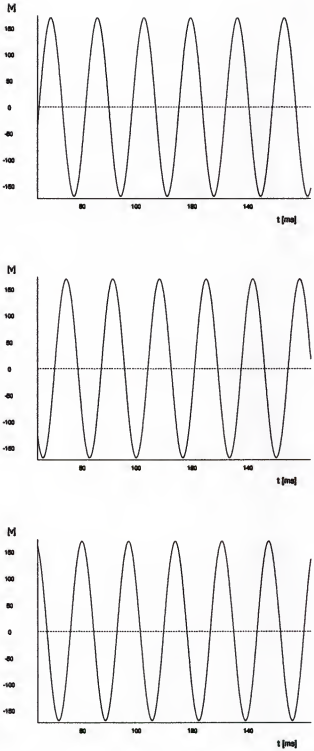

Figure 5.8 Three-phase voltage at the Custom bus (harmonics in feeder voltages)

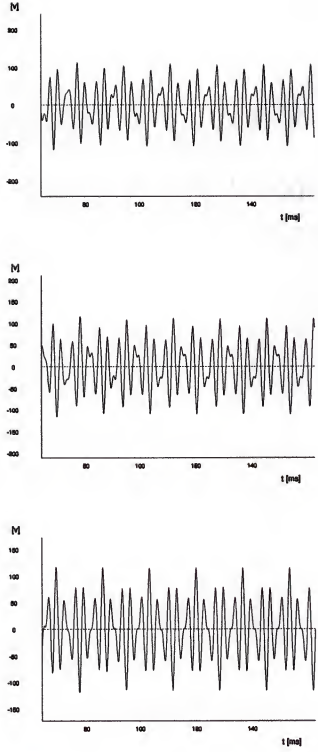

Figure 5.9 Three-phase converter output voltage (harmonics in feeder side)

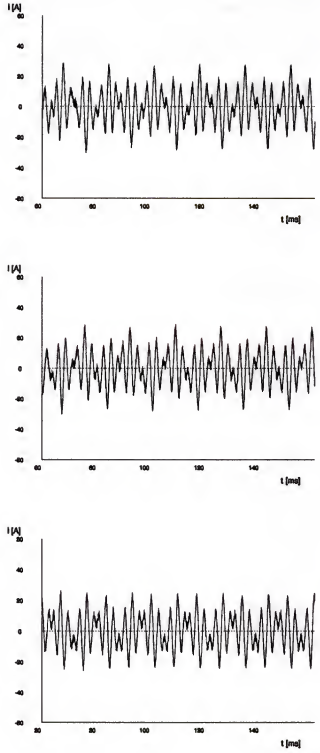

Figure 5.10 Three-phase filter inductor currents (harmonics in feeder side)

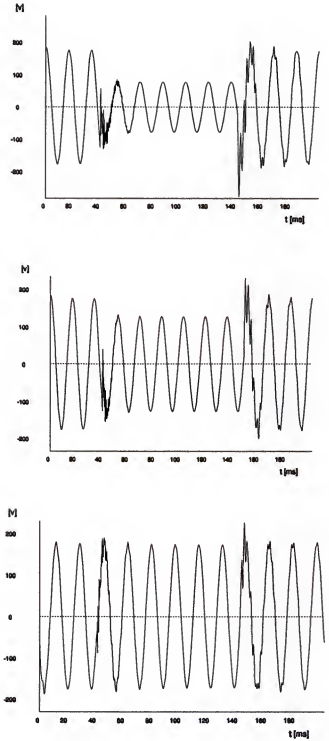

Figure 5.11 Three-phase feeder voltage with sags

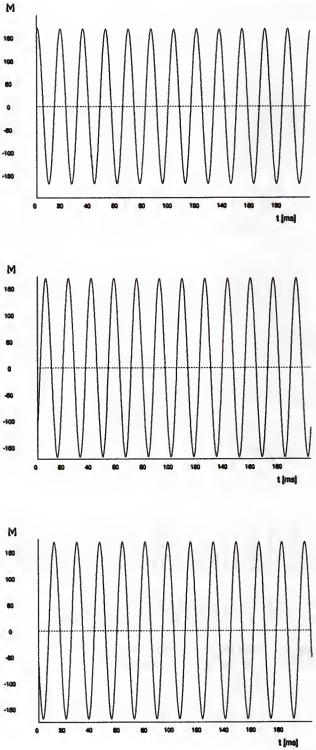

Figure 5.12 Three-phase Custom bus voltage with feeder voltage sags

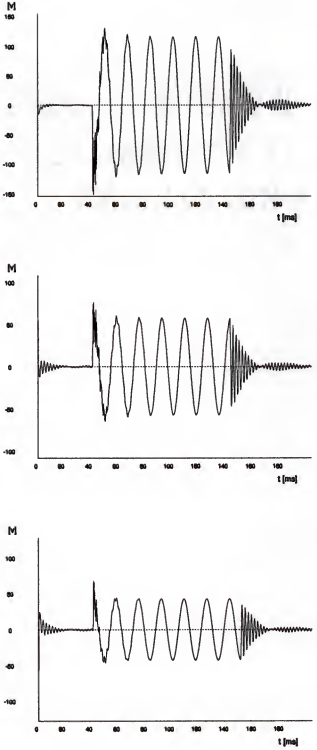

Figure 5.13 Three-phase inverter outputs with feeder voltage sags

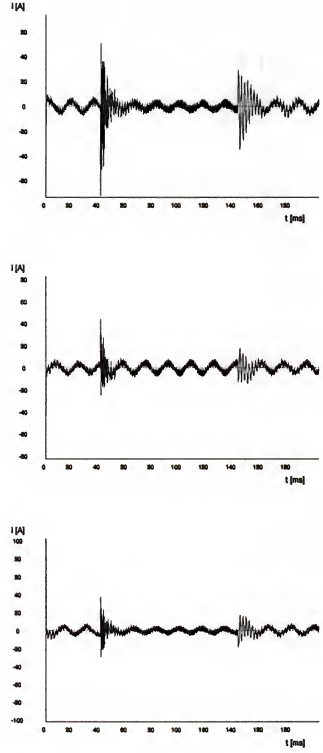

Figure 5.14 Three-phase inverter filter inductor currents with voltage sags

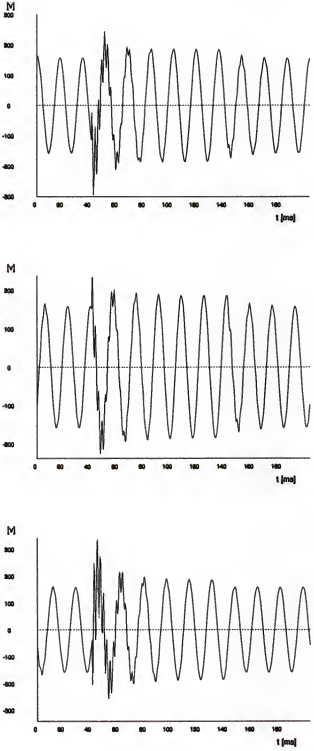

Figure 5.15 Three-phase feeder voltage swells

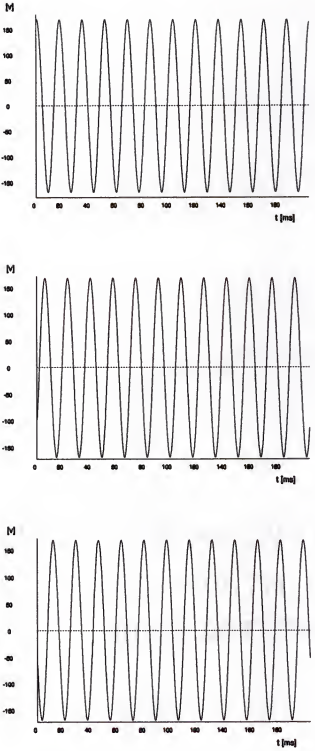

Figure 5.16 Three-phase Custom bus voltages with feeder voltage swells

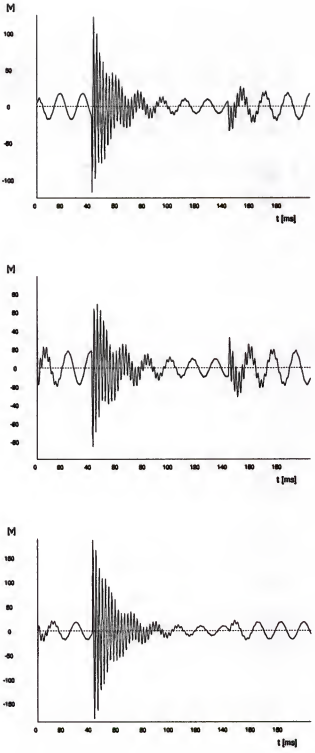

Figure 5.17 Three-phase inverter outputs with feeder voltage swells

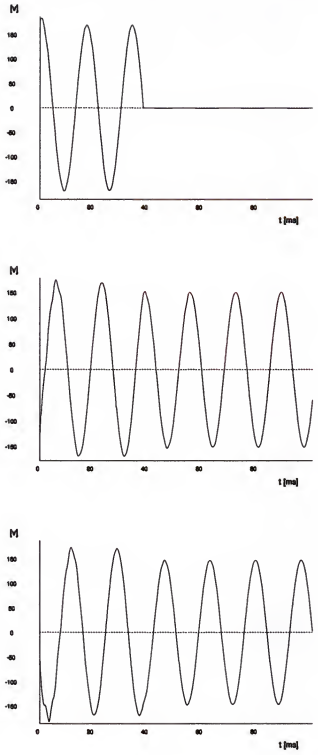

Figure 5.18 Three-phase feeder voltages with one phase outage

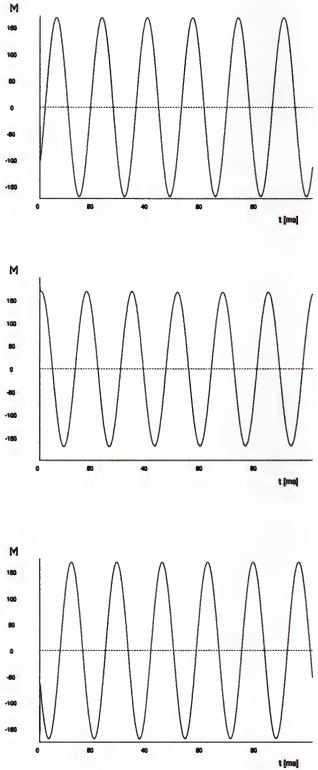

Figure 5. 19 Three-phase Custom bus voltages with one phase outage on feeder bus

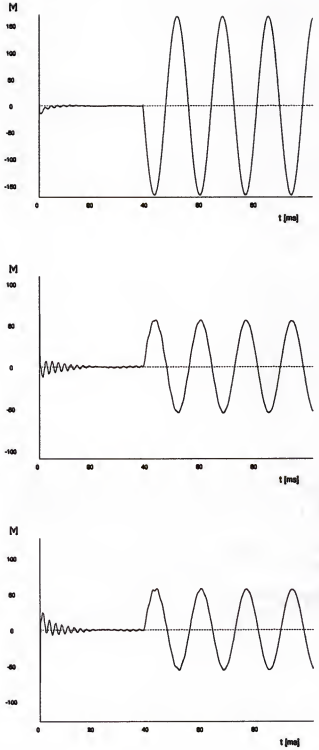

Figure 5.20 Three-phase inverter output with one phase outage

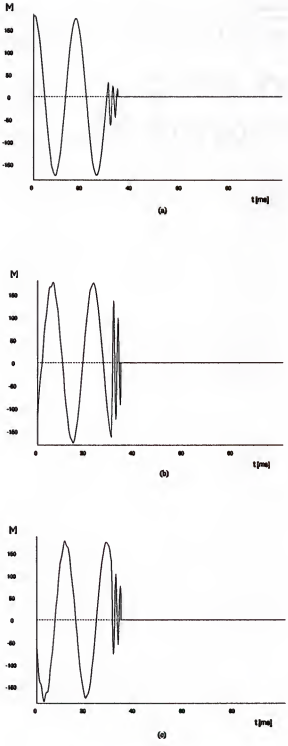

Figure 5.21 Three-phase feeder voltage outage

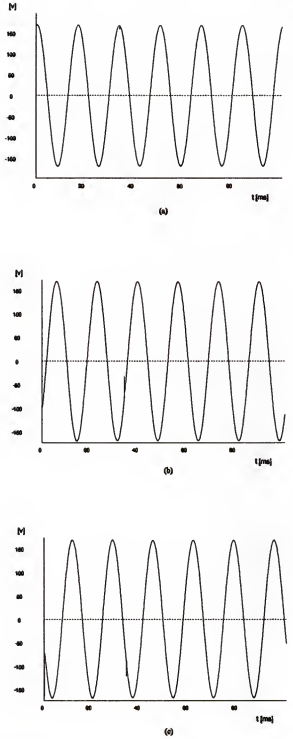

Figure 5.22 Three-phase Custom bus voltages with three-phase feeder outage

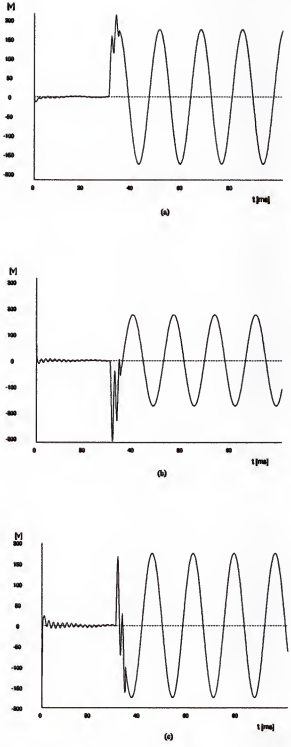

Figure 5.23 Three-phase inverter output with three-phase feeder outage

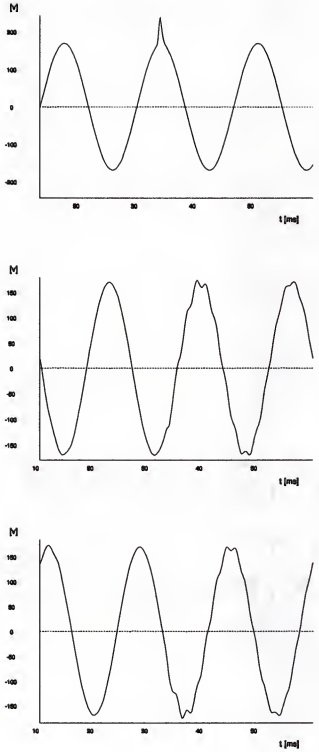

Figure 5.24 Three-phase feeder voltages with impulse disturbance

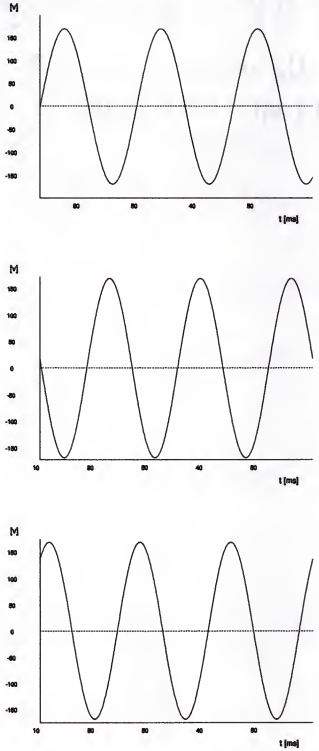

Figure 5.25 Three-phase Custom bus voltages with impulse on feeder side

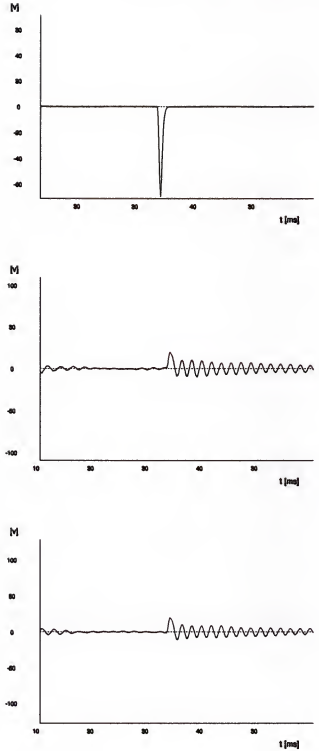

Figure 5.26 Three-phase inverter output with impulse on feeder side

5.3 One-cycle-switching

Solid-State-Breakers (SSB), as controlled by electronics devices, provide fast switching equipment for distribution systems. In conventional distribution systems, mechanical switches are widely used. However, mechanical switches typically take a long time to finish the switching operation. Typical switching times of mechanical switches are five to ten cycles, i.e., 90 milliseconds to 160 milliseconds. Therefore, if mechanical breakers are used as transfer switches, multi-cycle sags are possible at the feeder bus. If the mechanical switches are replaced by Solid-State-Breakers, the voltage sags can be limited to one cycle. This is so-called one-cycle-switching, and is shown in Figure 5.27.

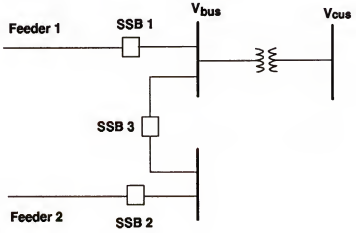

Figure 5.27 One-cycle-switching

In Figure 5.27, Feeder 1 supports the important Custom load V_{cus}. Feeder 1 and Feeder 2 are independent with SSB 3 normally-open. If a fault or other critical problem happens in Feeder 1, it is desirable that the Custom load be supported by Feeder 2 rather than Feeder 1. This is done by opening SSB 1 and closing SSB 3. The SSBs can implement the switching operation within one cycle. In this way, the Custom bus will only have less than one cycle voltage sags or outages. The Custom bus has a higher quality power supply in that the voltage sags or outage only exist for a few milliseconds rather than for dozens of milliseconds. It is noticed that Figure 5.27 is part of the miniature distribution system used in all the studies in this dissertation.

Furthermore, if the power electronic controller is installed between the feeder and the Custom bus, even higher quality power can be achieved. The principle is the same as that used in last section. The power electronics controller will compensate for the voltage sags for the one cycle shortage. In addition, the controller will also absorb the surges and oscillations caused by closing the breaker SSB 3. Figure 5.27 shows the application based on the miniature distribution system.

All three phases in Feeder 1 are tripped off sequentially at the instances when their line currents cross zero. The timing sequences of the switching operations are shown in Figure 5.28. In each phase of Figure 5.28, three curves are displayed with feeder voltage, SSB 1 current, and SSB 3 current. The feeder voltage at each phase suddenly changes due to the breaker opening, when its line current crosses zero. However, the voltage may be distorted because of the effect of other phases, as can be seen in phase B and phase C. The SSB 3 closes shortly after the SSB 1 opens. Due to

the power factor capacitors at both sides of the SSB 3, which are charged prior to the closing of SSB 3, the currents spike. By using the power electronic controller, each phase voltage is compensated, as shown in Figure 5.29. In this application, the control system is the closed-loop control system, as shown in equation 4.1. In Figure 5.29, the voltage spikes at the Custom bus appear. This is because of the low switching frequency, which can not recognize the high frequency ripple and sudden voltage changes. By using high switching frequency, the spikes may be eliminated.

Figure 5.30 shows the three-phase inverter output voltages. During switching period, the feeder voltages have dramatic deviations from the pure sinusoidal waveforms. Therefore, the inverter operates at a heavy duty condition, as far as the inverter output voltage is concerned.

One-cycle-switching is significant in that it changes the concept of distribution system switching operations, not only because of its fast switching, but also because of the flexibility of control. Since SSBs are actually designed using power electronics devices, they can be controlled by low voltage components or microprocessors. These switching devices can be used in high voltage and high power applications.

It is noticed that one-cycle-switching provides an alternative to power quality improvement. It only reduces the voltage sag period compared to mechanical switches, if power electronic controller is not applied. However, it produces high peak surges and high frequency oscillations. By using power electronic converters, long term voltage sags are overcome without introducing one-cycle-switching technique. The studies as performed here only describes a combination of these two applications.

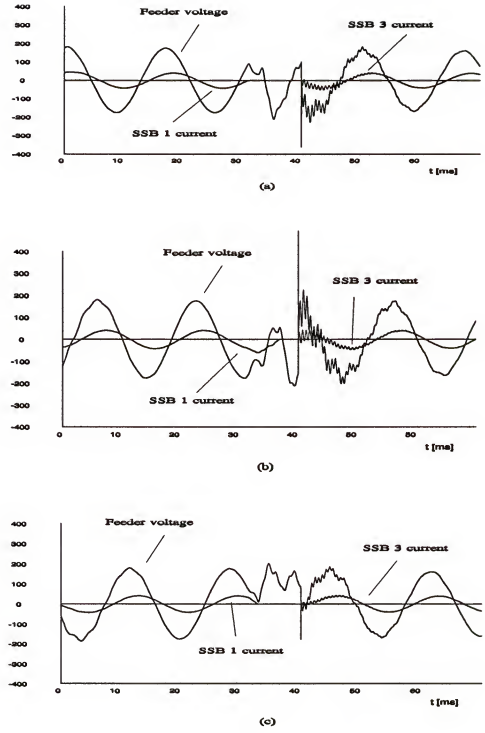

Figure 5.28 Three-phase feeder voltages and corresponding SSB currents

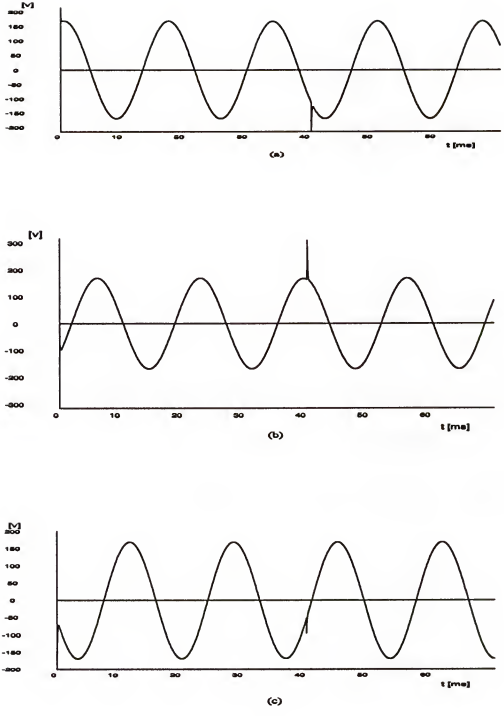

Figure 5.29 Three-phase Custom bus voltages

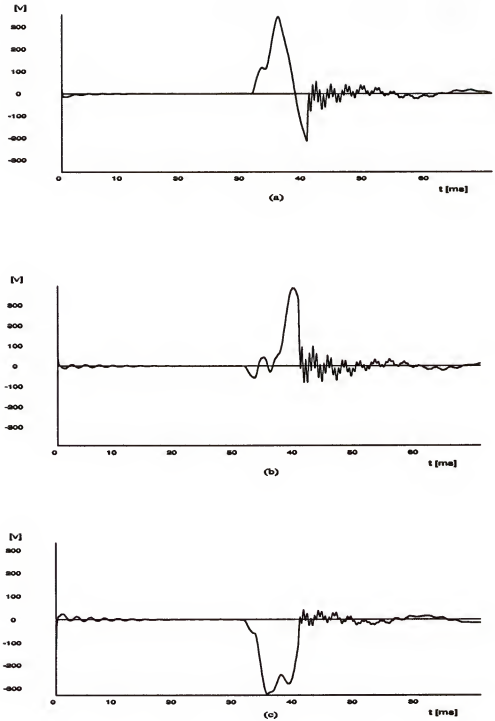

Figure 5.30 Three-phase inverter outputs

5.4 Power Quality Improvement for Dynamic Machine Loads

In the previous section, an equivalent load impedance was used at the Custom bus, which is assumed to be a static load with linear and time-invariant properties. However, real industrial loads are generally more complicated. There are various types of customer loads in the distribution systems, e.g. motors, rectifiers, heaters, etc. Furthermore, the loads connected at the Custom bus may be a combination of these various customers. If more realistic loads in distribution systems are taken into account, the results may not be so ideal as illustrated in last section.

To illustrate the effect of more realistic loads, a dynamic model of an induction motor load in parallel with a static load is assumed at the Custom bus. A simplified model of the three-phase system with feeder bus and converter is shown in Figure 5.31.

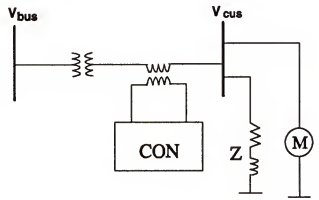

Figure 5.31 Dynamic induction motor load at the Custom bus

The loads at the Custom bus are assigned as follows. The motor has a 3 hp with running at 2 kVA load. The static load is 1 kVA. The total load at the Custom bus is 3 kVA. The parameters of the motor are listed in Appendix A, with an addition of load torque of 5 Nm. The static load with an equivalent impedance has the parameters as follows.

$R_L = 36.6\ \Omega$,

$X_L = 22.8\ \Omega$.

The rest of the parameters in the distribution system is the same as before, as shown in Figure 2.3 and listed in Appendix C.

As discussed in Chapter 3, the qd0 reference frame can be used for control analysis involving the dynamic machine loads. The closed-loop control system based on qd0 model was developed in Chapter 4, and its dynamic performance is predicted in Bode plots. The closed-loop compensator is based on the fact that the inverter has a high gain during steady state. Therefore, only a phase-lead compensator for both q and d axes is used. In the simulation, two coordinate systems exist with one being the qd0 system, and the other abc system. The qd0 system model is applied for closed-loop control implementation, while the abc system must be used for real converter implementation. In addition, the distribution feeder and motor load are part of the three-phase abc system. The interchange between the two systems is achieved by transformations between the abc and qd0 systems. Specifically, the motor terminal voltages are transformed to the qd components. In the inverter side, the duty ratios are transformed back to the abc system. Figure 5.32 shows the model used in the simulation.

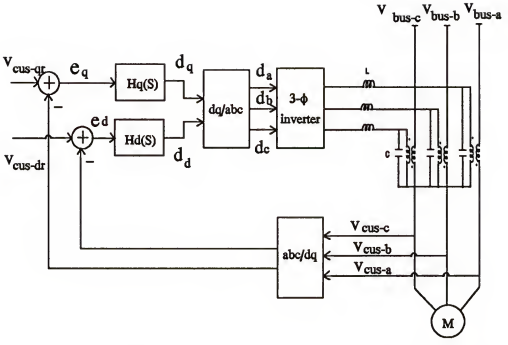

Figure 5.32 Interchange between three-phase and two-phase qd0 systems

Figure 5.33 shows the three-phase feeder voltages with sag caused by a line-to-ground fault in one phase. Figure 5.34 shows the Custom bus voltages, which are also the motor terminal voltages. Figure 5.35 shows the inverter output. The speed of the motor maintains constant during voltage sag on the feeder bus, as shown in Figure 5.36. However, the electromagnetic toque of the motor, as shown in Figure 5.37 exhibits a light torque pulsation, which is caused by current waveform distortion, as shown in Figure 5.38. The significance in the motor loads is that the motor behaves as an active current source rather than a passive network. For this, another converter topology may be needed to include the current control on the machine terminal, which leaves for future development.

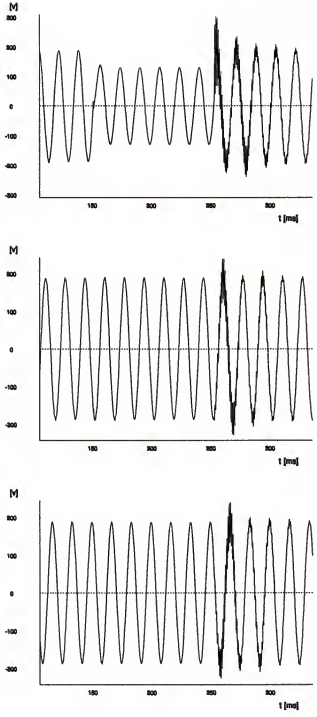

Figure 5.33 Three-phase feeder voltages with sag

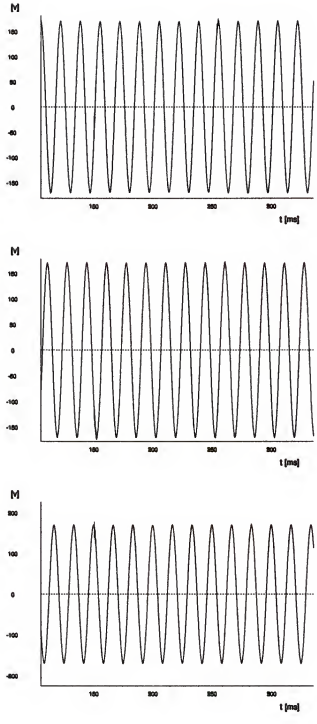

Figure 5.34 Three-phase Custom bus voltage

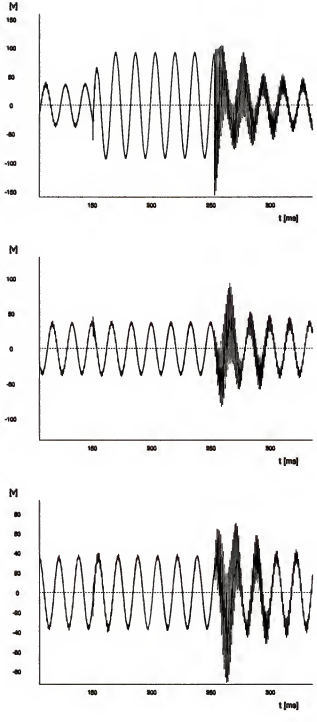

Figure 5.35 Three-phase inverter output

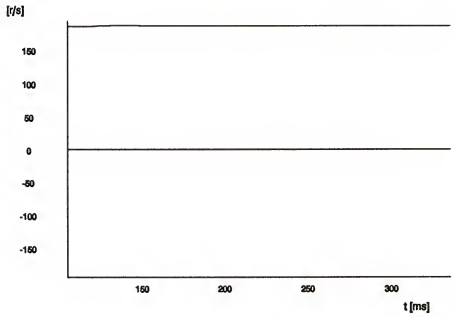

Figure 5.36 Motor speed

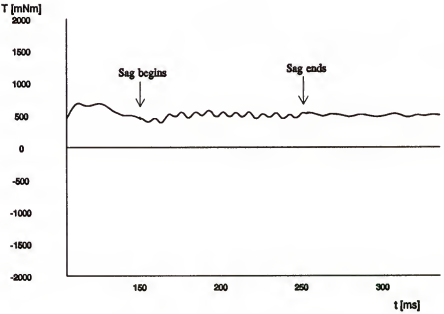

Figure 5.37 Electromagnetic Torque

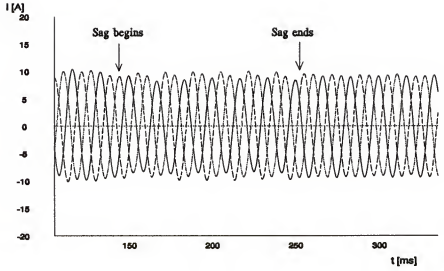

Figure 5.38 Three-phase armature winding currents

It should be pointed out that the qd0 model, as used for coupled dynamic load applications, is also valid for an uncoupled network load. An additional study was performed to apply the qd0 model for the nominal static load. The voltage sags are examined again in this study. The same system parameters are used. The three-phase feeder voltages are the same as those in Figure 5.11. From the simulation, the three-phase voltages at the Custom bus remain sinusoidal all the times. For comparison with previous results, the three-phase Custom bus voltages are shown in Figure 5.39. These voltages are overlaid on the same plot with the corresponding waveforms taken from per-phase abc control design in section 5.2.2. This further verifies that the single-phase control design model can be used for a three-phase uncoupled network. However, the qd0 model is valid for both uncoupled and coupled network loads.

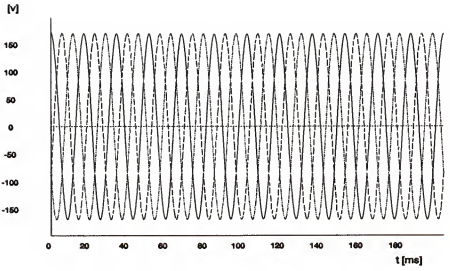

Figure 5.39 Comparison of three-phase Custom bus voltages with qd0 model vs. single-phase design model, for nominal static load.

5.5 Power Electronic Controller using Adaptive Control

The algorithm of one form of adaptive control was discussed in Chapter 4, where a closed-loop adaptive control system was proposed for the power electronics converter. In this section, simulation results will be shown to evaluate adaptive control. Overall, three cases are examined using adaptive control. The first one is the dynamic machine load with voltage sag on the feeder side, while the machine is running at a light load. The second one is also the dynamic machine load, but the motor operation is changed to a blocked rotor condition. From the discussion in Chapter 4, these two operating conditions are the two extreme cases. Furthermore, the third case examines the Custom load topology changed to an RLC static load. The same control law is used in all the cases.

The study of the adaptive control relies on the dynamic transfer functions of the different models, as described by Bode plots in Chapter 4. In the case the transfer function of the induction motor is based on the well-known steady state per-phase equivalent circuit. This assumption is made because the adaptive control is only valid for slowly changing systems. The fast electrical transients associated with the coupling inside the machine can not be neglected when using adaptive control. Under this circumstance, the motor is under steady state condition with different speeds. Therefore, the per-phase dynamic model of the motor can be used.

In addition, the distribution system is taken into account with the feeder bus connected to the infinite bus through an equivalent impedance. The equivalent model is shown in Figure 5.40, and the parameters are listed as follows based on the distribution system model in Figure 2.3.

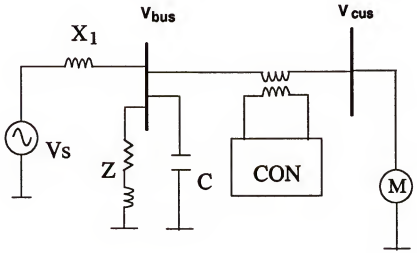

Figure 5.40 A simplified network for the adaptive control study

V_s = 120 V AC,

X_l = 1.2 Ω,

Z = 40.01+j 23.09 Ω,

C = 7.36 uF.

The machine parameters are listed in Appendix A.

The first example illustrates the adaptive control application in compensating the sag at the Custom bus. Figure 5.41 shows the feeder voltage with sag, as in the case studied previously. The worst case is examined here in which both the beginning and ending point of the sag appears at the peaks of the voltage waveform. Thus, the high peak oscillations exist in both cases, as shown at the Custom bus voltage in Figure 5.42. However, under steady state, the Custom bus voltage tracks the reference precisely during voltage sag at the feeder bus.

Prior to the voltage sag, the adaptive control has already reached a steady state for the inverter model and the compensator. The adaptation is examined by comparing the inverter output and output of the inverter model. The inverter and inverter model are represented by the plant and plant model as described in Chapter 4. The adaptation is shown in Figure 5.43, where the output of the plant model is approaching the plant output before the voltage sag. For this particular application, it takes almost 18000 iteration steps to reach the steady state, which is equivalent to 1.8 seconds with a 10 kHz sampling rate. Figure 5.44 shows the expanded waveforms of the plant output and plant model output voltage during voltage sag in the feeder bus.

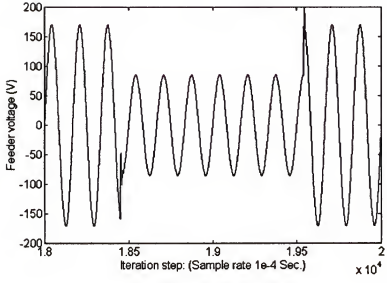

Figure 5.41 Voltage sag at the feeder bus

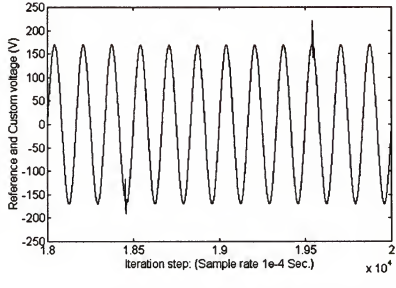

Figure 5.42 Reference and Custom bus voltage

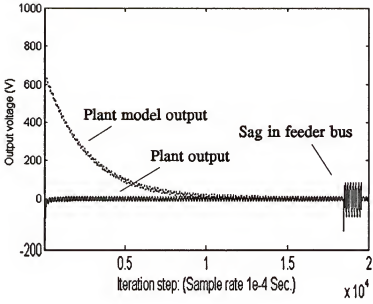

Figure 5.43 Inverter output and inverter model output

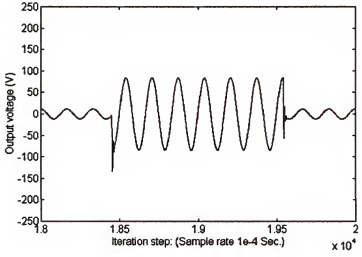

Figure 5.44 Expanded waveforms of inverter output and inverter model output

The second example illustrates the plant model change with the same topology as in the first example. In this application, the motor load at the Custom bus is suddenly changed to another operating point, a case which is much worse than in practical situations. Specifically, the rotor of the motor is blocked by external forces. Also, the inverter is providing a full voltage to the Custom load. The adaptive control responds to the changes by adjusting the plant model.

Figure 5.45 shows the adaptation of the plant model. While under steady state, the plant system is changed to second case, which corresponds to a motor operating condition change from no-load to blocked rotor. Accordingly, the plant model changes, as shown from its output, to respond the plant system changes, by changing its parameters. Thus, the output of the plant model is changed. Figure 5.46 shows an expanded waveform during the load operating condition changes.

Figure 5.47 shows the reference and Custom bus voltage during the plant system changes. The Custom bus voltage tracks the reference precisely. In fact, the adaptive control is mainly designed to deal with the plant system changes with the same topology, as in the case of this application.

This application involves electric machines over a large range of deviation in dynamic performance, i.e. from no-load to blocked rotor. Static loads in similar applications will yield the same results. Instead of testing all the cases separately, a more severe situation is examined in the following, to deal with the topology changes of plant system.

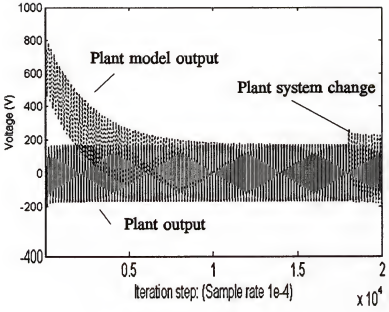

Figure 5.45 Inverter output and inverter model output in the case of the load operating condition changes

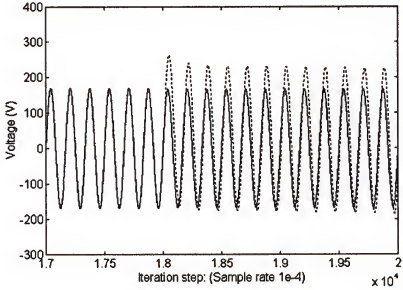

Figure 5.46 Expanded waveforms of Figure 5.45

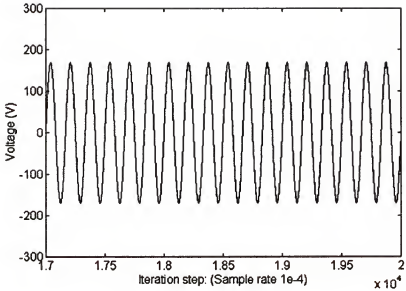

Figure 5.47 Reference and Custom bus voltage

Theoretically, adaptive control deals with a slowly changing plant system [46]. If the topology of the plant is changed, the control law in the compensator may not be suitable for the new plant. Fortunately, the inverter system with the different load topologies including the rotating machine loads have the similar characteristics, as discussed in Chapter 4. Therefore, adaptive control can be evaluated by examining the results when the adapter reaches a steady state.

In this application, the motor load is replaced by an RLC network, with C being the power factor correction capacitor in parallel with the RL equivalent load. The parameters of R and L are the same as used before and listed in Appendix C. The capacitance of the power factor correction capacitor is 100 uF. The same adaptive control structure with the same control law as used before is applied for this application.

In addition, the RLC static load operates at full load condition, i.e. 3 kVA. Meanwhile, the inverter supplies a full voltage to the Custom bus prior to the voltage sag on feeder bus. The system structure is similar to Figure 5.38 with only the motor load replaced by the RLC static load.

Figure 5.48 shows the feeder bus voltage. As used before, the worst cases are examined, in which the voltage sag is triggered at the negative peak of the voltage. Meanwhile, the voltage sag is cleared at the positive peak. During adaptation, the plant model rapidly approaches the real system, which can be seen from the initial outputs of these two systems, as shown in Figure 5.49. The adaptation is much faster than the motor load cases. Figure 5.50 shows the reference and Custom bus voltage for the static RLC load.

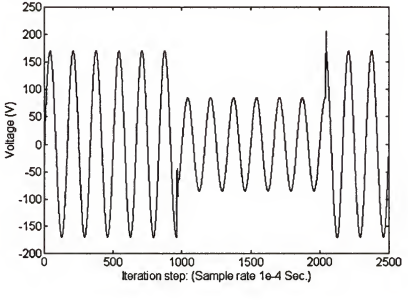

Figure 5.48 Feeder voltage

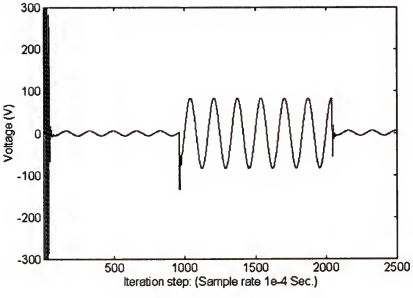

Figure 5.49 Inverter output and model output

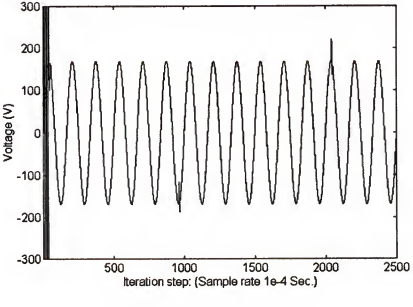

Figure 5.50 Reference and Custom bus voltage

The above three examples illustrate the adaptive control applications in coping with system changes involving load operating condition changes, as well as load topology changes. From the simulation results, the adaptive control can easily handle the load operating condition changes. For different load topologies, the dynamic machine load takes much a longer adaptation time than the static equivalent impedance load. From the theoretical analysis, the same control law can be used for all of the cases involving various distribution loads. Therefore, adaptive control serves as a multi-functional control technique, if all the loads as described are applied.

In the real system implementation of the adaptive control, several points are important. The first is the trade-off between the adaptation speed and transient response time. Normally, keeping longer adaptation is recommended, because the transient overshoot may be high using the above structure, and without any knowledge of the plant model. Also, the adaptive control may diverge, if the transient overshoot is too high because of the high gain of the inverter system. The second is the sampling rate used for discrete adaptive control. Increasing the sampling rate can reduce the adaptation speed. Nevertheless, increasing the sampling rate increases the cost as well. These are important in the application of adaptive control in power electronic controllers.

In conclusion, this chapter plays an important role in verifying the concept of using power electronic controller to improve distribution power quality. Detailed simulation results are provided showing power electronic converters solving typical power quality problems such as blocking harmonics, compensating voltage sags, absorbing voltage swells, high frequency oscillations and impulses. In addition, the

application of power electronic controllers in one-cycle-switching is addressed, showing that the converter not only compensates for the irregular voltage drops, but absorbs the surges.

In dealing with a dynamic machine load, a closed-loop qd0 model is used for control purposes. The simulation results also show that similar results as with static loads can be obtained by using the qd0 model. Furthermore, the simulation of the adaptive control system is performed as an approach to cope with the Custom load changes.

Further development is suggested following the analysis as performed in this chapter. As shown before, the qd0 model is valid for both uncoupled network loads and coupled dynamic machine loads. For uncoupled static loads, the qd0 model yields the exact same results as obtained from an equivalent single-phase model. However, for dynamic machine loads, which have a strong coupling between phases, the voltage waveforms remain sinusoidal, but the currents exhibit some distortion. Since the series converter is mainly applied for voltage control, another converter topology may be useful to deal with the current control.

CHAPTER 6

IMPLEMENTATION ISSUES

This chapter discusses some implementation issues for practical applications. The theory and applications as described in the previous chapters are sufficient to understand the principle of power electronics controllers for power quality improvement. Nevertheless, the topics presented here are helpful for further development in this area. The real issues in converter supply are addressed. A technique for converter supply is also discussed, which relies on a healthy feeder in the distribution system. Finally, the harmonic rejection issues regarding DC bus voltage are addressed.

6.1 A State-of-the-Art Technique for Converter Supply[1]

The DC-AC converters invert a DC source into an AC source. The DC voltage source could be a large capacitor for short disturbances or battery storage for UPS operation. These methods have some disadvantages in real system applications, from an operation point of view. Therefore, using other means for the converter DC power supply needs to be developed.

---

[1] This idea was originally conceived by Dr. Khai D.T. Ngo in a research meeting.

Referring to the miniature distribution system in Figure 2.3, using power lines to directly supply the DC-AC inverter is possible. The idea is to use three-phase or single-phase rectifiers to convert the AC voltage source, assuming the power lines which serve as the input for rectifiers do not need to support important loads. This assumption is made because rectifiers introduce harmonic distortions to the power lines. Using healthy feeders to support the controller can provide a continuous supply for the inverter, which is difficulty to achieve using batteries. This method was shown in the miniature distribution system, as in Figure 2.3. Figure 6.1 shows the detailed three-phase application related to the miniature system.

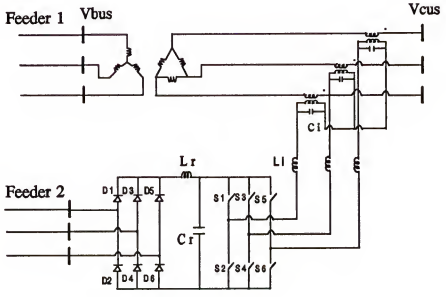

Figure 6.1 Rectifier-inverter set

In Figure 6.1, an L-C filter is used for DC linkage of rectifier and inverter, as noted by L_r and C_r. The selection of L_r and C_r is determined by the DC voltage requirement such as the ripple rate in the output voltage. The detailed design analysis is described in [38,39]. The parameters of the L-C filter is listed as the follows for future analysis.

L_r = 1.777 mH,

C_r = 100.0 uF.

It is noticed that the DC output voltage is fixed if an uncontrolled rectifier built with diodes is used. Furthermore, the inverter has certain requirements for the DC voltage source as well. Therefore, it is necessary to match the voltage level between the rectifier and inverter; otherwise, the inverter may not work properly for severe power quality problems at the Custom bus. The following analysis based on the prototype miniature distribution model can demonstrate how to reach a voltage match. If other topologies are used, the same principle is applied.

Assuming the rectifier is directly connected to the power line without a filter on the AC side, the DC voltage output from the three-phase rectifier depends on the AC voltage as in equation (6.1) [38]:

$$V_{DC} = 1.654 * V_m \tag{6.1}$$

in which V_m is the peak value of the per phase AC voltage.

The prototype distribution system has a line-to-line voltage of 208 V which creates a maximum output voltage V_{DC} = 280.9 V, according to (6.1). The rectifier which is built from diodes as shown in Figure 6.1 can obtain this voltage level.

The minimum DC voltage of the inverter is determined by the maximum inverter output voltage. Furthermore, the maximum inverter output voltage is determined by the worst case feeder bus voltage. It is recognized that the worst case in the feeder line is a complete voltage outage. Under this condition, the inverter operates in the Uninterruptible Power Supply (UPS) mode; i.e., the inverter will provide the full voltage to support the Custom bus while all three phases of the feeder bus are shorted to ground. The relationship between the DC voltage and the fundamental AC output of the inverter is discussed in Chapter 3, as in equation (3.1) [38,39].

According to equation (3.1), a three-phase 208 V line-to-line voltage output needs a minimum of 340 V DC to support full voltage, assuming the modulation index is 1.0. Comparing the output of the rectifier and inverter input requirement, the voltages do not match. Therefore, some voltage conversion technique has to be applied.

A simulation study was performed to explore feasibility in the above application. The rectifier-inverter scheme is applied with detailed models of the whole system; i.e., a detailed power system model, detailed control model, detailed inverter model and detailed rectifier model, referring to Figure 2.3 and Figure 6.1. For evaluation purposes, voltage sags are examined again in this application. Similar to the previous analysis, a fault at the feeder line causes voltage sags with an approximately 40 % voltage drop at the phase which suffers the fault. Therefore, the direct linkage between rectifier and inverter can be used in this case without compensating DC voltage.

Figure 6.2 and Figure 6.3 show the simulation results. From Figure 6.2, the voltage sags at the feeder bus do not exist at the Custom bus because of the compensation

by the inverter. A near perfect sinusoidal waveform at the Custom bus is achieved except for a small flaw. This shortcoming is due to the DC bus voltage drop in which the rectifier can not respond fast enough to the sudden voltage demand at the inverter output.

Figure 6.3 shows the rectifier input and output waveforms. The input voltage and current waveforms are distorted as discussed in Chapter 2. On the DC bus voltage waveform there are several points which may be important in practice. One is the peak DC voltage which needs to be suppressed to protect the devices. The other is the transient voltage at the DC bus which occurs because of the sudden change in output demand. In order to obtain a waveform without notches at the Custom bus, the DC voltage has to be compensated.

Another effect is the DC voltage ripple which depends on the Lr-Cr filter. However, a high quality DC bus voltage is not necessary in our applications even though it has direct impact on the output voltage, according to the conventional open-loop control. Because of the closed-loop control technique and high switching frequency, the voltage ripples in the DC bus do not have any impact on the output voltage. The closed-loop control adjusts the output, depending on the error between the reference and measurement. This is another significant effect in using the closed-loop control compared to the open-loop control. A more detailed analysis will be provided in the next section in studying the effect of the DC bus voltage harmonics on the output voltage in closed-loop system.

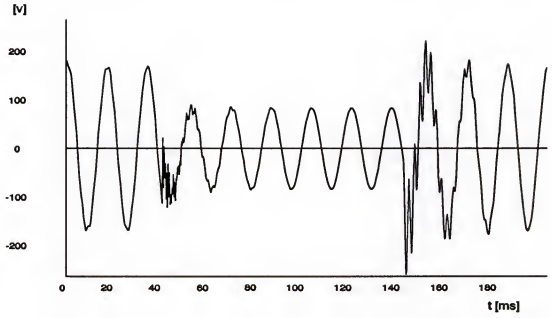

(a)

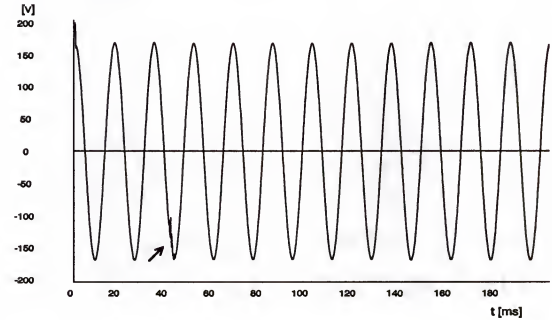

(b)

Figure 6.2 Voltages at (a) the feeder bus, and (b) the Custom bus

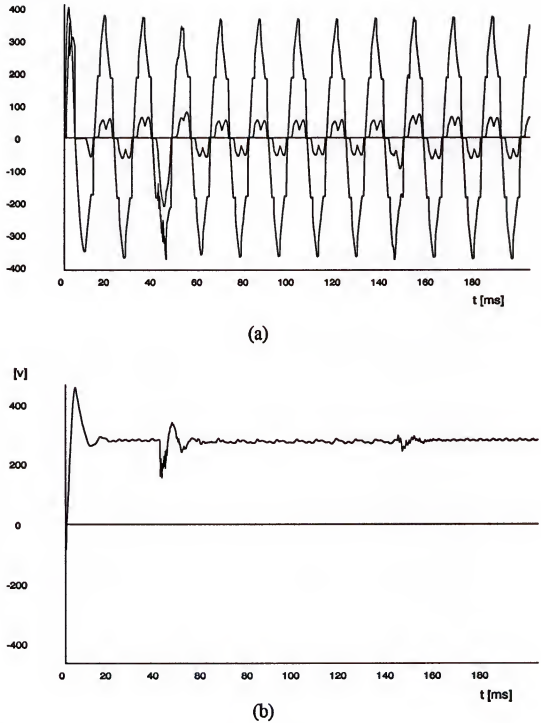

Figure 6.3 Rectifier input and output with inverter compensating voltage sags
(a) Rectifier input voltage and current, (b) DC bus voltage

Finally, other suggestions for using healthy feeders to support inverters are provided. If the important load at the Custom bus is single-phase, the rectifier can be connected to the other phases in which the inverter takes care of power quality problems resulting from both the feeder line and unbalanced harmonics. Also, Feeder 1 can serve as an input for the rectifier if there are no long-term power quality problems in the feeder side. The energy stored in the DC link capacitor can support the inverter for a while in case a voltage abnormality exists at the feeder bus. However, this method may have a stability problem because the system containing feeder bus, converter output, and rectifier actually constitutes a closed-loop system. More detailed analysis needs to be performed in order to implement this application.

6.2 Harmonic Rejection and Sensitivity Analysis

As illustrated previously, the closed-loop control system has the advantage of rejecting harmonic ripple parasitic on the DC bus voltage. This section provides an analytical solution for it. Also, a sensitivity analysis is performed to study the effect of the compensator deviation on the output voltage.

6.2.1 Harmonic Rejection

In order to investigate the effect of the DC harmonic ripple on the output voltage, the transfer function from the DC bus voltage to converter output can be derived. As pointed out previously, the describing functions which represent low frequency components are used as in [29]. Based on Figure 3.5, the equation (3.4) can be rewritten as follows.

$$v_{ab} = d*v_g \tag{6.2}$$

where both d and v_s are nonlinear.

Furthermore, the voltage equation (3.5) can be written as

$$v_{ab} = dv_g = v_o + L\frac{di_1}{dt} \tag{6.3}$$

The inductor current i_1 can be written as

$$i_1 = c\frac{dv_o}{dt} + i_o \tag{6.4}$$

Meanwhile, the load current can be written as in (6.5), if the Custom load is assumed to be an equivalent impedance.

$$R_L i_o + L_L\frac{di_o}{dt} = v_{cus} \tag{6.5}$$

As before, the feeder bus voltage V_{bus} is taken to be zero in deriving the transfer function. Therefore, the Custom bus voltage as in (6.5) is equal to the converter output voltage V_o. Using the small signal perturbation technique [40], one can rewrite the state space equations as follows.

$$L\frac{d\hat{i}}{dt} = D\hat{v}_g + V_g\hat{d} - \hat{v}_o \tag{6.6}$$

$$c\frac{d\hat{v}_o}{dt} = \hat{i} - \hat{i}_o \tag{6.7}$$

$$L_L \frac{d\hat{i}_o}{dt} = \hat{v}_o - R_L \hat{i}_o \tag{6.8}$$

In equation (6.6), D is the steady state duty ratio, and V_g is the steady state DC bus voltage. Thus, by taking the Laplace transform, one can obtain the transfer function as in (6.9).

$$\hat{v}_o(S) = \frac{SL_L + R_L}{X(S)} V_g * \hat{d}(S) + \frac{SL_L + R_L}{X(S)} D * \hat{v}_g(S) \tag{6.9}$$

where X(S) is given by (6.10).

$$X(S) = R_L + (L + L_L)S + LR_L CS^2 + LL_L CS^3 \tag{6.10}$$

One can see the transfer function from the duty ratio d(S) to the converter output $v_0(S)$ is the same as that in equation (3.12). The transfer function from DC bus voltage $v_g(S)$ to converter output is a new term which can be taken as a disturbance or noise. Based on equation (6.9), the closed-loop control system can be redrawn as in Figure 6.4, without taking the feeder bus into account. The transfer functions $G_1(s)$ and $G_2(s)$ are given by (6.11) and (6.12).

$$G_1(S) = \frac{R_L + SL_L}{X(S)} V_g \tag{6.11}$$

$$G_2(S) = \frac{R_L + SL_L}{X(S)} D \tag{6.12}$$

Based on equation (6.12) and Figure 6.4, the harmonic rejection effect of the closed-loop system can be evaluated by the transfer function from $v_g(S)$ to $v_o(S)$, which is given by (6.13).

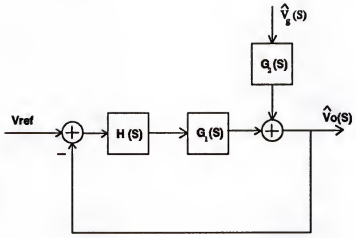

Figure 6.4 Closed-loop control system for DC bus harmonic rejection

$$\frac{\hat{V}_o(S)}{\hat{V}_g(S)} = \frac{G_2(S)}{1+H(S)G_1(S)} \tag{6.13}$$

Assuming the loop gain $H(S)G_1(S)$ is high, one can consider the denominator of (6.13) as H(S)G1(S). Approximately, the harmonic rejection can be represented by (6.14), which is derived by substituting (6.11) and (6.12) into (6.13).

$$\frac{\hat{V}_o(S)}{\hat{V}_g(S)} \approx \frac{D}{H(S)V_g} \tag{6.14}$$

Under steady state, the duty ratio is less than one. And, H(S) is larger than one. Thus, the harmonic noise on DC bus is at least attenuated by a factor of V_g. In the example as discussed before, which has a 280.9 V DC for three-phase and 162.2 V DC for single-phase, the output voltage will have at most 0.062 V voltage ripple, if the DC bus voltage has a 10 V peak harmonic ripple.

6.2.2 Sensitivity Analysis

The sensitivity of the closed-loop system to the deviation of the compensator was also studied by removing the disturbance input from the system. As can be seen in equation (6.13), the deviation of the compensator also affects the transfer function from the disturbance to the output. A similar analysis can be applied for that case.

Figure 6.9 shows the Bode-plot of the closed-loop transfer function. From the figure, the gain is almost a constant under 1 kHz. Also, the phase angle is 0 degree under 1 kHz. Therefore, the closed-loop system will follow the reference very precisely.

In the following, a quantitative example will be provided to examine the sensitivity of the closed-loop system to the compensator gain under steady state condition. From Figure 6.5, each parameter in the transfer function can be represented by a constant, as in equation (6.15).

$$V_o = \frac{HG_1}{1+HG_1} V_{ref} \tag{6.15}$$

By taking the derivative of the equation (6.15), one can get the sensitivity factor as given by (6.16).

$$\frac{\Delta V_o}{\Delta H} \approx \frac{dV_o}{dH} = \frac{G_1 V_{ref}}{(1+HG_1)^2} \tag{6.16}$$

Using the example given before, one can examine how the output is affected by the gain deviation of the compensator. The gain of the converter during steady state is 44.2 dB, i.e. 162.2. The gain of the original compensator H is taken as 1. The reference voltage is 169.7 V. Assuming a deviation factor of 2 for the compensator

gain, one expects an approximate 8.17 V deviation at the output voltage, if the inverter supplies a full voltage with a peak value of 169.7 V.

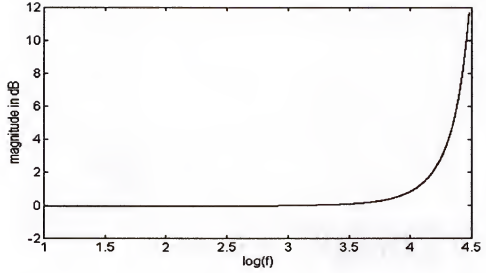

(a)

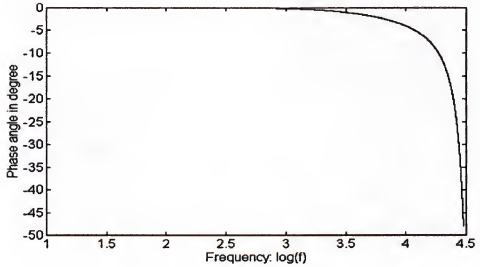

(b)

Figure 6.5 Bode plot of the closed-loop transfer function

CHAPTER 7

CONCLUSION

The dissertation describes one of the most challenging topics in present day electric power engineering: power electronics applications in solving distribution power quality problems. The dissertation includes descriptions of problems in the power quality area, investigation of possible solutions using power electronics controllers, theoretical background analyses of power electronics converters and computer simulations to verify the concepts, advanced control systems design and implementations using state-of-the-art methods.

The dissertation first introduces the power quality problems which plague present distribution systems. Various power quality phenomena are investigated using computer simulations based on a typical distribution system. The power quality phenomena causing concern in distribution systems include harmonic distortions, voltage sags, voltage swells, outages, transients, impulses, and noise. In addition, low power factor is a problem from a stabilizing voltage point of view and reducing losses in equipment. The waveforms obtained through computer simulations are comparable to those acquired from real distribution systems. The advantage of computer simulations is providing flexibility to analyze the power quality phenomena indepth. On the other hand, measuring the power quality phenomena in a real system is not always feasible.

Due to the complexity of distribution systems, many studies are based on some approximations as seen in the literature. This is especially recommended in studying a system with rotating electric machines, because they are non-linear and dynamic loads. The dissertation not only concentrates on the static loads, but it investigates dynamic loads of rotating electric machinery as well, using detailed computer simulation models. The phenomena uncovered through computer simulation upgrades the results obtained by conventional and simplified models used to represent motor loads.

The dissertation investigates power electronic converters, especially the series connected PWM DC-AC inverter, by evaluating theoretical background and illustrating various applications. Dynamic models of power electronic converters are derived, based on different load types. For static and uncoupled network loads, the single-phase inverter model can be used for analysis of three-phase systems. For dynamic and coupled loads, a generalized qd reference model is developed for typical rotating machinery loads.

Furthermore, a control system is developed for each type of application based on the developed model. In general, closed-loop control is applied in all of the applications. Of special interest is the adaptive control which serves as a multi-functional controller for any type of load.

The dissertation verifies the concepts by using computer simulations to cover various power quality phenomena. The studies are as follows: blocking harmonic distortions existing in the feeder side, compensating voltage sags caused by unbalanced faults, absorbing voltage swells resulting from large motor load trip-off, compensating

outages, absorbing low rise time impulses or surges. The results are generally the same: the Custom bus maintains high quality power with regular sinusoidal waveforms.

The dissertation also covers another application: one-cycle-switching. By using power electronic devices, mechanical breakers can be replaced by Solid-State-Breakers (SSBs). The advantages are obvious. The switching speed of SSBs is much faster than that of mechanical breakers. Moreover, SSBs can be controlled by microprocessors which provide flexibility of operation. Applying SSBs in distribution systems improve power quality as well, because the time interval of voltage sags caused by closing or opening mechanical breakers is reduced. Furthermore, power electronics converters can be applied in a complementary mode to completely compensate voltage sags and absorb surges.

Finally, the dissertation discusses implementation issues, a rectifier-inverter set is proposed using a healthy AC bus to support the power electronic controller for the Custom bus. Because the DC bus voltage is rectified, harmonic ripple is of concern as well. The dissertation examines the effect of the harmonic ripple on the output voltage. It is concluded that the closed-loop control plays an important role in all of the applications, including rejecting harmonic ripple.

The dissertation covers several areas which are related to power quality control. It investigates distribution power quality phenomena in-depth. The power electronics of DC-AC inverters are studied in-depth as well. Control system design techniques are addressed, and a multi-functional control system is developed for the power electronics controller.

For further analysis, the current control using other converter topologies may be needed for dynamic machine load applications. As discussed in the dissertation, dynamic machine loads behave as current source at the Custom, for which the series converter may not be so efficient to cope with the current transients. Furthermore, the adaptive control may be applied to the qd0 dynamic machine model to cope with the load changes. These are of concerns in future development.

As another candidate of the control system, robust control may be applied. The dissertation investigates various Custom loads, from which the band of the dynamic performance can be developed. Thus, a control system with fixed parameters can be designed to deal with all the dynamic loads. The advantage of robust control over adaptive control is that it reduces the cost in designing the control systems.

Furthermore, the assumption of a high loop gain is made in control system, because a unit feedback is applied. Thus, the phase lead-lag compensator is designed. In practice, the feedback gain is a fraction because the voltage comparison is based on a low voltage scale. Therefore, the compensator with certain gain needs to be designed in order to maintain a high loop gain.

In power electronics, loss analysis can be performed including the DC-AC inverters. In this dissertation, a 20 kHz switching frequency is applied in order to obtain a high quality power. However, the inverter may have a great amount of switching losses due to the high switching frequency. Further analysis needs to be carried out in order to determine the overall efficiency of using power electronics converters.

APPENDIX A

INDUCTION MOTOR DATA

NEMA: Design B

RATINGS:

3 hp, 208 V, 3 phase, 4 poles, 60 cycle.

Electrical parameters:

Stator resistance:	$r1 = 0.21772\ (\Omega)$,
Stator leakage inductance:	$l1 = 0.001904$ (H),
Rotor resistance referred to the stator:	$r2' = 0.2631\ (\Omega)$,
Rotor leakage inductance referred to the stator:	$r2' = 0.002477$ (H),
Magnetizing inductance:	$lm = 0.054243$ (H).

Mechanical parameters:

Moment of inertia:	$0.063\ kg.m^2$,
Damping coefficient:	0.002 N.m.s.

APPENDIX B

ALGEBRAIC EQUATIONS OF TRANSFORMATION MATRICES

B-1 Transformation between abc and ofb Variables

The transformations between the abc variables and ofb variables are performed as follows [29,30]:

$$x_{ofb} = T^{-1} x_{abc} \tag{B-1}$$

$$x_{abc} = T x_{ofb} \tag{B-2}$$

Where the matrices T and T^{-1} are given by (B-3) and (B-4).

$$T = \frac{1}{\sqrt{3}} \begin{bmatrix} 1 & e^{-j\theta} & e^{j\theta} \\ 1 & e^{-j(\theta-120^\circ)} & e^{j(\theta-120^\circ)} \\ 1 & e^{-j(\theta+120^\circ)} & e^{j(\theta+120^\circ)} \end{bmatrix} \tag{B-3}$$

$$T^{-1} = \frac{1}{\sqrt{3}} \begin{bmatrix} 1 & 1 & 1 \\ e^{j\theta} & e^{j(\theta-120^\circ)} & e^{j(\theta+120^\circ)} \\ e^{-j\theta} & e^{-j(\theta-120^\circ)} & e^{-j(\theta+120^\circ)} \end{bmatrix} \tag{B-4}$$

where the angle θ is given by (B-5)

$$\theta = \int_{o}^{t} \omega(\tau) d\tau \tag{B-5}$$

and $\omega(\tau)$ is the angular speed of the reference frame. In the applications used in this dissertation, $\omega(\tau)$ is assumed to be a constant with 60 Hz frequency.

By taking the first order derivative of (B-2), one can obtain a differential equation, as in (B-6).

$$\dot{x}_{abc} = \dot{T}\, x_{qfb} + T\, \dot{x}_{qfb} \tag{B-6}$$

Furthermore, the second order derivative of (B-2) yields:

$$\ddot{x}_{abc} = \ddot{T}\, x_{qfb} + 2\, \dot{T}\, \dot{x}_{qfb} + T\, \ddot{x}_{qfb} \tag{B-7}$$

where $\dot{T}$ and $\ddot{T}$ are given by:

$$\dot{T} = \frac{1}{\sqrt{3}} \begin{bmatrix} 0 & -j\omega e^{-j\theta} & j\omega e^{j\theta} \\ 0 & -j\omega e^{-j(\theta-120^{o})} & j\omega e^{j(\theta-120^{o})} \\ 0 & -j\omega e^{-j(\theta+120^{o})} & j\omega e^{j(\theta+120^{o})} \end{bmatrix} \tag{B-8}$$

$$\ddot{T} = \frac{1}{\sqrt{3}} \begin{bmatrix} 0 & -\omega^2 e^{-j\theta} & -\omega^2 e^{j\theta} \\ 0 & -\omega^2 e^{-j(\theta-120^{o})} & -\omega^2 e^{j(\theta-120^{o})} \\ 0 & -\omega^2 e^{-j(\theta+120^{o})} & -\omega^2 e^{j(\theta+120^{o})} \end{bmatrix} \tag{B-9}$$

B-2 Transformation between abc and qd0 Variables

The transformations between the abc variables and qd0 variables are performed as follows [27]:

$$x_{qd0} = K\, x_{abc} \tag{B-10}$$

$$x_{abc} = K^{-1}\, x_{qd0} \tag{B-11}$$

Where the matrices K and K^{-1} are given by (B-12) and (B-13).

$$K = \frac{2}{3}\begin{bmatrix} \cos\theta & \cos(\theta-120^o) & \cos(\theta+120^o) \\ \sin\theta & \sin(\theta-120^o) & \sin(\theta+120^o) \\ \frac{1}{2} & \frac{1}{2} & \frac{1}{2} \end{bmatrix} \tag{B-12}$$

$$K^{-1} = \begin{bmatrix} \cos\theta & \sin\theta & 1 \\ \cos(\theta-120^o) & \sin(\theta-120^o) & 1 \\ \cos(\theta+120^o) & \sin(\theta+120^o) & 1 \end{bmatrix} \tag{B-13}$$

By taking the first order derivative of (B-11), one can obtain a differential equation, as in (B-14).

$$\dot{x}_{abc} = \dot{K}^{-1} x_{qd0} + K\, \dot{x}_{qd0} \tag{B-14}$$

Furthermore, the second order derivative of (B-11) yields:

$$\ddot{x}_{abc} = \ddot{K}^{-1}\, x_{qd0} + 2\, \dot{K}^{-1}\, \dot{x}_{qd0} + K^{-1}\, \ddot{x}_{qd0} \tag{B-15}$$

where $\dot{K}^{-1}$ and $\ddot{K}^{-1}$ are given by:

$$\dot{K}^{-1} = \begin{bmatrix} -\omega\sin\theta & \omega\cos\theta & 0 \\ -\omega\sin(\theta-120^o) & \omega\cos(\theta-120^o) & 0 \\ -\omega\sin(\theta+120^o) & \omega\cos(\theta+120^o) & 0 \end{bmatrix} \tag{B-16}$$

$$\ddot{K}^{-1} = \begin{bmatrix} -\omega^2\cos\theta & -\omega^2\sin\theta & 0 \\ -\omega^2\cos(\theta-120^o) & -\omega^2\sin(\theta-120^o) & 0 \\ -\omega^2\cos(\theta+120^o) & -\omega^2\sin(\theta+120^o) & 0 \end{bmatrix} \tag{B-17}$$

APPENDIX C

PARAMETERS USED IN THE DISSERTATION

C-1 Laboratory Model Distribution System

(Referring to Figure 2.2 and 2.3)

System rating: 15 kVA, 208 V line-to-line, 3 phase.

Transformers:

(1) Main transformer on the source side: 30 kVA, Y/Δ, 208 V/480V, X_L=6%.

(2) Transformer on the feeder 1 and feeder 2: 3 kVA, Δ/Y, 480 V/208V, X_L=6%.

(The 3 kVA transformer on feeder 1 must be replaced by 6 kVA to carry full loads on this feeder).

(3) Transformer on the feeder 3: 15 kVA, Δ/Y, 480 V / 208 V, X_L=6%.

(4) The back-to-back transformers on Custom load side: 3 kVA, Δ/Y, 480V/208V, X_L=6%.

(5) Transformer in connecting the inverter and distribution line: 3x1 kVA, single-phase, 460V/230V.

Loads:

(1) Loads on the distribution feeders 1 and 2:

Z_1=82.3+j51 Ω, C_1=5uF (Δ),

Z_2=32.6+j20.3 Ω, C_2=3uF (Δ),

(2) Load on the distribution feeder 3:

Z_3=5.1+j3.17 Ω.

Distribution line impedances (equivalent):

Z_s=0.375+1.003 Ω.

(3) Custom load:

3 kVA: Z=12.2+j7.6 Ω,

0.3 kVA: Z=122+j76 Ω.

C-2 Inverter Filter Parameters

L=0.256 mH,

C=95uF,

Transformer (see above).

C-3 Control System

Transfer function of the phase lead compensator:

$$H(S) = \frac{1+7.54*10^{-5}S}{1+1.3*10^{-5}S} \qquad \text{(C-1)}$$

APPENDIX D

DIGITAL ALGORITHMS

The control system as discussed in the dissertation can be implemented by digital equipment such as microprocessors. Rather than using analog components to build the functional blocks to represent mathematical equations which are normally differential equations in linear systems, the microprocessors solve the equations based on difference equations. All analog signals will be digitized into the discrete-time domain. The digitization is based on sampling the continuous signal at certain equal base instances. The speed is evaluated by sampling rate. The fundamental digital controls are discussed in Franklin [49] and Leigh [50].

In a digital system, analysis is normally performed in Z-domain which corresponds to difference equations. In a continuous time system, Laplace transform, known as in the S-domain, is used; this was applied in Chapter 4 to study the dynamic performance of the control system and design compensators for a closed-loop system. The S-domain equations need to be converted to the Z-domain in order to implement digital control. There are several techniques available to transform S-domain equations to Z-domain. In the applications as performed in this dissertation, a very widely used technique--Bilinear transformation--is applied. The detailed description of the Bilinear transformation is described in [51].

The Bilinear transformation uses the linear relationship as in (D-1) to substitute the S variable in a continuous frequency domain equation.

$$S = \frac{2}{T_s}\frac{Z-1}{Z+1} \tag{D-1}$$

where T_s is the sampling period.

Using this formula, the transfer functions in the S-domain can be converted to Z-domain. Substituting this into the inverter and system model as in equation (4.9), one can get the transfer function in the discrete-time domain as in (D-2):

$$\frac{V_o(Z)}{D(Z)} = \frac{\sum_{i=0}^{3} A_i(Z^{-i})}{\sum_{j=0}^{3} B_j(Z^{-j})} \tag{D-2}$$

where A_i and B_i are the coefficients composed of inverter filter and Custom load parameters. The summation from zero to three is used because the system is in a third order. The detailed derivations are not provided here.

In equation (D-2), the element Z^{-1} is simply a time-step delay, in which the delay is determined by the sampling rate. The equation is linear because the numerator and denominator are polynomials. The inverse Z-Transform yields a difference equation which shows the input and output relationship in discrete-time system, as in (D-3).

$$v_o(k) = -\frac{\sum_{i=1}^{3} B_i}{B_o} v_o(k-i) + \frac{\sum_{j=0}^{3} A_j}{B_1} d(k-j) \tag{D-3}$$

Furthermore, the compensator as designed in Chapter 4 can be transformed to the Z-domain as well. From equation (4.1), a difference equation can be derived using the

Bilinear transformation, as in (D-4).

$$d(k) = c_1 d(k-1) + c_2 e(k) + c_3 e(k-1) \qquad \text{(D-4)}$$

In addition, the adaptive control as discussed in Chapter 4 and Chapter 5, relies on digital control to carry out iteration steps.

REFERENCES

[1] Narain G. Hingorani, "CUSTOM POWER Technology," Electric Power Research Institute (EPRI), Palo Alto, California, USA, December 1, 1992.

[2] Narain G. Hingorani, "Introducing CUSTOM POWER," IEEE Spectrum, Volume 32, June, 1995, pp 41- 48.

[3] Narain G. Hingorani, "Flexible ac transmission," IEEE Spectrum, Volume 30, April 1993, pp 41- 48.

[4] Dennis P. Carroll, K.D.T. Ngo, G.B. Chung, A.Maheshwari, S.B. Swindler, "High Frequency Link Converters as Elements in Flexible AC Transmission Systems," Annual Report submitted to Electric Power Research Institute (EPRI), Project RP4000-19, Palo Alto, California, USA, August 1991.

[5] IEEE Tutorial Course, "Adjustable Speed Drives," Course Text 92 EHO 362-4-PWR, IEEE, Inc. Piscataway, NJ, 1992.

[6] David E. Rice, "Adjustable Speed Drive and Power Rectifier Harmonics -- Their Effect on Power Systems Components," IEEE Transactions on Industry Applications, Vol. IA-22, No.1, January/February 1986, pp 161-177.

[7] Mark F. McGranaghan, David R. Mueller, Mark J. Samotyj, "Voltage Sags in industrial Systems," IEEE Transactions on Industry Applications, Vol. 29, No. 2,March/April 1993, pp 397-403.

[8] Jeff Harvey, "System Engineering Avoids Electrical Disasters," Power Quality Assurance, July/August 1993, pp 15-24.

[9] Chingchi Chen, Deepakraj M. Divan, "Simple Topologies for Single Phase AC line Conditioning," IEEE Industry Applications Meeting, Dearborn, MI, 1991, pp 911-917.

[10] Fang Zheng Peng, Hirofumi Akagi, and Akira Nabae, "A New Approach to Harmonic Compensation in Power Systems - A Combined System of Shunt Passive and Series Active Filters," IEEE Transactions on Industry Applications, Vol. 26, No. 6. November/December 1990, pp 983-990.

[11] F.Z. Peng, H.Akagi, A.Nabae, "A novel harmonic power filter," IEEE Power Electronics Specialists Conference (PESC) record, Kyoto, Japan, April, 1988, pp 1151-1157.

[12] Richard Petrecca, Nicholas Abi-Samra, "Active Power Line Conditioning: A New Approach to Power Quality," Power Quality Assurance, July/August 1993.

[13] Joe F. Chicharo, and Haihong Wang, "Power System Harmonic Signal Estimation and Retieval for Active Power Filter Applications," IEEE Transactions on Power Electronics, Vol. 9, No. 6. November 1994, pp 580-586.

[14] Juan C. Balda, Syh C. Low, Kraig J. Olejniczak, "An Analysis of Active Power Line Conditioners Using the ElectroMagnetic Transients Program," IEEE Industry Applications Meeting, Houston, Texas, 1992, pp 1327-1334.

[15] Alexandre Campos, Geza Joos, Phoivos D. Ziogas, James F. Lindsay, "Analysis and design of a series voltage unbalance compensator based on a three-phase VSI operating with unbalanced switching functions," IEEE Transactions on Power Electronics, Vol. 9, Number 3, May 1994, pp 269-274.

[16] V.B. Bhavaraju, P. Enjeti, "A Novel Active Line Conditioner for A Three-Phase System," IEEE Industry Applications Meeting, Toronto, Canada, 1993, pp 979-985.

[17] Roger C. Dugan, Larry A. Ray, D. Daniel Sabin, Gene Baker, Clyde Gilker, Ashok Sundaram, "Impact of fast tripping of utility breakers on industrial load interruptions," IEEE Industry Applications Meeting, Denver, Colorado, USA, October 1994, pp 2326-2333.

[18] Stephen B. Smith, Ronald B. Standler, "The effects of Surges on Electronic Applications," IEEE Transactions on Power Delivery, Vol. 7, No. 3, July 1992, pp 1275-1282.

[19] A. Kusko, D. Galler, N. Medora, "Output Impedance of PWM UPS Inverter-Feedback vs. Filters," IEEE Industry Applications Society Annual Meeting, Seattle, Washington, October 7-12, 1990, pp 1044-1048.

[20] Akira Nabae, Hirotami Nakano, Yositsugu Okamura, "A Novel Control Strategy of the Inverter with Sinusoidal Voltage and Current Outputs," IEEE Power Electronics Specialists Conference Record, 1994, Taiwan, R.O. China, pp 154-159.

[21] Qunying Yao, D.G. Holmes, "A Simple, Novel Method for Variable-Hysteresis-Band Current Control of a Three Phase Inverter with Constant Switching

Frequency," IEEE Industry Applications Conference Record, 1993, Toronto, Canada, pp 1122-1129.

[22] Seong-Sik Min, Kyu-Chan Lee, Jhong-Whan Song, Kyu-Bock Cho, "A Fuzzy Current Controller for Field-Oriented Controlled Induction Machine by Fuzzy Rule," IEEE Power Electronics Specialists Conference Record, June 1992, Toledo, Spain, pp 265-270.

[23] Herve Pouliquen, Khaled Elloumi, Miao-Xin Wang, "Real Time PWM Control Converters Using Three Phase Elements Polynomial Regulations," IEEE Power Electronics Specialists Conference Record, June 1992, Toledo, Spain, pp 451-458.

[24] M.A. Dzieniakowski, M.P. Kazmierkowski, "Microprocessor-Based Novel Current Regulator for VSI-PWM Inverters," IEEE Power Electronics Specialists Conference Record, June 1992, Toledo, Spain, pp 459-464.

[25] Hong Le-Huy, Karim Slimani, Philippe Viarouge, "Analysis and Implementation of a Real-Time Predictive Current Controller for Permanent-Magnet Synchronous Servo Drives," IEEE Industry Applications Meeting, Dearborn, Michigan, 1991, pp 996-1002.

[26] Paul C. Krause, "Analysis of Electric Machinery," McGraw-Hill Inc., 1986.

[27] Y. Murai, H.Ishikawa, T.A. Lipo, "New Series Resonant DC Link Inverter for Electric Vehicle Drives," IEEE Industry Applications Conference Record, October 2-5, 1994, Denver, Colorado, pp 443-447.

[28] Takao Kawabata, Takeshi Miyasgita, Yushin Yamamoto, "Digital Control of Three Phase PWM Inverter with L-C Filter," IEEE Power Electronics Specialists Conference Record, Kyoto, Japan, April 1988, pp 634-643.

[29] Khai D.T.Ngo, "Low Frequency Characterization of PWM Converters," IEEE Transactions on Power Electronics, Vol. PE-1, Number 4, October 1986, pp 224-230.

[30] D.C. White and H.H. Woodson, "Electromechanical Energy Conversion," John Wiley and Sons Inc., New York,1959.

[31] G. Joos, P.D. Ziogas, D. Vincenti, "A Three Phase Model Reference Adaptive PWM Technique with Improve Features," IEEE Industry Applications Meeting, Seattle, Washington, October 1990, pp 997-1004.

[32] Bonneville Power Administration, "ElectroMagnetic Transients Program (EMTP)

Reference Manual," Bonneville Power Administration, Portland, Oregon, USA, August 1986.

[33] K.U.Leuven EMTP Center, "Alternative Transients Program (ATP) Rule Book," Former European EMTP Center, Leuven, Belgium, July 1987.

[34] Wilson E. Kazibwe, "Electric Power Quality Control Techniques," Van Nostrand Reinhold, New York, 1993.

[24] Yuexin Yin, "A Comprehensive Analysis of Electrical Machinery With Adjustable Speed Drives Using Electromagnetic Transients Program (EMTP) Simulation," Master's thesis, University of Florida, Gainesville, May 1993.

[35] Yuexin Yin, "Universal Machine Modeling in EMTP," A Short Course on Power System Analysis Using the ElectroMagnetic Transients Program, Latest version, May 1995, University of Florida, Continuing Education Department, Gainesville.

[36] Yuexin Yin, "Power Electronics and Motor Drives" A Short Course on Power System Analysis Using the ElectroMagnetic Transients Program, Latest version, May 1995, University of Florida, Continuing Education Department, Gainesville.

[37] Juan A. Martinez, "Rotating Machine Model", Lecture notes presented to the Leuven EMTP Short Course, July 1991, Leuven, Belgium.

[38] Muhammad H. Rashid, "Power Electronics: Circuit, Devices, and Applications," Prentice-Hall, Inc., Englewood Cliffs, NJ, 1993.

[39] Ned Mohan, Tore M.Undeland, William P. Robbins, "POWER ELECTRONICS: Converters, Applications, and Design," John Wiley & Sons, Inc., New York, 1989.

[40] John G. Kassakian, Martin F. Schlecht, George C. Verghese, "Principles of Power Electronics," Addison-Wesley Publishing Company, Reading, MA, 1991.

[41] Robert John Dirkman, "Generalized State Space Averaging," IEEE Power Electronics Specialists Conference (PESC) record, Albuquerque, New Mexico, 1983, pp 283-294.

[42] Richard C. Dorf, "Modern Control Systems," 5th edition, Addison-Wesley Publishing Company, Reading, MA, 1989.

[43] Katsuhiko Ogata, "Modern Control Engineering," Prentice-Hall, Englewood Cliffs, NJ, 1970.

[44] E.B. Dahlin, "Designing and Tuning Digital Controllers," Instrumentation & Control Systems, Vol. 42, No. 6, June 1968, pp 77-83.

[45] A.T. Touchstone, and A.B. Corripio, "Adaptive Control through Instrumental Variable Estimation of Discrete Model Parameters," Proceedings of ISA/77, Anaheim, CA. May 1977, pp 57-64.

[46] A.B. Corripio, P.M. Tompkins, "Industrial Application of a Self-Tuning Feedback Control Algorithm," ISA Transactions, Vol. 20, No.2, 1981.

[47] Ray-Shyang Lai and Khai D.T. Ngo, "A New Method for Reduction of Switching Loss in a Full-Bridge Inverter," IEEE Transactions on Power Electronics, Vol. 10, No.3, May 1995, pp 326-332.

[48] IEEE Standard Collection, "Surge Protection," C62, 1992.

[49] Gene F. Franklin, "Digital Control of Dynamic Systems," Addison-Wesley Publishing Company Inc., Reading, MA, 1990.

[50] J.R. Leigh, "Applied Digital Control: Theory, Design and Implementation," Prentice-Hall, Englewood Cliffs, NJ,1985.

[51] Robert D. Strum, Donald E. Kirk, "First Principle of Discrete Systems and Digital Signal Processing," Addison-Wesley Publishing Company, Inc. Reading, MA, 1989.

BIOGRAPHICAL SKETCH

Yuexin Yin was born in 1963, in China. He received his B.S.E.E. degree in 1986, from Nanjing Institute of Technology in China and his M.E. degree in 1993 from the University of Florida, USA. He was a faculty member in Nanjing Institute of Technology from 1986 to 1989 where he received the Outstanding Research Award and Outstanding Teaching Award. From 1990 to 1991, he was a full-time research assistant with the European EMTP Center located in Leuven, Belgium, to help further develop the power system simulation package ElectroMagnetic Transients Program (EMTP). He has given lectures in EMTP short courses on the topics of Universal Machine modeling, power electronics, and motor drives. Mr. Yin has been a consultant with Westinghouse Electric Corporation, Marine Division, California, and has done consulting projects with Brookhaven National Laboratory in New York and several other companies. Mr. Yin's professional interests include power system modeling, power quality, power electronics and electric drives, and control systems.

I certify that I have read this study and that in my opinion it confirms to acceptable standards of scholarly presentation and is fully adequate, in scope and quality, as a dissertation for the degree of Doctor of Philosophy.

Dennis P. Carroll, Chairman
Professor of Electrical and
Computer Engineering

I certify that I have read this study and that in my opinion it confirms to acceptable standards of scholarly presentation and is fully adequate, in scope and quality, as a dissertation for the degree of Doctor of Philosophy.

Martin A. Uman
Professor of Electrical and
Computer Engineering

I certify that I have read this study and that in my opinion it confirms to acceptable standards of scholarly presentation and is fully adequate, in scope and quality, as a dissertation for the degree of Doctor of Philosophy.

Khai D.T. Ngo
Associate Professor of
Electrical and Computer
Engineering

I certify that I have read this study and that in my opinion it confirms to acceptable standards of scholarly presentation and is fully adequate, in scope and quality, as a dissertation for the degree of Doctor of Philosophy.

Haniph A. Latchman
Associate Professor of
Electrical and Computer
Engineering

I certify that I have read this study and that in my opinion it confirms to acceptable standards of scholarly presentation and is fully adequate, in scope and quality, as a dissertation for the degree of Doctor of Philosophy.

Barney L. Capehart
Professor of Industrial and
Systems Engineering

This dissertation was submitted to the Graduate Faculty of the College of Engineering and to the Graduate School and was accepted as partial fulfillment of the requirements for the degree of Doctor of Philosophy.

December, 1995

Winfred M. Phillips
Dean, College of Engineering

Karen A. Holbrook
Dean, Graduate School